

METEOR-Berichte

Long-term monitoring of fluid and solid emissions at the African-Eurasian tectonic boundary in the ALBORan Sea and the Gulf of CADIZ

Cruise No. M167

11.10.2020 – 05.11.2020

Emden (Germany) – Emden (Germany)

ALBOCA II



Menapace W., Chahid D., Duarte D., Fleischmann T., Heitmann-Bacza C., Kramer L., Krupiński S., Leymann T., Mai A., Morales N., Otte F., Schmidt C., Tamborrino L., Vittori V., Xu S., Zehnle H., Zhang J.

Chief Scientist: Dr. Walter Menapace
MARUM - Center for Marine Environmental Sciences
University of Bremen

2021

Table of Contents

1	Cruise Summary	3
1.1	Summary in English.....	3
1.2	Zusammenfassung.....	3
2	Participants.....	4
2.1	Principal Investigators.....	4
2.2	Scientific Party.....	4
2.3	Participating Institutions	5
3	Research Program.....	5
3.1	Description of the Work Area	5
3.2	Aims of the Cruise	8
4	Narrative of the Cruise	10
5	Methodology and Preliminary Results.....	13
5.1	Hydroacoustics (Parasound & Multibeam).....	13
5.2	Sediment Sampling & Sedimentology.....	24
5.3	Physical Properties.....	30
5.4	Pore water Sampling & Geochemistry.....	35
5.5	Microbiology.....	39
5.6	BlueROV.....	40
5.7	ROV SQUID.....	50
5.7.4	MeBo CORKs.....	58
6	Ship's Meteorological Station	61
7	Station List M167.....	63
7.1	Overall Station List	63
7.2	Profiles Station List.....	66
8	Data and Sample Storage and Availability.....	68
9	Acknowledgements.....	68
10	References.....	68
11	Appendices.....	71
11.1	Lithologs	71

1 Cruise Summary

1.1 Summary in English

RV Meteor expedition M167 (ALBOCA II) main objective was to study the recent state of fluid and solid emissions at the plate boundary between Eurasia and Africa and retrieve three long-term datasets of in situ temperature, pressure and conductivity data. Shipboard sampling of gas and pore waters from the recovered cores further aimed at post-cruise analyses of fluid-rock interactions and fluid flow processes at depth. These research activities, together with comprehensive seafloor mapping and ROV dives, focused on i) the Gulf of Cadiz accretionary prism and, to a lesser extent, ii) the Alboran Sea Carboneras fault. From October 18 to 29, 2020, the M167 cruise collected a total of 55,55 m of sediment cores, conducted 11 ROV dives (7 SQUID + 4 BlueROV) and mapped approximately 7220 km² of seafloor. 8 new mud volcanoes were discovered during the cruise (Marie Tharp, Goldberry, Maria Bianca Cita, Isengard, Gondor, El Profesor, Tokyo, EUMR), which are located outside the predominant mud volcano distribution in the area. We also revisited various small mud volcanoes (Averroes, Boabdil, Atlas, Student, Fiuza) and the large Yuma, Ginsburg, Jesus Baraza, Al Idrisi and Gemini, where we sampled the most recent mud flows with thin hemipelagic cover on their summits. The recovered cores reflect a wide suite of mud breccias, that will provide insight into the dynamics of mud volcanism in the region. Onboard total alkalinity and chlorinity of collected pore waters further showed a systematic trend for these mud volcanoes, being respectively higher and lower compared to mean seawater values, when active fluid flow was present. Physical properties measured both on the ship and onshore also highlight the differences between gas-rich and gas-poor mud breccia, marking how these sediments could be profoundly influenced by gas seepage. During the ROV dives conducted we were able to recover two of the three observatories deployed in 2018 and we also tested cutting-edge seafloor visualization techniques and new technologies (3D photomosaicking, modified BlueROV system).

1.2 Zusammenfassung

Das Hauptziel der RV Meteor Expedition M167 (ALBOCA II) bestand darin, den aktuellen Zustand der Flüssigkeits- und Feststoffemissionen an der Plattengrenze zwischen Eurasien und Afrika zu untersuchen und drei Langzeitdatensätze von In-situ-Temperatur-, Druck- und Leitfähigkeitsdaten zu erhalten. Probenahmen von Gas und Porenwasser aus den geborgenen Bohrkernen an Bord, die weiter auf Analysen von Fluid-Gesteins-Interaktionen und Fluidströmungsprozessen in der Tiefe nach der Forschungsfahrt abzielen. Diese Forschungsaktivitäten konzentrierten sich zusammen mit umfassenden Kartierungen des Meeresbodens und ROV-Tauchgängen auf i) das Akkretionsprisma des Golfs von Cadiz und in geringerem Maße ii) die Alboran Sea Carboneras Störung. Vom 18. bis 29. Oktober 2020 sammelte die M167 insgesamt 55,55 m Sedimentkerne, führte 11 ROV-Tauchgänge (7 SQUID + 4 BlueROV) durch und kartierte ca. 7220 km² Meeresboden. Während der Forschungsfahrt wurden 8 neue Schlammvulkane entdeckt (Marie Tharp, Goldberry, Maria Bianca Cita, Isengard, Gondor, El Profesor, Tokio, EUMR), die sich außerhalb das vorherrschende Schlammvulkangebiet in der Region befinden. Wir besuchten auch verschiedene kleine Schlammvulkane (Averroes, Boabdil, Atlas, Student, Fiuza) und die großen Yuma, Ginsburg, Jesus Baraza, Al Idrisi und Gemini, wo wir auf ihren Gipfeln die jüngsten Schlammflüsse mit

dünnen hemipelagische Bedeckung untersuchten. Die gewonnenen Kerne spiegeln eine breite Palette von Schlammbrekzien wider, die einen Einblick in die Dynamik des Schlammvulkanismus in der Region geben werden. Die Gesamtalkalität und Chlorinität an Bord des gesammelten Porenwassers zeigten weiterhin einen systematischen Trend für diese Schlammvulkane, die im Vergleich zu den mittleren Meerwasserwerten jeweils höher bzw. niedriger waren, wenn ein aktiver Flüssigkeitsfluss vorhanden war. Physikalische Eigenschaften, die sowohl auf dem Schiff als auch an Land gemessen wurden, verdeutlichen auch die Unterschiede zwischen gasreicher und gasarmer Schlammbrekzien und zeigen, wie diese Sedimente durch das Eindringen von Gas tiefgreifend beeinflusst werden könnten. Während der durchgeführten ROV-Tauchgänge konnten wir zwei der drei im Jahr 2018 eingesetzten Observatorien bergen und wir testeten auch modernste Techniken zur Visualisierung des Meeresbodens und neue Technologien (3D-Photomosaicking, modifiziertes BlueROV System).

2 Participants

2.1 Principal Investigators

Name	Institution
Menapace, Walter, Dr.	MARUM
Kopf, Achim, Prof.	MARUM
Schmidt, Christopher, Dr.	GEOMAR

2.2 Scientific Party

Name	Discipline	Institution
Menapace, Walter, Dr.	Chief Scientist/Marine Geology	MARUM
Duarte, Debora, Dr.	Hydroacoustics/Observer	IPMA
Kramer, Laura	Hydroacoustics	MARUM
Xu, Shuhui, PhD	Hydroacoustics/Phys. Props.	MARUM
Tamborrino, Leonardo, PhD	Sedimentology	MARUM
Morales, Natasha	Sedimentology/Curator	MARUM
Zhang, Junli, PhD	Phys. Props.	MARUM
Fleischmann, Timo	Coring/Observatories/ROV SQUID	MARUM
Krupiński, Szymon, Dr.	Coring/BlueROV	MARUM
Schmidt, Christopher, Dr.	Geochemistry	GEOMAR
Zehle, Hanna, PhD	Microbiology/Geochemistry	MPI
Leymann, Tom	ROV SQUID	MARUM
Mai, Hoang Anh	ROV SQUID	MARUM
Vittori, Vincent	ROV SQUID	MARUM
Chahid, Driss, Dr.	Observer	UM5
Heitmann-Bacza, Carola	Meteorology	DWD
Otte, Frank	Meteorology (technician)	DWD

2.3 Participating Institutions

MARUM	Zentrum für Marine Umweltwissenschaften, Bremen
GEOMAR	Helmholtz-Zentrum für Ozeanforschung, Kiel
DWD	Deutscher Wetterdienst - Seeschiffahrtsberatung, Hamburg
MPI	Max Planck Institut für Marine Mikrobiologie, Bremen
IPMA	Instituto Português do Mar e da Atmosfera, Lisbon
UM5	Mohammed V University, Rabat, Morocco

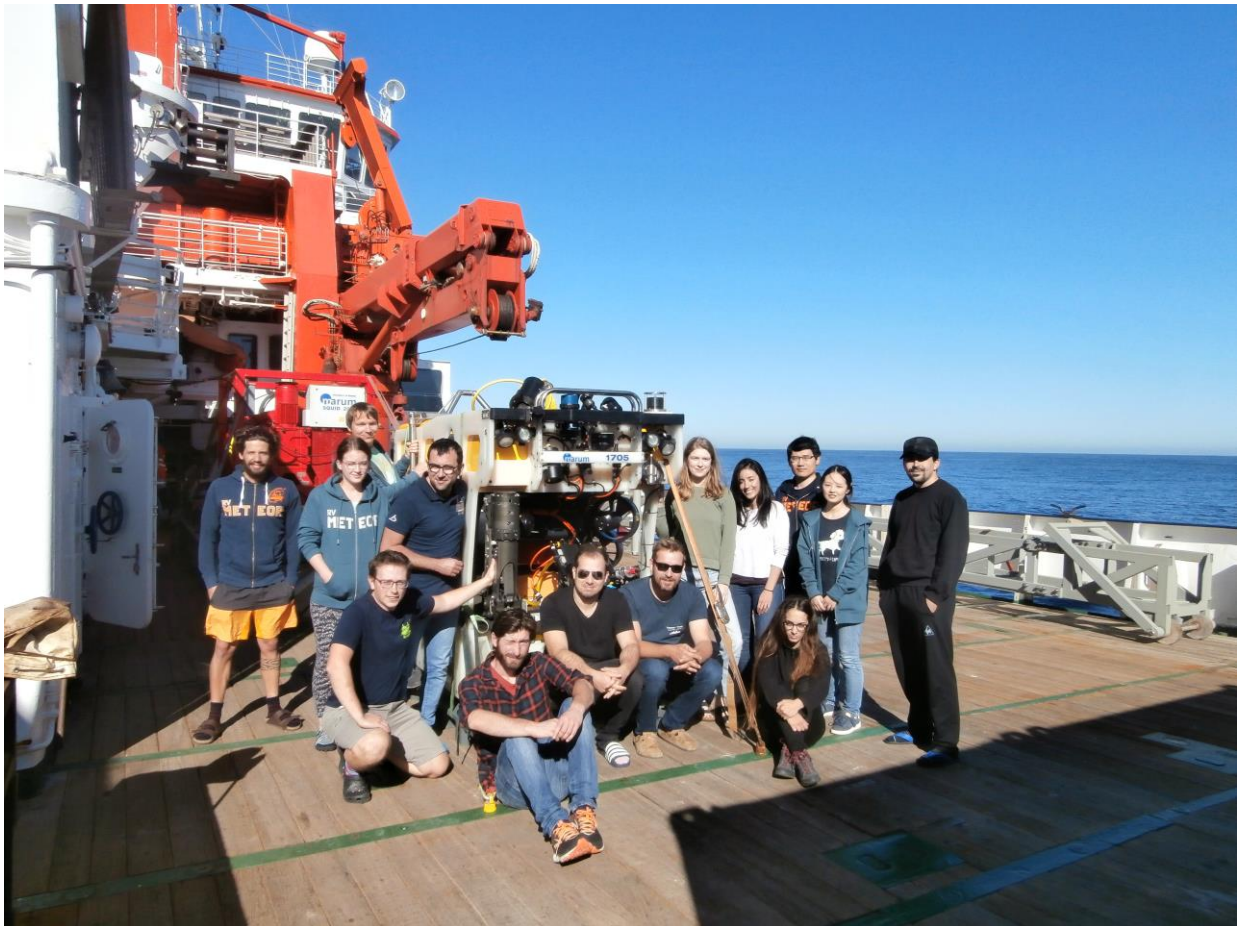


Figure 2.1: Scientific crew on the deck of RV Meteor during the M167 expedition.

3 Research Program

3.1 Description of the Work Area

(W. Menapace)

Gulf of Cadiz

The Gulf of Cadiz (GoC), main focus of the M167 expedition, is located on the South-West Iberian Margin (Atlantic Ocean), between the West Iberian Peninsula and Morocco (Fig. 3.1). The geological history of the area is highly complex and dictated by the interplay between the Eurasian and the African Plates. Subduction has developed during the Miocene, possibly due to roll-back of the oceanic crust slab towards the west, and correspondent emplacement of the Gibraltar Arc in the current position (Duarte et al., 2013). Simultaneously to the westward

motion of the Gibraltar Arc, the GoC accretionary wedge was building up to form the present allochthonous deposits, previously called the “Olistostrome” complex (Medialdea et al., 2004) and now referred to as the Accretionary Wedge complex. Miocene deformation was followed by a compressional regime that lasted from the Pliocene until today (Gómez de la Peña et al., 2018).

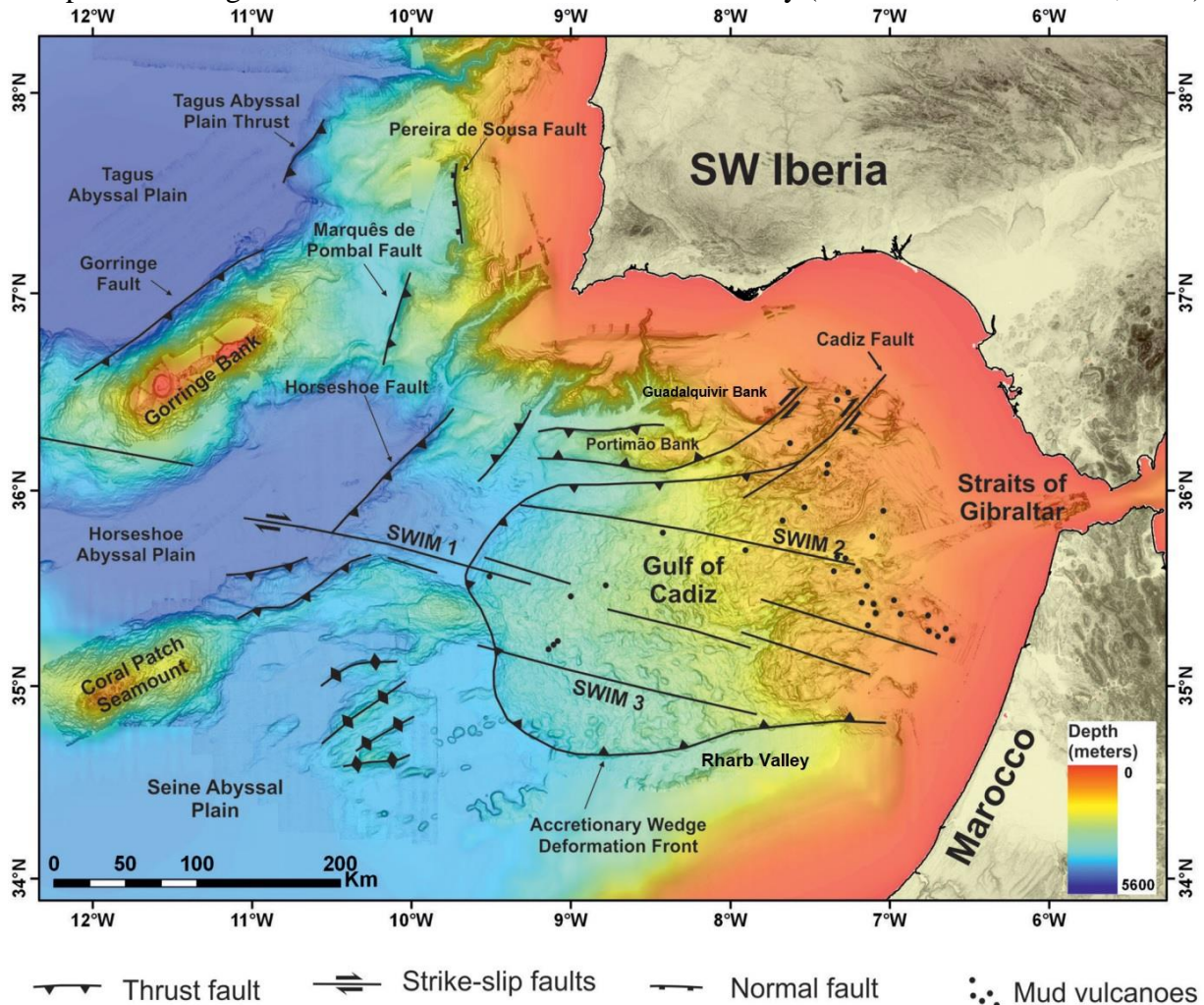


Figure 3.1: Simplified tectonic map of the Gulf of Cadiz (Cunha et al., 2012).

The current state of subduction is unclear: some authors suggest part of the region is inactive (Platt et al., 2013), whereas some others defend the opposite idea (Gutscher et al., 2012). Despite that, the convergence rate between the Iberian and Nubian subplates (respectively belonging to Eurasia and Africa) is $\sim 4\text{--}6$ mm/yr with a WNW-ESE direction (Cunha et al., 2012). The convergence is accommodated by a series of right-lateral strike-slip faults which are called the SWIM lineaments (from South-Western Iberian Margin), hypothesized as the current plates' boundary (Figure 2, Zitellini et al., 2009). Several pull-apart basins are also scattered along the SWIM faults, further confirmation of the ongoing strike-slip tectonics (Crutchley et al., 2011)

Deep EQs, related to the slab rollback (Spakman et al., 2018), and intermediate ones, from the transpression west of Gibraltar, are distributed in the region, but almost none of them is located beneath the accretionary prism (Silva et al., 2017). The extremely low taper angle of 2° might also hint towards a weak decollement, which could help explain the absence of shallow EQs (Gutscher et al., 2009). This paradox has ultimately led scientists to believe that an incipient subduction zone is currently forming west of the Gibraltar arc (Duarte et al., 2013); also

supported by the evidence of several $M_w > 7$ EQs around the Goringe Bank and the Horseshoe Plain (Silva et al., 2017).

The GoC shows all the classical signs of an accretionary wedge sequence, with abundant thrust faults (Gutscher et al., 2009), scattered but numerous MVs (Medialdea et al., 2009), and active fluid flow structures (León et al., 2010). The accretionary wedge is limited on the east by the Gibraltar Arc, on the west by both the Horseshoe and Seine Abyssal Plains, whereas it is bounded north and south by the Guadalquivir/Portimao Banks and the Rharb Valley, respectively (Zitellini et al., 2009). It can be divided into an upper part, composed by a two-lobed structure of possible gravitative origin, and a lower part, constituting the main tectonically accreted sediments (Gutscher et al., 2009). This complex geometry has also been reconstructed analogically through sandbox models (Duarte et al., 2011), which again suggested that subduction was actively playing a role in shaping what has been identified as an accretionary wedge.

Alboran Sea

In the eastern Alboran Sea (western end of the Mediterranean Sea) a complex distribution of sinistral SW-NE and dextral SE-NW trending strike-slip faults exist between the Moroccan and the Spanish margin. Similar to the Gulf of Cadiz, this region has suffered large earthquakes in the past, which repeatedly destroyed coastal communities between the 15th and 19th century, such as the cities of Vera and Almeria (Gràcia et al., 2006 and references therein). Some of these faults extend up to 100 km in the Alboran Sea and continue on land, e.g. the Carboneras fault in southern Spain, which has been identified as a potential candidate of large earthquakes of up to $M7.2$ (Gràcia et al., 2006). Therefore, the fault system in the Alboran Sea constitutes a significant earthquake and tsunami threat to coastal communities neighboring the western Mediterranean Sea (Gràcia et al., 2019) and has been investigated during both the M149 and M167 expeditions.

Mud volcanism

MVs in the GoC were first discovered during the TTR-9 (Training-through-Research) cruise, back in 1999 (Ivanov, 2000). Since then, the number of such structures identified on the seafloor has risen to >90 (Hüpers et al., 2019). Through an ever-increasing bathymetric coverage, several MVs areas have been identified. MVs are distributed mostly in the upper part of the accretionary wedge (Somoza et al., 2003), although they can also be found further downslope in smaller numbers (Pinheiro et al., 2003), as well as on the Horseshoe Abyssal Plain (Hensen et al., 2015) (Fig. 3.2).

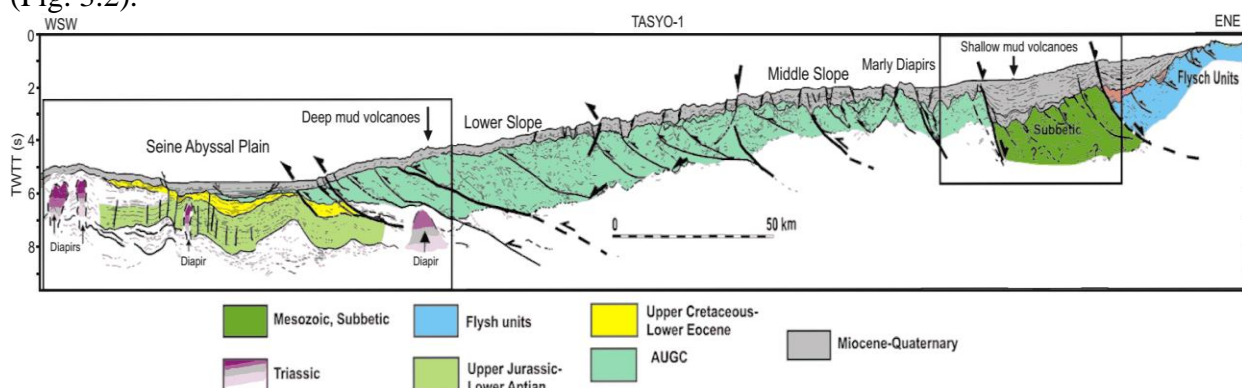


Figure 3.2: Interpretation by Medialdea et al. (2009) of the seismic line TASYO-1 cross-cutting the accretionary prism. In the boxes are highlighted the two main areas where MVs are present.

Numerous multi-channel seismic lines (MCS) cross-cutting the accretionary prism revealed how the salt diapirism in the area is undoubtedly linked to the emplacement of MVs, where Triassic salt rises in the sedimentary sequence under tectonic overload, and the extensive presence of faults favor the ascent of mud towards the seafloor (Medialdea et al., 2009;). On the other hand, the fluids expelled from the MVs are clearly linked to clay dehydration, with few other processes overprinting their signature, e.g. dissolution of evaporites, carbonate precipitation (Hensen et al., 2007). Several studies also point to a crustal source of the fluids, which show a stronger signal in the deep-water MVs due to the thinner sediment package overlying the basement (Scholz et al., 2009).

Mainly because of their connection with the deepest part of the accretionary prism, MVs are highly episodic features, acting as valves to dissipate excess pore pressure (Menapace et al., 2017). Common indicators of episodicity are different generations of mud flows draping the edifices or interfingering pelagic sedimentation below the seafloor, presence of mineral deposition fronts at depth (from changes of seepage intensity), and different morpho-structures (i.e. moats, carbonate crusts, multiple coalescent cones, etc) which could hint toward activity vs quiescence. Such episodicity has been investigated in the GoC by means of bathymetric and seismic surveys (Toyos et al., 2016), corroborated by fluids (Haffert & Haeckel, 2019) and solids (Vanneste et al., 2103) geochemistry. However, it is still fairly obscure which are the main drivers behind these sporadic bursts in activity. It is hypothesized that different events could trigger MVs eruptions (e.g. gas accumulation, sedimentary overburden), but EQs are the only ones for which a direct cause-effect relationship has been established (Manga et al., 2009).

The M167 expedition was aiming to clarify the relation between MVs and both active tectonics and seismicity in the GoC, improving our understanding of these complex seafloor structures.

3.2 Aims of the Cruise

(W. Menapace)

Earthquakes (EQs) and landslides are the most common causes of tsunamis, all of which represent a major threat along the Southwestern European continental margin (e.g. Great Lisbon EQ of 1755, $M_w > 8.5$). The most crucial knowledge for hazard mitigation is given by the recurrence intervals, the preconditioning factors and the triggers that favor such events in a determined region.

The westernmost portion of the Mediterranean Sea is tectonically complex, given the controversial views on the nature and location of the Africa-Eurasia plate boundary and the significance of the Azores-Gibraltar transform fault. At the same time, this region has suffered from frequent, large magnitude earthquakes with epicenters both on- and offshore, and has an instrumental seismic record too imprecise for reliable risk assessment or determination of recurrence times in the seismic cycle.

In this regard, the objective of expedition M167 was to study the recent condition of fluid and solid emissions at the plate boundary between Eurasia and Africa and retrieve three long-term dataset of in situ temperature, pressure and conductivity data (2018-2020). Due to the privileged location of these so called “MeBo CORKS” observatories on two active faults and on

the Ginsburg mud volcano (MV), the monitored parameters will allow us to shed much needed light on the relationship between EQs and fluid emission in the Gulf of Cadiz. The expedition M167 scientific objectives will contribute to understand the episodic nature of the Southwestern Iberian Margin's seismicity and its tectonic settings by answering three critical questions:

- Which structures (MVs, faults, pockmarks) show fluid advection and how is it related to the tectonic or sedimentary processes in the accretionary prism?
- How are the lineament faults connected to the distribution of active/inactive MVs throughout the GoC?
- Can geochemical fluid signatures, also in comparison with M149 data, shed some light on deep fluid pathways in the GoC?
- What does monitoring of active fluid emission features reveal about seismicity in the 2018-2020 period?
- How can new, innovative, techniques (photomosaicking) and technologies (BlueROV) help scientists reach these goals?

In order to answer these questions, the scientific program included the following approaches:

i) recover the “MeBo CORKs” observatories to assess episodic emission of sediments and/or fluids in key locations instrumented during the M149 with the ROV SQUID; ii) testing the modified BlueROV system developed by MARUM; iii) sample sediment material from deep-seated faults as well as from active mud volcanoes using gravity coring; iv) acquire photo-/videomosaicking and microbiological samples with the ROV SQUID to investigate ongoing biogeochemical processes on active MVs; and v) sample newly discovered MVs fields and active fluid emission features.

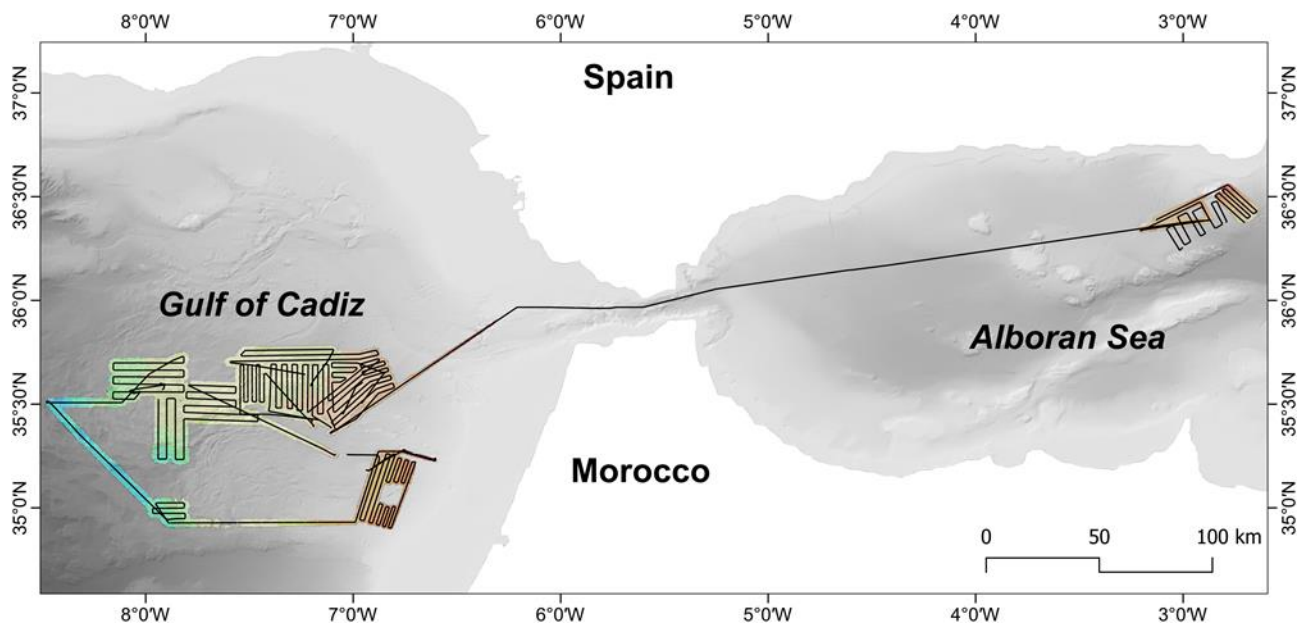


Figure 3.3: Track chart of RV Meteor Cruise M167 in the working areas (black lines), with the acquired bathymetry underneath.

Specifically, the work program encompassed primarily observatories recovery, gravity coring (for sediments, pore fluids and microbiological samples) and the acquisition of hydrographic data (Parasound and multibeam). A total of 4 dive sites were visited multiple times with the ROV SQUID. Once completed the main task of retrieving the MeBo observatories, the ROV focused on photomosaicking of key seafloor features. The gravity coring was located in

strategic positions along prominent fault zones (e.g., Lineament South and Center, Carboneras fault) as well as on mud volcanoes in the vicinity of those same faults (Ginsburg, Yuma, Rabat) and on suspected mud volcanoes or seepage features detected during the M149 (Fig. 3.3).

4 Narrative of the Cruise

(W. Menapace)

On October 10 the scientific crew was allowed to embark the RV Meteor after four days of quarantine in a Bremerhaven Hotel, and being tested negative for COVID-19. A bus transfer from the hotel to the ship, berthed in Emden, delivered the scientists safely to the vessel. The RV Meteor left port on the morning of October 11, passing through the sluice gate that connects the Harbor of Emden with the Wadden Sea, after both the ROV SQUID and all the scientific equipment was safely unpacked and prepared for transit.

For most part of the week from October 12, the ship steamed towards the easternmost of the M167 two study areas, the Alboran Sea. The transit, which started with a somewhat rough crossing of the English Channel, ended on the 17th night with a quiet entrance in the Mediterranean Sea. During the whole week the scientists, which were mostly new to the ship, had the chance to get acquainted with the life on board, laboratories were prepared for the first “core on deck”, science meetings were held daily in the conference room, and the first multibeam profiles were taken in Portuguese EEZ, in order to contribute to the DAM Underway Bathymetry project.

On Sunday the 18th the first station was reached and, due to a calm sea state, two ROV SQUID dives were performed, in order to retrieve the first of three CORK observatories deployed on the seafloor during the M149 expedition (2018). The observatories tasks were to record water pressure and temperature in the boreholes over the years and document the activity of the target structures. Unfortunately, the first dive failed due to an hydraulic problem and on a subsequent deployment the CORK could not be found. After the dive a small COTS-ROV from MARUM was successfully deployed in the water column. This so called “BlueROV” underwent a number of modifications compared to the original product with respect to manipulation, control, etc.; making it a versatile and affordable instrument for shallow seafloor exploration. During the night the Carboneras fault was extensively mapped and a series of interesting Parasound profiles perpendicular to it were produced, showing both ductile and fragile deformation of the sedimentary layers. Taking advantage of the good weather and the perfect sea conditions on Monday the 19th the ROV SQUID was deployed again to look for the missing CORK. The dive was successful with the instrument safely retrieved, and the RV Meteor then steamed away in the direction of the Gulf of Cadiz.

The Gulf of Cadiz was reached on the morning of the 20th but prohibitive weather condition impeded a safe SQUID deployment, therefore several meters of sediments were obtained using the gravity corer (Fig. 4.1). Different mud breccia facies, a typical sediment constituting the main solid emissions of mud volcanoes, were retrieved from different structures of the Moroccan mud volcanic field: Ginsburg, Yuma, Boabdil, and Averroes. For post-cruise gas, fluid and microbiological analyses, the scientists collected numerous sediment and fluid samples immediately after the gravity corer was on deck. In addition, detailed sedimentological descriptions and physical properties analyses were performed onboard. Those sample will be

studied in order to determine the geochemical composition of the porewater, as well as the presence of microbial activity, in an effort to shed some light on the origin of the fluids and the life which they could fuel.

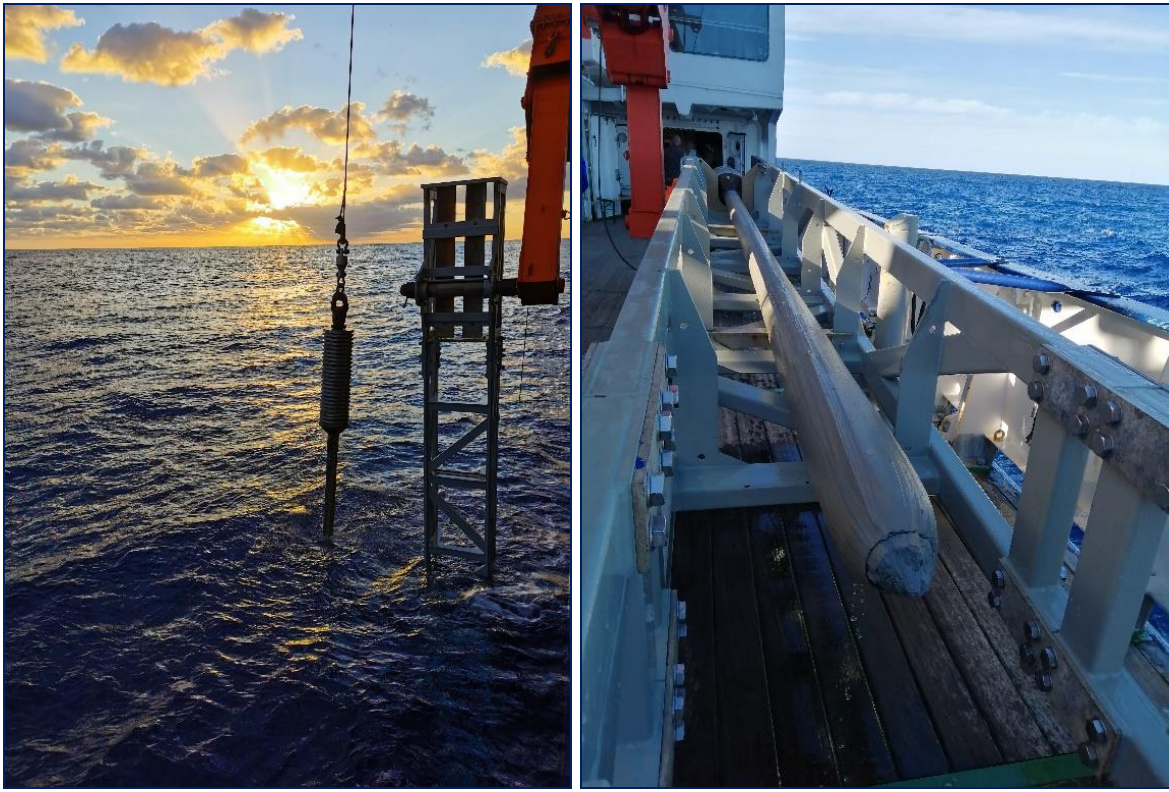


Figure 4.1: a) gravity coring at dawn (Photo: Natasha Morales), b) full recovery of extremely dense mud breccia (Photo: Leonardo Tamborrino)

On the 21st and part of the 22nd the coring continued on different structures, which then proved to be newly discovered mud volcanoes situated in the northern part of the Moroccan mud volcanic field. In the afternoon of the 22nd the wave height $<2\text{m}$ made possible an ROV deployment, concluded with the retrieval of the second CORK observatory, installed on the active Ginsburg mud volcano. On Friday, Saturday and Sunday (23rd, 24th and 25th), complicit the excellent weather, various dives were performed on Ginsburg MV, on the Lineament Center and on a coral mound structure, both with the ROV SQUID and with the BlueROV (this last one for testing purposes). The goal was to produce a 3D Photomosaicking reconstruction of the seafloor on these extremely interesting targets. Meanwhile, coring and surveying various morphological features which proved to be unknown mud volcanoes, circular depressions, diapiric ridges and coral mounds, was also continued between dives. Preliminary assessment of the pore fluids chemistry done onboard suggests widespread freshening on the active mud volcanoes summits, whereas high salinity fluids were sampled in depressed structures possibly related to upward fluid circulation.

At the beginning of the week starting on October 26 the RV Meteor sailed towards the western part of the Gulf of Cadiz, in order to sample some deep-water mud volcanoes (MVs) and a new MV field. The deeper MVs are interesting because they are following the traces of both Lineament South and Center, potentially showing different source fluids/sediments than the bigger expulsion features on the eastern part of the accretionary prism. The samples acquired will thus allow to paint a more complete picture of the Gulf of Cadiz mud volcanism, possibly

revealing key information from the subducting plate. The new MVs field in the Portuguese EEZ was reached on the morning of the 27th, after a night spent by thoroughly mapping the area. Some structures in this area were discovered during the M149 in 2018, but no complete map was done until now. The scientists managed to sample and confirm two of the MVs, but then the winch used for gravity coring broke down, making coring operations unfeasible for the rest of the day.

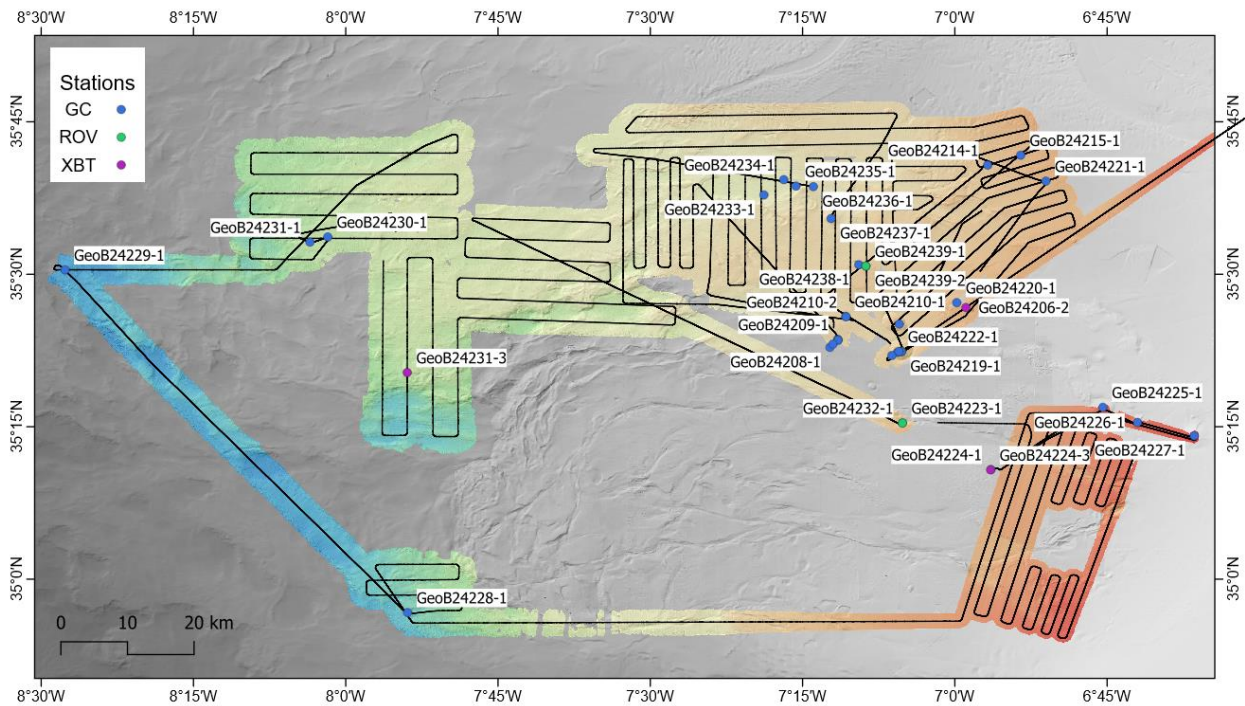


Figure 4.2: Overview of stations and bathymetry/Parasound profiles in the GoC main study area.

Talking advantage of a window of good weather, on the 28th October the vessel headed to the Lineament Center, at the location of the third CORK observatory. Despite a serious hydraulic malfunction which impeded the use of the ROV mechanical arm, the ROV team managed to build an extension for the same arm, making the retrieval of the CORK possible. Unexpectedly, just before arrival on deck, the (flooded) observatory exploded and all its instrumentation got lost in the water column. After that, the scientific program was concluded by coring different structures along the northern boundary of the Southern Lobe. Again, a new MV was discovered and the known Atlas, Student and Jesus Baraza MVs were sampled, showing an amazing variety of mud breccias and confirming once again the extreme variability of these seafloor features in the Gulf of Cadiz (Fig. 4.2).

On the 29th afternoon the ship started the transit towards Emden, reaching its final destination on November 4. The M167 equipment and samples were safely packed during transit and unloaded on November 6, while the scientist disembarked the vessel a day earlier.

5 Methodology and Preliminary Results

5.1 Hydroacoustics (Parasound & Multibeam)

(L. Kramer, D. Duarte; S. Xu)

5.1.1 Introduction and Aim

The hydroacoustic studies onboard R/V METEOR included seafloor mapping and profiling of the uppermost subseafloor sediments. The aim of these studies was to determine gravity coring sites and to identify new mud volcanoes or active/recently active seepage sites. Additionally, their association to tectonic structures (e.g. the SWIM strike-slip faults) has been investigated.

Fluid flow and seepage are expressed in characteristic features both at seabed and in the subsurface. The morphological expression of seepage includes a wide variety of features (Judd and Hovland, 2007), the two most common being mud volcanoes – conical-shaped positive morphological features – and pockmarks – crater-like negative topographic features at the seabed. Evidences for fluid flow in the subseafloor sediments is inferred by the observation of geophysical indicators, such as acoustic blanking, enhanced reflections and gas chimneys or migration pathways. Often, these indicators are observed in association with others resulting from the presence of gas in the water column like acoustic plumes (flares).

For the acquisition of bathymetric and backscatter data the multibeam Kongsberg Simrad systems EM122 and EM710 was used, and for sub-bottom profiling the Atlas Parasound P70. These systems are described in detail below. The cruise preparation relied on bathymetry data that was collected with the EM122 system during the M149 expedition in 2018. The existing maps were expanded and enhanced during cruise M167.

5.1.2 Methodology

5.1.2.1 Multibeam bathymetry and backscatter mapping (*KONGSBERG EM122 and EM710*)

Data Acquisition

Two multibeam systems are available onboard R/V METEOR for bathymetric mapping of the seafloor: the KONGSBERG EM710 for shallow-water and the KONGSBERG EM122 for deep-water conditions. Due to the depths recorded in the study areas – the Gulf of Cadiz and the Alboran Sea - the seafloor surveying was mainly performed with the EM122 system. In the Alboran Sea the EM710 was used in addition to the EM122 to map the seafloor in water depths of less than 700 m.

The EM122 system is a hull-mounted deep water MBES providing accurate bathymetric mapping down to full ocean depth. The system contains two linear transducer arrays in a Mills cross configuration with separate units for transmitting and receiving. The technical specifications of the EM122 system are enumerated in Table 1. The EM122 system used a nominal frequency of 12 kHz with a beam width configuration of 2° (TX) by 2° (RX). For beam spacing the “high-density-equidistant” mode was chosen, which provides 432 independent depth values (soundings) perpendicular to the track for each ping. Using the two-way-travel-time and the beam angle known for each beam, and considering the ray bending due to refraction in the water column by sound speed variations, depth and position are calculated for each beam. A combination of amplitude (for the central beams) and phase (slant beams) is used to provide a

measurement accuracy practically independent of the beam pointing angle. Furthermore, the EM122 system applies the “dual swath” technology: instead of one ping two pings are simultaneously transmitted and recorded, one slightly tilted forward and the second backward. This enables a denser bottom coverage which allows higher survey speeds. For multibeam mapping surveys speeds of 9 to 11 knots were carried out. The Ping Mode was set to Auto, which enabled the system to use CW (continuous wave) pulses in shallow modes and FM or “chirp” pulses in deep modes. es. FM or “chirp” pulses transmit more energy into the water, thus enabling greater ranges of the beams leading to a better across-track coverage of the seafloor particularly at greater depth.

The EM710 is a 0.5° by 1° broadband MBES, operating in the 70 to 100 kHz band. The system was mainly used in water depths less than 700 m. At these depths, it has a better resolution and a wider swath than the EM122. Basic principles are identical to those of the EM122, the differences are: i) a higher sonar frequency which also means considerably smaller transducer arrays, ii) a beam footprint of 0.5° by 1° , iii) a total swath width of up to 140° instead of 150° , iv) the number of beams (256 instead of 288) and v) 400 soundings per ping instead of 432. Further technical specifications and applied settings during the cruise are displayed in Table 5.1.

Table 5.1: EM122 and EM710 technical specifications and settings during M167 on R/V METEOR.

	EM122	EM710
	<i>Technical specifications</i>	
Main operational frequency	12 kHz	100 kHz
Angular coverage sector	150°	140°
Number of beams per swath	288	256
Number of soundings per swath	432	400
Beam width	$1 \times 2^\circ$	$0.5 \times 1^\circ$
Pulse length	1 ms CW to 100 ms FM	0.2 ms CW to 200 ms FM
Depth range	20 - 11000m	20 – 2000 m
	<i>Settings during cruise</i>	
Swath width used	120°	120°
Beam spacing mode	High density equidistant	High density equidistant
Dual Swath mode	Off: Alboran Sea On: Gulf of Cadiz	Off: Alboran Sea
Ping Mode	Auto	Auto
Tilt angle of the transmitted beam array	3°	3°
Used Areas	Area in Interest	Chella Bank (Alboran Sea) Southern Gulf of Cadiz

Using the two-way-travel-time (TWT), the beam angle known for each beam and considering the ray bending due to refraction in the water column by sound speed variations, a seafloor depth is calculated for each beam. Additionally, sound velocity profiles were updated if

a major change in the physical properties of the water column was expected due. These profiles were calculated from several XBT (Expendable Bathythermograph) during the cruise and where either directly applied to the Kongsberg’s acquisition software SIS or used for correcting already collected bathymetric data (Fig 5.1).

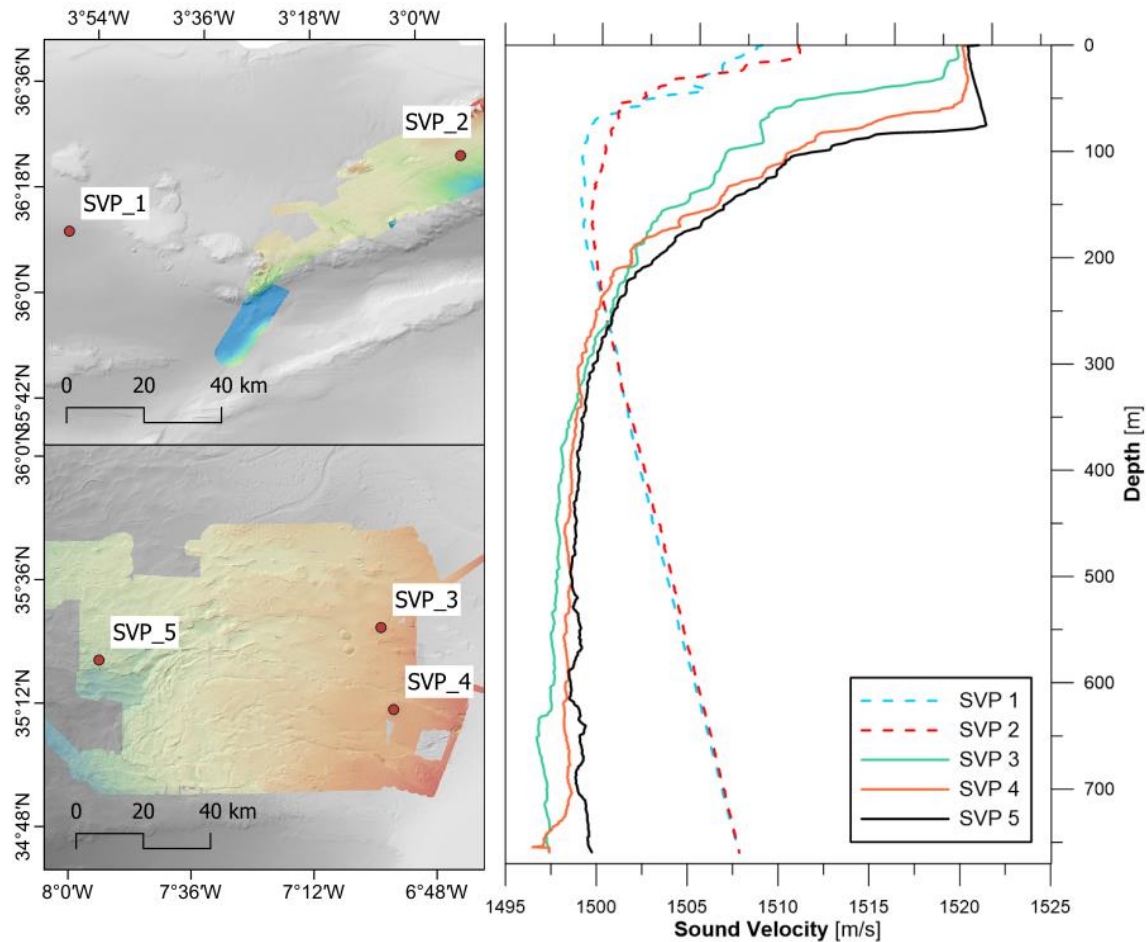


Figure 5.1: Locations and sound velocity profiles of XBT measurements. XBT-1 and -2 were carried out in the Alboran Sea (upper map), whereas XBT-3 to -5 were taken in the Gulf of Cadiz (lower map).

The collected depth data from each sounding also contains the amplitude of the return sound pulse, which is called backscatter data. The backscatter signal depends on the physical nature of the seafloor, orientation of the illuminate surface and the frequency and angle used. Acoustic backscatter data are used for classifying seafloor types: a weak return signal (low amplitude) indicates a soft-bottom substrate, and a strong return signal (high amplitude) indicates a hard-bottom substrate.

Data quality and processing

Monitoring and quality control of the data was conducted with the Kongsberg Seafloor Information System (SIS). The software controls the sector coverage (angle, beam spacing), depth settings (swath mode, ping mode) and transmission control (pitch stabilization). The data was stored every 30 minutes as an *.ALL file with all required information about ship motion, GPS, vessel speed, number of beams, total time, and track.

The multibeam data was post-processed with the MB-System (Caress and Chayes, 1996) and the Generic Mapping Tool software (GMT; Wessel and Smith, 1998). The following steps were carried out:

- Pre-processing and converting the data to editable MB-format using *mbpreprocess*
- Applying SVP with *mbsvpselect* [either collected XBT profiles, or a profile generated by a historical database from the 1982 Climatological Atlas of the World Ocean (Levitus, 1982) using *mblevitus*]
- Applying tide correction by utilising OSU Tidal Prediction Software (OTPS) distribution (volkov.oce.orst.edu/tides/otps.html)
- Manual editing of the data set with *mbeditviz*
- Correcting amplitude (aka backscatter) and sidescan (time series) values based on a function of grazing angle with respect to the seafloor (slope) with *mbackangle*
- Applying the changes to the raw files, creating processed files with *mbprocess*
- Grid the data, using netCDF (GMT) file format (Ryan et al., 2009) via *mbgrid*

Additionally, Global Mapper™ was used during the cruise for on-board geographical data compilation and visualization. The open source geographic information system QGIS was used to generate maps and carry out morphometric analyses.

5.1.2.2 Sub-bottom profiling (TELEDYNE ATLAS PARASOUND PS70)

Data acquisition

The sub-bottom profiler Parasound P70 (Atlas Hydrographic GmbH, Bremen) was operated to provide high resolution information of the uppermost 50-100 m of the subseafloor sediments. This system is a hull mounted parametric echo-sounder which utilizes the parametric effect based on non-linear relations of pressure and density during sonar propagation. Two high intensity waves with frequencies of 18-20 kHz (primary high frequency, PHF) and 22-24 kHz were used to create a secondary high (about 40-42 kHz) and a secondary low frequency (SLF) of about 4 kHz. While the SLF is used for the sub-bottom profiling, the PHF signal can be recorded synchronously to image potential gas bubbles, plankton, fishes or nepheloid layers in the water column. The footprint corresponds to size of about 7% of the water depth due to an opening angle of the transducer array of 4° by 5°. The technical specifications of the P70 system as well as the chosen setting during cruise M167 are enumerated in Table 5.2.

Table 5.2: P70 technical specifications and settings during M167 of R/V METEOR.

Technical specifications	
Depth range	11000 m
Penetration	Max. >200 m
Frequencies	PHF of 18 kHz, adjustable to 18.5-28 kHz SLF of 0.5-10 kHz, SHF of 36.5-48 kHz
Pulse interval	500 ms in shallow waters 1000 ms in deep waters
Pulse length	0.25 ms
Vertical resolution	0.188 m
Number of transducers	128, on a rectangular plate of approximately 1 m ²

Settings during cruise		
Desired SLF	4 kHz (in the Alboran Sea), 3.5 kHz (in the Gulf of Cadiz)	
Pulse type	Continuous Wave with a length of 250 ms	
Pulse shape	Rectangular	
Depth Search Mode	Variable Min/Max Depth Limit	
Window System Sounding Depth	Other / EM122	

Data quality and processing

For the standard operation, a parametric frequency of 4 kHz in the Alboran Sea and 3.5 kHz in the Gulf of Cadiz as well as a sinusoidal source wavelet of 2 periods was chosen to provide a good relation between signal penetration and vertical resolution. The transmission sequence was established as a single pulse mode with manual system depth of the multibeam echosounder EM122 system. The PHF and SLF signal were recorded permanently. The Parastore software was used for the monitoring and quality control of the incoming data. It controls the data recording, processing, and visualization.

All raw data were stored in the *.ASD data format, which contains the data of the full water column of each signal as well as the full set of system parameters. Additionally, the data was recorded in compressed *.PS3 files every 100 mb or 60 min, with the carrier frequency and the necessary geographical coordinates (UTM 29/30 and Lat/Lon).

For further processing the *.PS3 file format was converted utilizing the PS32SGY software developed by H.Keil & V.Spiess, MTU-GeoB, University of Bremen, Germany. During this process, a Time Domain Filter (2 – 6 kHz) and Resampling (Factor 2) were carried out. Furthermore, the envelope of each profile was calculated. The acquired data was imported to the IHS Kingdom Suite for visualization and interpretation. Further data processing included the filtering with a band pass filter to improve the signal-to-noise ratio.

5.1.2.3 Hydroacoustic Data Management

Table 5.3 shows statistics of the conducted hydroacoustic surveys during M167 and illustrates the amount of storage data needed on the cruise.

Table 5.3: Hydroacoustic survey statistics.

Device	EM122	EM710	PS70
Total Time	201 h	14 h	175 h
Total Track Length	2762 km	454 km	2356 km
Raw Data Amount (including water column data for EM122 and EM710)	32.0 GB	8.0 GB	35.6 GB
Processed Data	57.9 GB	7.33 GB	--

5.1.3 Preliminary Results

5.1.3.1 Transit through the Portuguese EEZ

During the transit to the study area, multibeam bathymetry was recorded in the Portuguese EEZ in order to contribute to the DAM Underway Bathymetry project. The data was acquired at ~12 knots.

5.1.3.2 Alboran Sea

Multibeam bathymetry was acquired in the Northern Alboran Sea (Fig. 5.2), in water depths of 96 to 1367 meters. This survey was conducted to investigate the Carboneras Fault, complementing data previously acquired in the area (cruise M149). Parasound profiles (11 km survey, Fig. b dashed line) were also acquired to observe sub-bottom deformation in the fault zone. The Carboneras fault is a NE-SW left-lateral strike-slip fault zone that extends from the onshore to the Alboran Sea basin (Rutter et al., 2012). It has been active since Late Miocene.

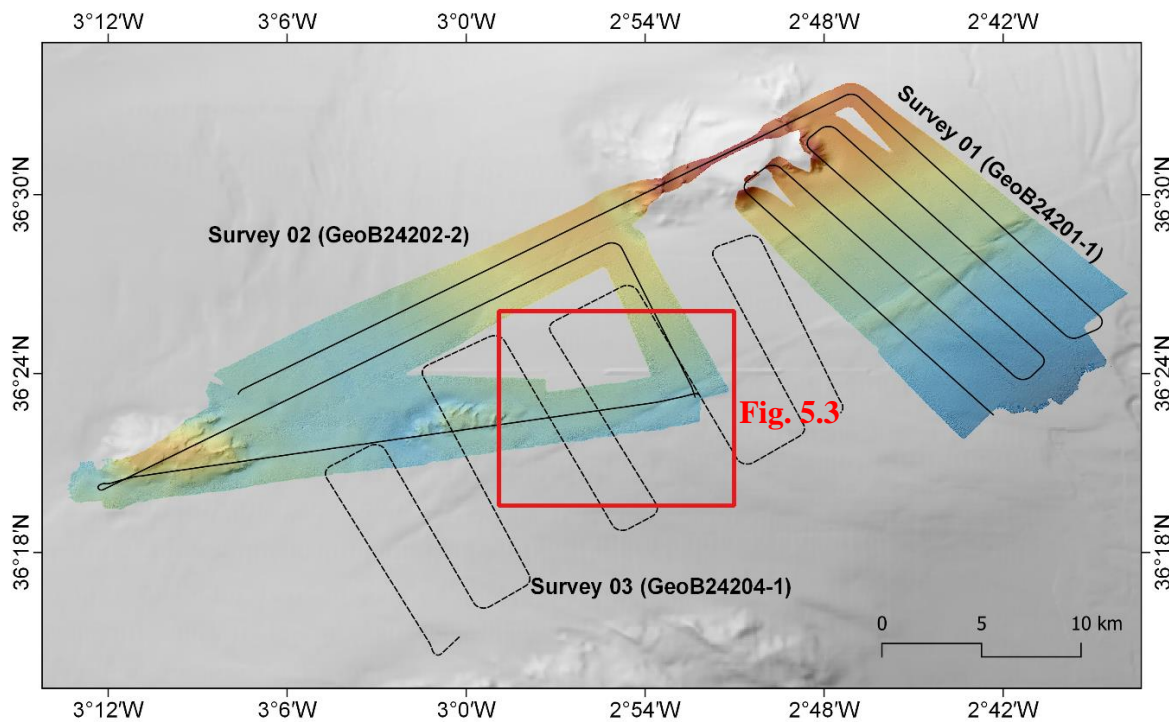


Figure 5.2: Multibeam bathymetry and tracks of the sub-bottom profiles acquired in the Alboran Sea during the M167 ALBOA II cruise. The red box shows the image section shown in Fig. 5.3.

In the bathymetric data acquired during cruises M167 and M149 (Hüpers et al., 2018), the seafloor expression of the Carboneras Fault extends for ~40 km. In the NE area of the fault, a upwarped region of the seabed is observed, delimited by two semi-parallel lineaments (Fig. 5.3). In the Parasound profiles, the fault corresponds to an uplifted area where ductile and fragile deformation are observed (it could possibly be related to the upper section of a positive flower-structure). To the SW, only one lineament is observed at the seafloor, marking a change of depths. The fault zone separates well-stratified parallel and continuous reflections of a 60 ms to 80 ms TWT sedimentary sequence.

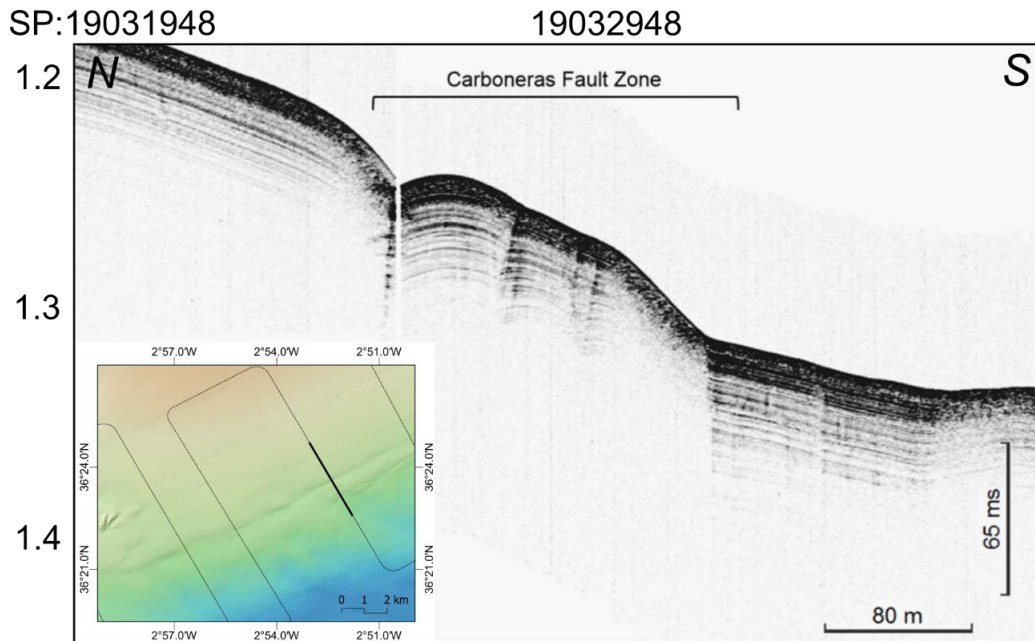


Figure 5.3: NNW-SSE trending sub-bottom profile crossing the Carboneras Fault zone. Small bathymetric map showing survey tracks and the location of the PS section.

5.1.3.3 Gulf of Cadiz

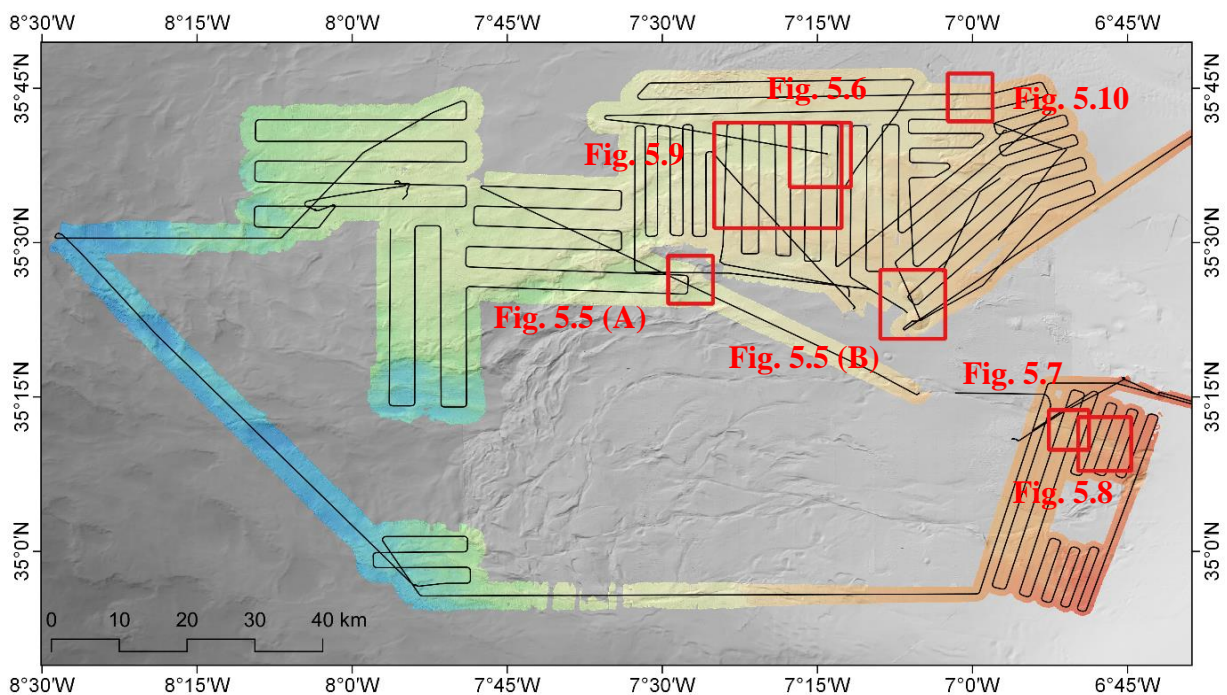


Figure 5.4: Multibeam bathymetry and tracks of the sub-bottom profiles acquired in the Gulf of Cadiz during the M167 ALBOA II cruise. The red boxes show image sections shown in Figs. 5.5 to 5.10.

Several multibeam bathymetry and Parasound surveys were collected in the Gulf of Cadiz accretionary prism (Fig. 5.4), in water depths from 414 to 2444 meters. These surveys were integrated with data previously acquired in the area, during the M149 expedition. The aim was to investigate the existence of previously unknown mud volcanoes and study in more detail other structures that deform the present-day seafloor (e.g. diapiric ridges, circular depressions, and strike-slip faults).

Mud Volcanoes

The existence of mud volcanoes (MVs) is well-known in the Gulf of Cadiz (e.g. Pinheiro et al., 2003; Hensen et al., 2007). During the M167 surveys, several MVs were identified both in the bathymetric and the Parasound data, including previously known ones (e.g. Atlas, Jesus Baraza, Student, Yuma and Ginsburg MVs) and multiple unknown MVs (Fig. 5.4). Of those, eight have been confirmed through the recollection of mud breccia sediments (see “Sedimentology” chapter).

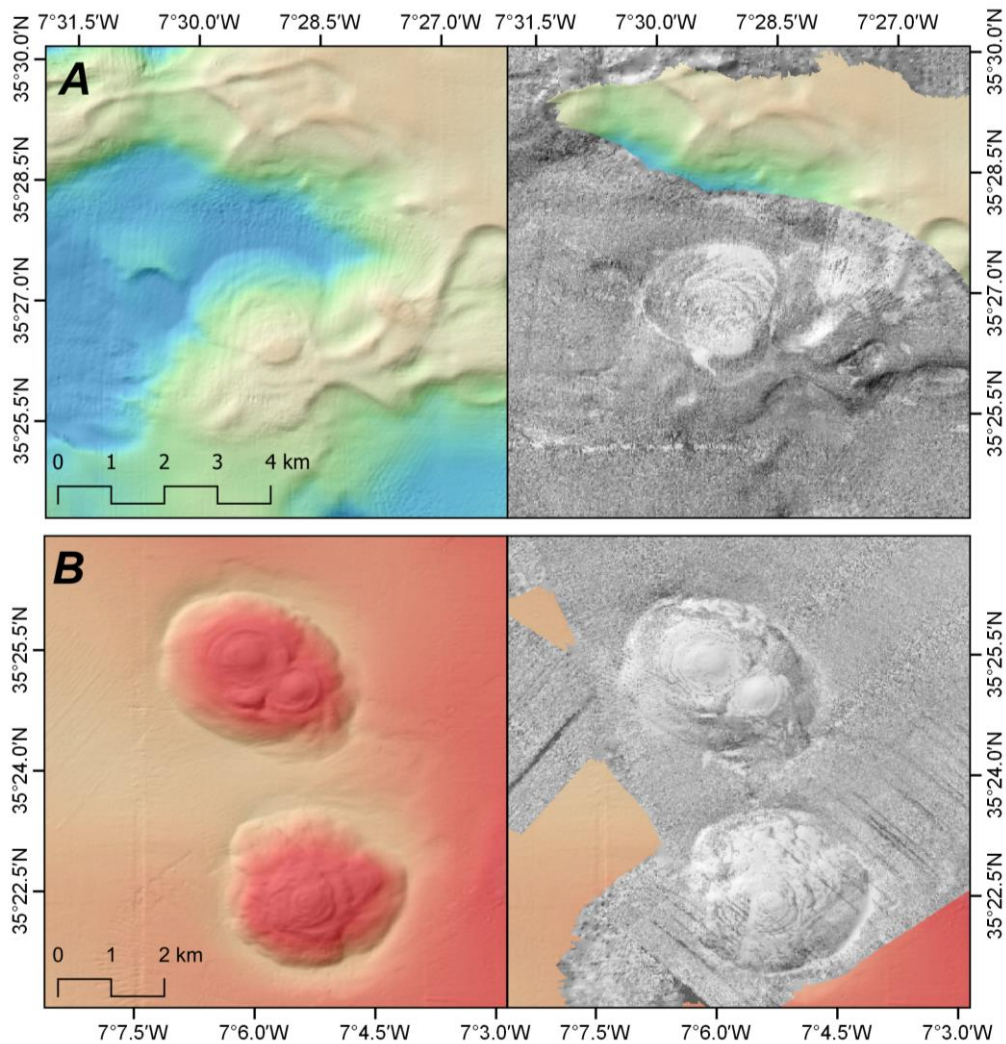


Figure 5.5: Bathymetric and backscatter maps of the El Cid MV (A) as well as the Ginsburg and Yuma MVs (B), in the Central Gulf of Cadiz.

In the bathymetric map, mud volcanoes can be recognised as positive reliefs with a circular to sub-circular shape and cone-shaped profile. Additionally, associated mud flows (e.g. El Cid MV; Fig. 5.5), a depressed area around the structure rim (e.g. Ginsburg MV; Fig. 5.5) and terraces (e.g. Jesus Baraza MV; Fig. 5.6) can be recognised in the bathymetric map as well as in the backscatter map. In the Parasound profiles, MVs are characterized by a cone-shaped structure with transparent seismic facies (Fig. 5.6), cutting through parallel and continuous sedimentary deposits. In some cases, it was possible to observe the mud volcanoes characteristic “Christmas tree” structure, with transparent acoustic lenses interspersed with parallel, laminated sedimentary layer being observed in the flanks of the MV cone (Fig. 5.6).

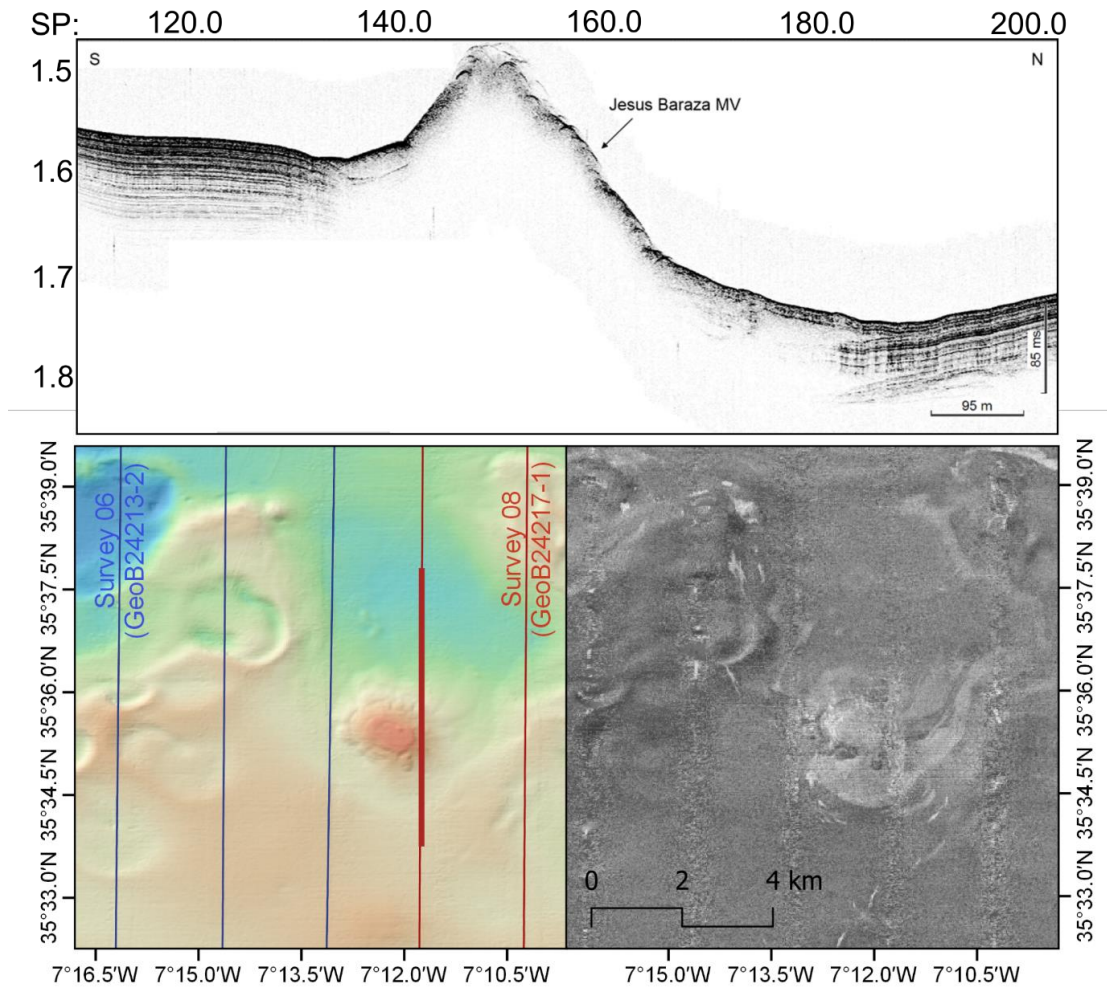


Figure 5.6: N-S Parasound profile crossing through the Jesus Baraza Mud Volcano, in the Central Gulf of Cadiz, as well as the bathymetric and backscatter map of the area, surrounding the mud volcano.

Strike-slip faults

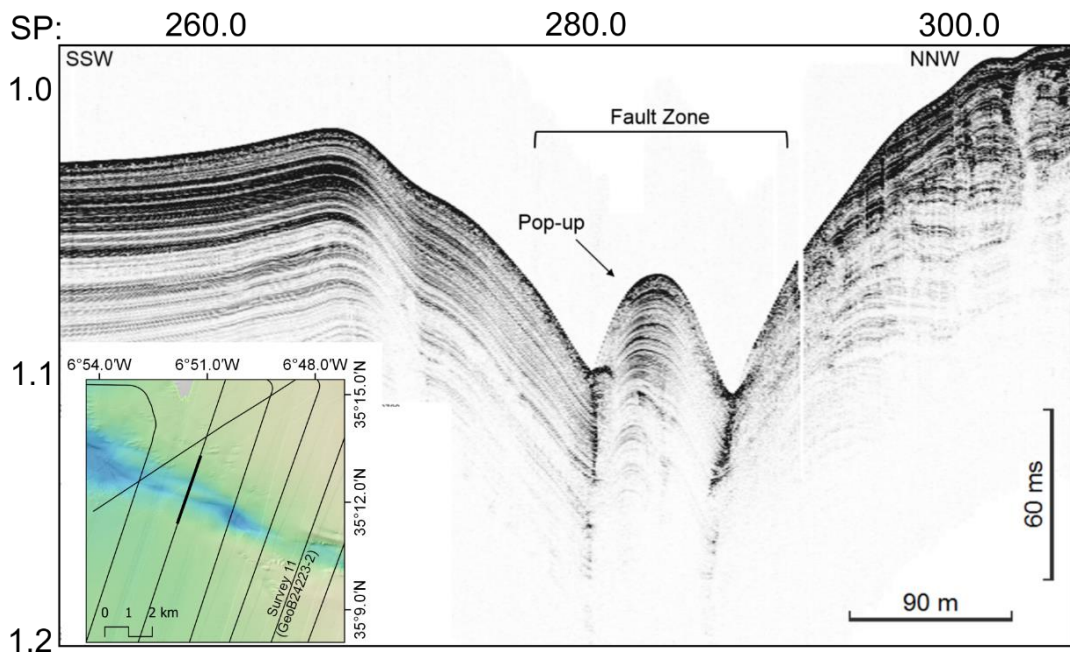


Figure 5.7: NNE-SSW Parasound profile showing a transpressional section of the northernmost fault zone. Small bathymetric map showing survey tracks and the location of the Parasound section.

On the Moroccan Margin, two semi-parallel NW-SE strike-slip faults are observed in the bathymetric map (Fig. d). These features are part of the SWIM lineaments, that can be traced all along the Gulf of Cadiz accretionary wedge (e.g. Zitellini et al., 2009). The southernmost fault shows an important branch with ENE-WSW orientation (Fig. 5.4).

Transpressional and transtensional zones are observed along the faults, characterised by pop-up structures and sigmoidal-shaped pull-apart basins, that are observed in the bathymetric map and the Parasound profiles (Fig. 5.7).

Coral Mounds and Contourite Features

Several cold-water coral mounds were identified in the bathymetric map (Fig. 5.4), integrating the known coral mound province in the Moroccan margin (Hebbeln et al., 2019 and references therein). In the Parasound profiles, they are characterised by circular to oval or vertically elongated shapes with transparent facies (Fig. 5.8). Exposed and buried corals were observed during the surveys (e.g. Fig. 5.8), suggesting several mound formation episodes.

Commonly, coral mounds were observed near contourite drifts (Fig. 5.8). These deposits exhibit aggradational sheeted geometries at the base, evolving upward into mounded geometries. Internally, they are characterised by well-stratified, laterally continuous, medium to high amplitude reflections. Internal discontinuities are also observed, marked by toplap terminations on the underlying strata and/or downlap terminations on the overlying strata.

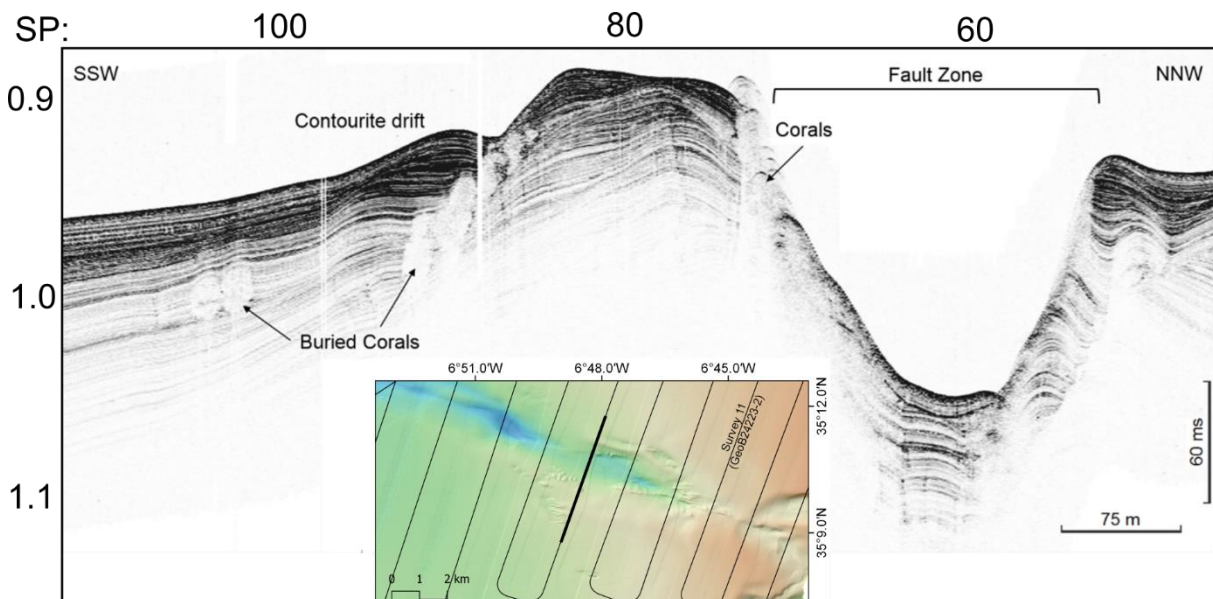


Figure 5.8: NNE-SSW Parasound profile showing buried and exposed cold-water corals, developed in close relation with contourite drifts. To the NNW of the profile the northernmost strike-slip fault is observed (pull-apart basin), with corals developing on its flanks. Small bathymetric map showing survey tracks and the location of the PS section.

Other structures

In the proximity of Lineament North, three main morpho-bathymetric areas are observed (Figs. 5.4, 5.9, 5.10):

Diapiric ridges and circular or sub-circular depressions Sector

Elongated diapiric ridges, with various orientations, deform the present-day seafloor by folding the overburden sediments (Fig. 5.4). These features seem to form a network of ridges,

that occasionally encase the depositional strata. In the Parasound profiles, salt bodies are characterised by transparent facies, topped by chaotic reflectors or by folded semi-parallel sedimentary strata. Circular to sub-circular depressions are observed in this sector (Fig. 5.9), characterised by chaotic to transparent seismic facies at their base. These were interpreted as mass transport deposits (MTDs), related to diapiric vertical migration on the subsurface, which created steep slopes on the seabed and, therefore, caused instability and the formation of MTDs.

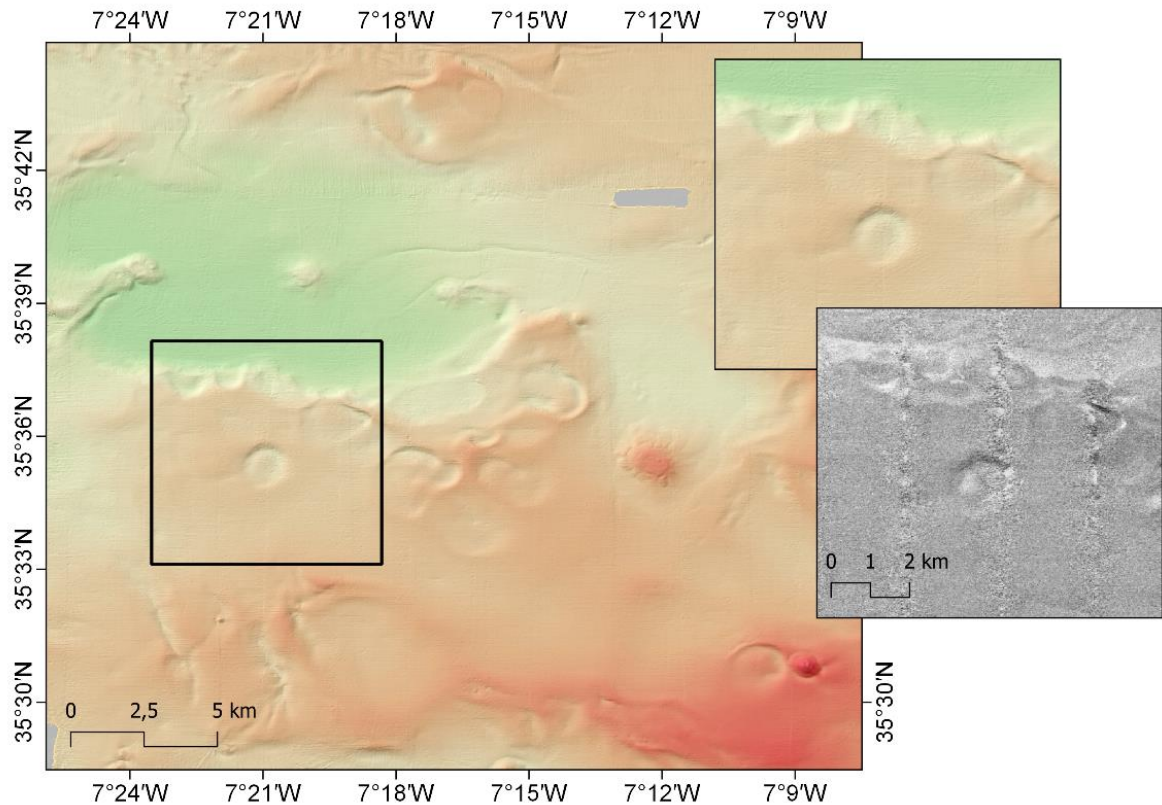


Figure 5.9: Bathymetric and backscatter maps of an area showing sub-circular to circular depressions and diapiric ridges in the Central Gulf of Cadiz.

Gentle Seafloor Sector

The gentle seafloor sector is covered by a chaotic facies deposit (Fig. 5.9), that is locally channelised and pierced by mud volcanoes and was also interpreted as MTDs. The sedimentary strata below this MTD is not visible in the Parasound profiles (Fig. 5.10).

Rough Seafloor Sector

In this sector, the seafloor is characterised by a sequence of semi-parallel highs and lows (Fig. 5.4). Diapiric ridges and erosive channels are also observed in the area (Fig. 5.4). In the Parasound profiles, medium to high amplitude, continuous reflections are observed (Fig. 5.10). These deposits are often folded, partially showing transparent facies (Fig. 5.10). On its base, transparent to chaotic facies can be recognised (Fig. 5.10), which probably correspond to salt or muddy deposits. This complex geometry was interpreted as resulting from gravitational gliding of the sedimentary strata above a mobile layer of salt or mud.

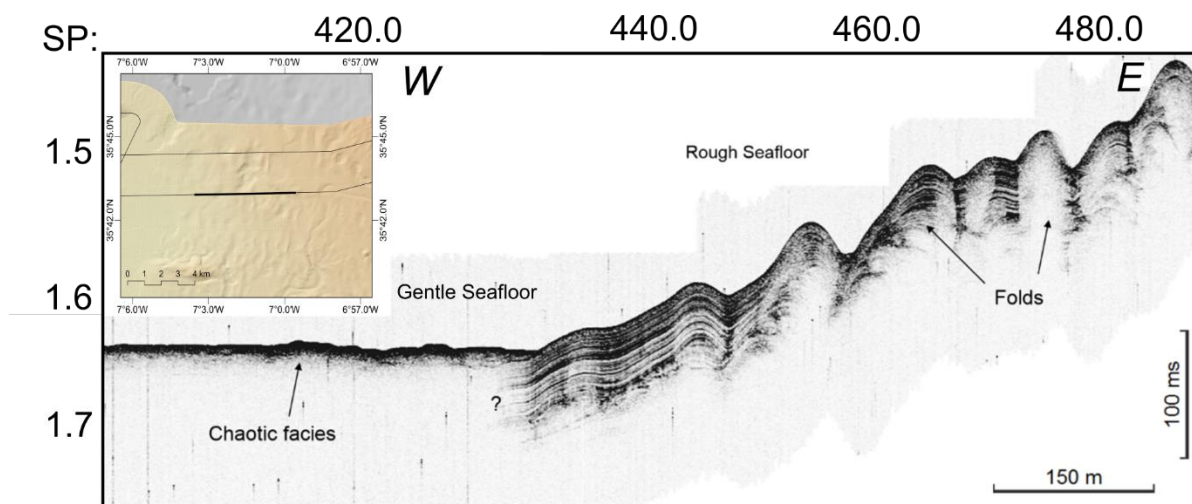


Figure 5.10: W-E Parasound profile showing the chaotic facies and folding observed in the Gentle and Rough Seafloor Sectors. Small bathymetric map showing survey tracks and the location of the PS section.

5.2 Sediment Sampling & Sedimentology

(L. Tamborrino, N. Morales, J. Zhang, T. Fleischmann, S. Krupiński, W. Menapace)

5.2.1 Introduction

One of the main objectives of expedition M167 was to sample sediments from active faults and mud volcanoes in the Gulf of Cadiz (Atlantic Ocean). Seafloor sampling was conducted with a gravity corer (GC), from which a total of 26 cores from 24 working stations (Fig. 5.15) were retrieved, covering about 55,55 m of sediment material from water depths ranging between 211 m and 2276 m. The complete station list for sediment samples can be consulted in Table 5.3.

5.2.2 Methodology

Sediment sampling

The coring activities started on 20.10.2020 at 11:14 (UTC) on the Ginsburg MV (35°22.300'N, 7°05.651'W) and finished on 29.10.2020 at 10:13 (UTC) on the Student MV (35°30.799'N, 7°08.754'W). A gravity corer (GC) with a core barrel length of 5,75 m or 4,5 m and a weight of 1.5 tons were deployed to recover sediment sequences. The device was lowered to the seafloor at a constant velocity of 1 m/s and the obtained cores were collected with solid plastic liners of 12 cm diameter. The positioning of every deployment was supported by a Posidonia transponder installed at 50 m distance from the core barrel on the GC cable.

Once on board, the liner was removed from the barrel, cut into 1-m sections and closed with caps on both ends (Fig 5.11a). Each section was labelled according to the GeoB numbering system used by the University of Bremen for sampling, storage and data management purposes (Fig. 5.11b).

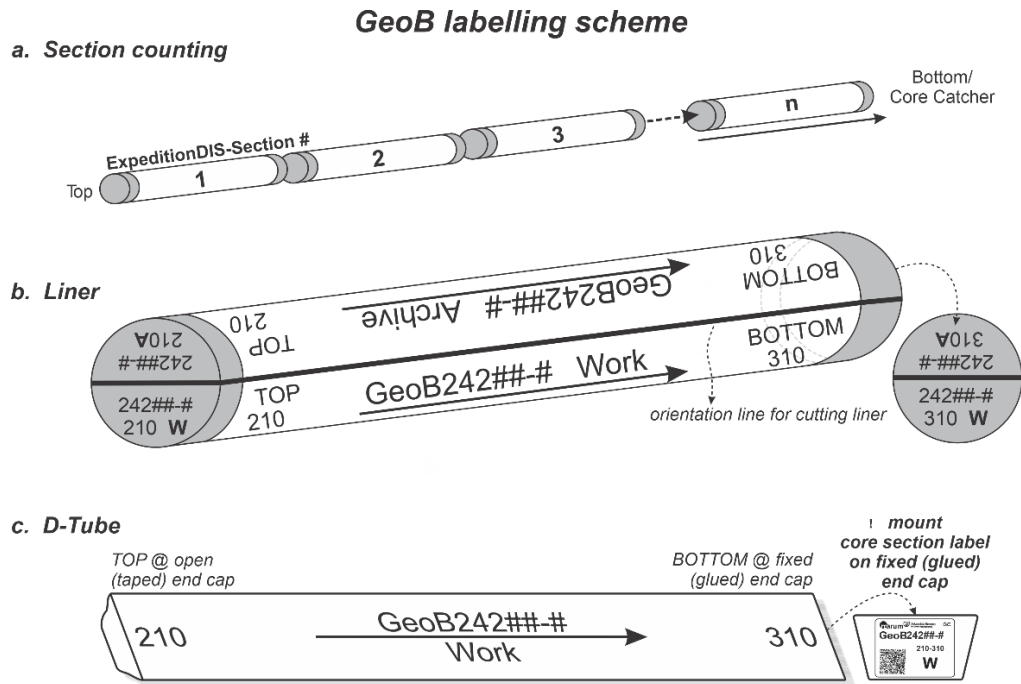


Figure 5.11: GeoB labelling scheme (modified from MARUM chief scientist guidelines)

On the whole round sections (WR) sampling of head space gas (HS) was conducted immediately after each section was cut on deck. 3 cm holes were drilled into the liner in order to take additional gas samples (see “Geochemistry” chapter)

Subsequently, all the cores were split lengthwise and divided into working (W) and archive (A) halves. The working halves (W) were used to take samples for shipboard and post-cruise measurements such as pore water (IW), physical properties (WC), and sediments (BAG). Archive halves (A) were used for sedimentological investigations including core descriptions and Line Scanner imaging. After the necessary samples were taken and the description and imaging were finished, both halves were packed in D-Tubes (Fig. 5.11c) and then stored in the ship’s cooling room at 4°C in order to maintain seafloor temperature. At the end of the expedition, the collected station and sample information saved in the ExpeditionDIS database system was compiled for curation and the sediment cores were transported back to Germany and stored in the MARUM Core Repository at the University of Bremen.

A push corer device - here PC (20 cm length and 8 cm diameter) - deployed by the ROV SQUID was also used to recover sediment material, which was mostly sampled for microbiology, pore water and gas analyses.

Sediment core description

Detailed core descriptions were done onboard for each section using visual core description sheets (VCD) from the MARUM (GeoB) protocol and then transferred and digitized into composite graphical lithologs. The sedimentary description was made following the conventional IODP convention and included grain size, color, sedimentary fabric and primary structures, presence of fossils or fauna, bioturbation and/or coring disturbance, identification of paleo-redox fronts, presence of gas hydrates, authigenic minerals such as sulphides or carbonates, organic matter-rich sediments, etc. The color designation (hue, value and chroma) of the cored material was determined visually using the Munsell Soil Color Chart (Munsell Color Co., 1975). All core descriptions are provided in the Appendix 10.11.

Sediment core imaging

After being described, all core sections were imaged using the smartcube® Camera Image Scanner SmartCIS 1600LS line scanning system of the MARUM GeoB Core Repository (www.marum.de/en/Infrastructure/GeoB-smartCIS-1600-Line-Scanner.html) to obtain a more detailed graphical analysis of the cores that complement the visual core description (Fig. 5.12).

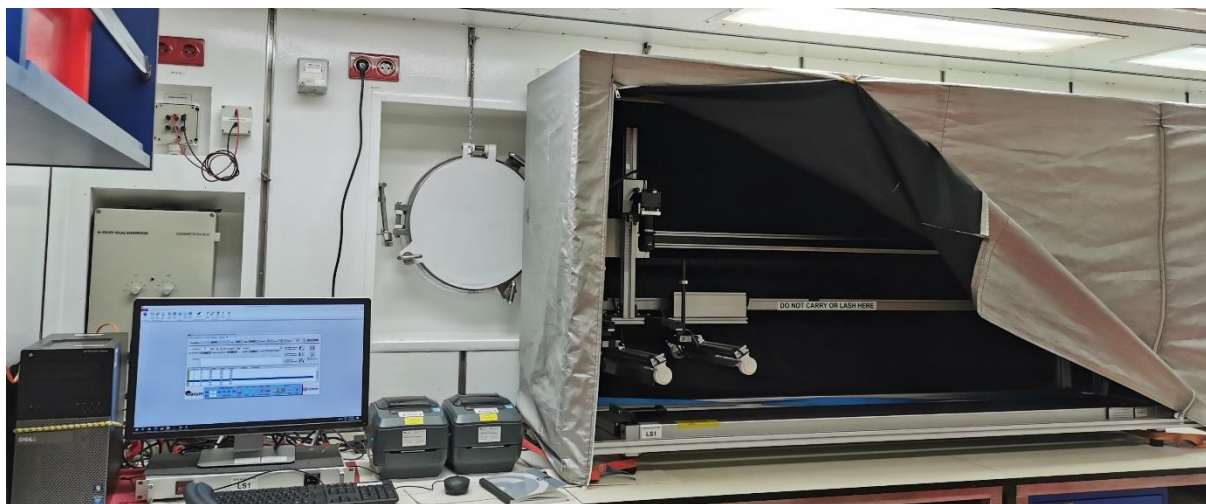


Figure 5.12: Assembled Line Scanner in the Universal Laboratory on board the RV Meteor

Split surfaces of each section were freshly scraped immediately prior to imaging in order to capture the ephemeral nature of sedimentary features, as the sediment can oxidize in a short time span. All images were acquired at a standard resolution of 500dpi. In order to retain the relative variability in sediment lightness throughout the expedition, the camera aperture was fixed at f/8. This aperture setting imaged most sediments without the need for further adjustment. All sections were scanned with a camera height of 29 cm, which is ideally suited for gravity cores. Two light sources were used to improve lighting condition and reduce potential shadow effects on rough surfaces.

A white calibration of the system was carried out daily, using a standardized white tile. Absolute color reproduction of the scanned images is ensured through the automatic application of an IT8.7/2-target referenced ICC-profile, built in the steering software of the line scanner. Section images were directly saved to the ExpeditionDIS database system as JPEG files. Output also included a tab-delimited text file with red, green, blue, lightness (%) values as well as red/blue ratios in 1 mm down-core resolution for each section. Line scan images are compiled into lithologs and provided in the Appendix 10.11, with their respective visual core descriptions (VCD).

5.2.3 Preliminary Results

A total of 32 gravity cores were collected from MVs on the Atlantic Moroccan margin, linked to the accretionary wedge of the Gulf of Cadiz. The total sediment recovery is 55.55 m corresponding to the 32.49 % recovery considered the gear length deployed (Tab. XX). Sampling was carried out to collect or update information on the processes related to known MVs (Ginsburg, Averroes, Boabdil, Yuma, Gemini II, Al Idrisi, Atlas, Student, Jesus Baraza, Fiuza), as well as checking the mud volcanism activity of potential MVs detected by MBES during the M167 cruise (Marie Tharp, Goldberry, Maria Bianca Cita, Isengard, Gondor, El

Profesor, Tokyo, EUMR). Empty gravity corer was collected in 6 stations, although in two cases, sediments on the external surface of the GC pipe were indicative of mud volcanism and fluid seepage (respectively, GeoB24220-1, GoldBerry MV, and GeoB24235-1, pockmark E of Atlas MV). On three occasions, we recovered a bent pipe with a relatively small sediment recovery (up to 100 cm).

Table 5.3: Basic information of the gravity cores collected during the M167 cruise. In parenthesis are the names proposed for the new MVs discoveries.

GeoB number	Site	Gear length	Recovery	Main sedimentology
GeoB24206-1	Summit Ginsburg MV	575	255	Hemipelagic sediment on top of mud breccia
GeoB24207-1	W flank Ginsburg MV	575	360	Mud breccia
GeoB24208-1	Pockmark SW Averroes Mv	575	369	Mud breccia
GeoB24209-1	Averroes MV	575	100	Mud breccia
GeoB24209-3	Averroes MV	450	61	Mud breccia
GeoB24210-1	Boabdil MV	450	46	Mud breccia
GeoB24210-2	Boabdil MV	450	69	Mud breccia
GeoB24211-1	Yuma MV	450	225	Mud breccia
GeoB24212-1	Averroes MV	450	0	Empty
GeoB24213-1	Background pockmark	450	416	Hemipelagic sediment
GeoB24214-1	Pot. MV #1 N of Tangier MV (M. Tharp MV)	450	215	Mud breccia
GeoB24215-1	Pot. MV #2 N of Tangier MV	450	0	Empty
GeoB24215-2	Pot. MV #2 N of Tangier MV	450	0	Empty
GeoB24219-1	Ginsburg MV	575	129	Mud breccia
GeoB24220-1	Pot. MV W of Al Gacel (Goldberry MV)	575	0	Empty, but H ₂ S smell on GC pipe
GeoB24221-1	Pot. MV #2 N of Tangier MV (M.B. Cita MV)	575	430	Hemipelagic sediment with H ₂ S smell (buried MV)
GeoB24222-1	Ginsburg MV	575	241	Mud breccia
GeoB24225-1	Gemini II MV	575	274	Mud breccia
GeoB24226-1	Fiuza MV	575	161	Mud breccia
GeoB24227-1	Al Idrisi MV	575	67	Mud breccia
GeoB24228-1	Pot. MV#1 Lineament South (Isengard MV)	575	65	Mud breccia
GeoB24228-2	Pot. MV#1 Lineament South (Isengard MV)	575	0	Empty
GeoB24229-1	Pot. MV#3 Lineament Center (Gondor MV)	575	343	Hemipelagic sediment with H ₂ S smell (buried MV)
GeoB24230-1	Pot. MV#1 New MVs Field (El Profesor MV)	575	31	Hemipelagic sediment with H ₂ S smell (buried MV)
GeoB24231-1	Pot. MV#1 New MVs Field (Tokyo MV)	400	266	Hemipelagic sediment (buried MV)
GeoB24233-1	Plain SW Atlas MV	575	145	Hemipelagic sediment
GeoB24234-1	Atlas MV	575	272	Hemipelagic sediment on top of mud breccia
GeoB24235-1	Pockmark E of Atlas MV	575	0	only CC - hemipelagic sediment with H ₂ S smell
GeoB24236-1	Pot. MV E of Atlas MV (EUMR MV)	575	241	Mud breccia
GeoB24237-1	Jesus Baraza MV	575	132	Mud breccia
GeoB24238-1	Depression W of Student MV	575	433	Hemipelagic sediment
GeoB24239-1	Student MV	575	209	Mud breccia

Four main types of sediment were detected in the GCs collected during the M167 cruise (Fig. 5.13). Brownish slightly-bioturbated silty mud with a variable content of sandy particles

and carbonate material (likely nannofossil ooze with foraminifera) has been detected in the relatively long GCs collected in the plain area for sampling background sediments for geochemical purposes (GeoB24413-1, 24433-1 and 24438-1). No evident bedding and coarsening/fining of the grain size leads to classifying these deposits as hemipelagic sediments. However, nodules and layers of fine sand occur in one core (GeoB24438-1) but are related to bioturbation. Gray silty mud in anoxic conditions (strong H₂S) covered by variable oxidized sediments was collected on an MV-like structure and were interpreted as buried MV facies. The buried MV facies is composed of hemipelagic sediments and/or material re-suspended from mud breccia, likely affected by circulation of reducing fluids from the underlying mud breccia). Unique anoxic silty mud sediments, characterized by H₂S smell and inferred gas hydrates, were sampled in an active pockmark close to Ginsburg MV (GeoB24408-1). Greenish-gray mud breccia with polygenetic clasts represents the most common sedimentological facies encountered in the GCs recovered during the M167 cruise.

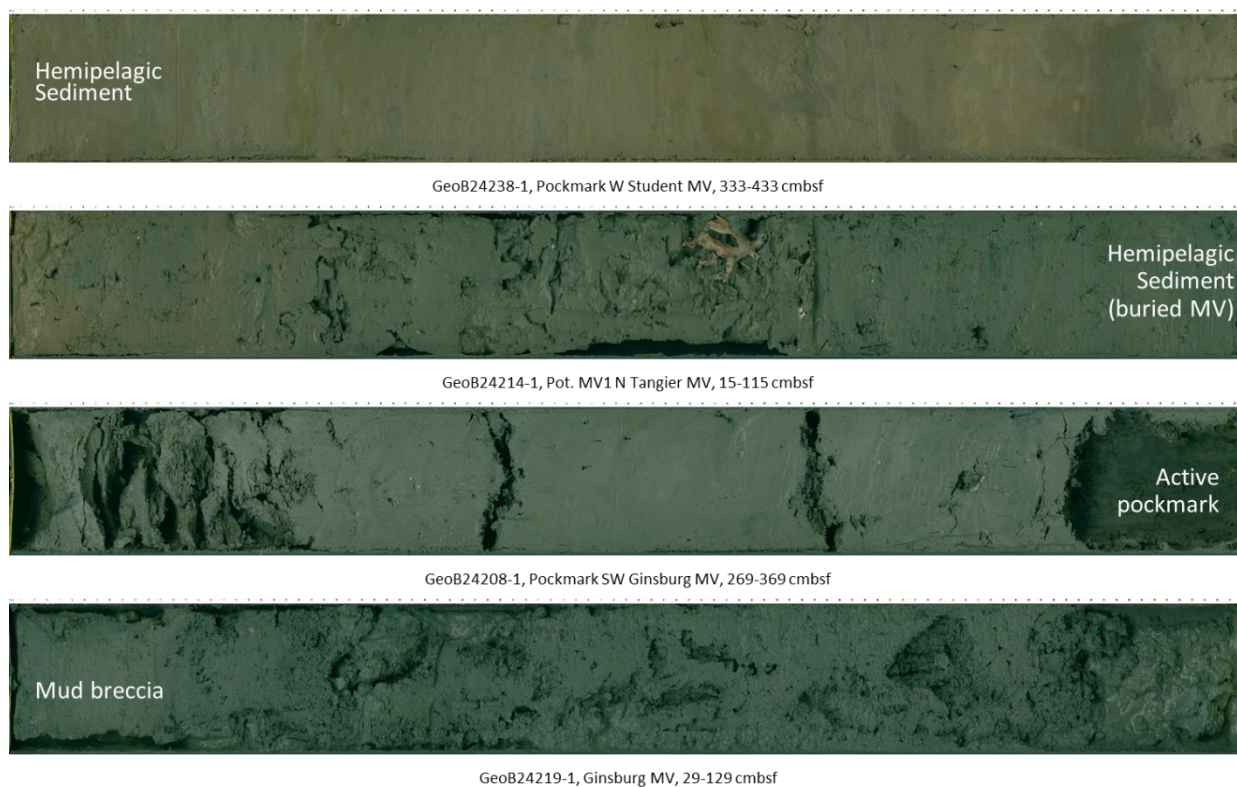


Figure 5.13: Gravity core sections representative of the main different sedimentological facies encountered in the sediment samples collected during the M167 cruise.

The sedimentological variability among the mud breccias has been qualitatively outlined into four main types of mud breccia, although small details can be observed among the different MVs (Fig. 5.14). The large number of GCs collected on the Ginsburg MV allow to describe the most generic features of the mud breccia from the MVs of the Gulf of Cadiz. The Ginsburg-type is made by greenish gray matrix with polygenetic breccia (mostly $\phi \sim 0.3$ cm), H₂S smell and sparse sub-cm mud clasts. In some MVs (Fig. 5.14), the mud breccia can be extremely stiff, with decompression cracks, indicative of a rheological nature derived from reduced water content and/or clay composition. A mud breccia with high water content, moussy texture and a large amount of the 0.3-0.5-cm-like clasts in a grey matrix was uniquely recovered in Jesus Baraza

MV. Similar to Jesus Baraza MV, the mud breccia from Al Idrisi MV has a large content of clasts ($\phi \sim 0.4\text{-}0.8\text{ cm}$), although immersed in a more greenish-like mud.

A layer of variable thickness of yellowish-brownish oxidized water-saturated sediments covers all the mud breccias. In few cases, the mud breccia hosts large bioclasts, including fragments (rubble to frameworks) of cold-water corals (mostly *L. Pertusa*). Variable can be the water content and the stiffness-compactness of the mud breccia, which generally decrease and increase with depth, respectively.

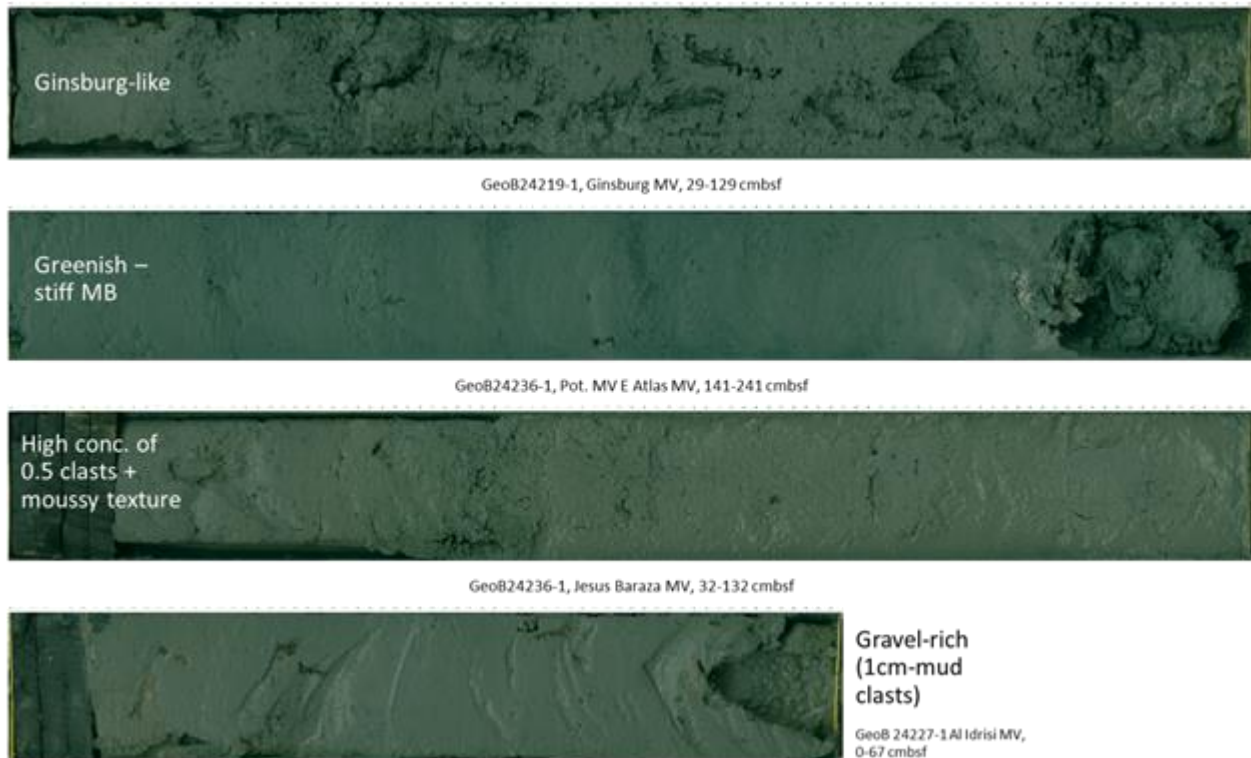


Figure 5.14: different kinds of mud breccias identified from the GCs collected in the Gulf of Cadiz during the M167 cruise. Abbreviations: MV, mud volcano; MB, mud breccia

Variability of mud breccias from different mud volcanoes is highlighted by the spatial distribution of the GCs sampled. Greenish gray mud breccia with a strong H_2S smell is related to the shallow MVs (Gemini II, Fiuza, Al Idrisi). These shallow MVs are characterized by moussy texture, presence of (authigenic) carbonate-rich layers and relatively large clast. This makes these MVs considered relatively active MVs, as well as Jesus Baraza MV. Failed and short gravity cores from Boabdil and Averroes MVs are potentially indicative of the occurrence of large clasts and/or compacted mud breccia in the near-shallow seafloor. Deep MVs like El Professor and Tokyo present exclusively the buried MV facies. MVs located on the Lineaments (South and North, respectively), like Isengard and Atlas MVs present a similar very cohesive mud breccia, although these two MVs are geographically quite distant. M. Tharp and M.B. Cita MVs have a similar composition to the Ginsburg-like mud breccia, but they are characterized by a conspicuous amount of cold-water coral fragments.

Detailed information on the gravity cores collected in the M167 cruise is described in the visual core description in Appendix 10.11. Metadata information of the gravity cores is reported in the station list.

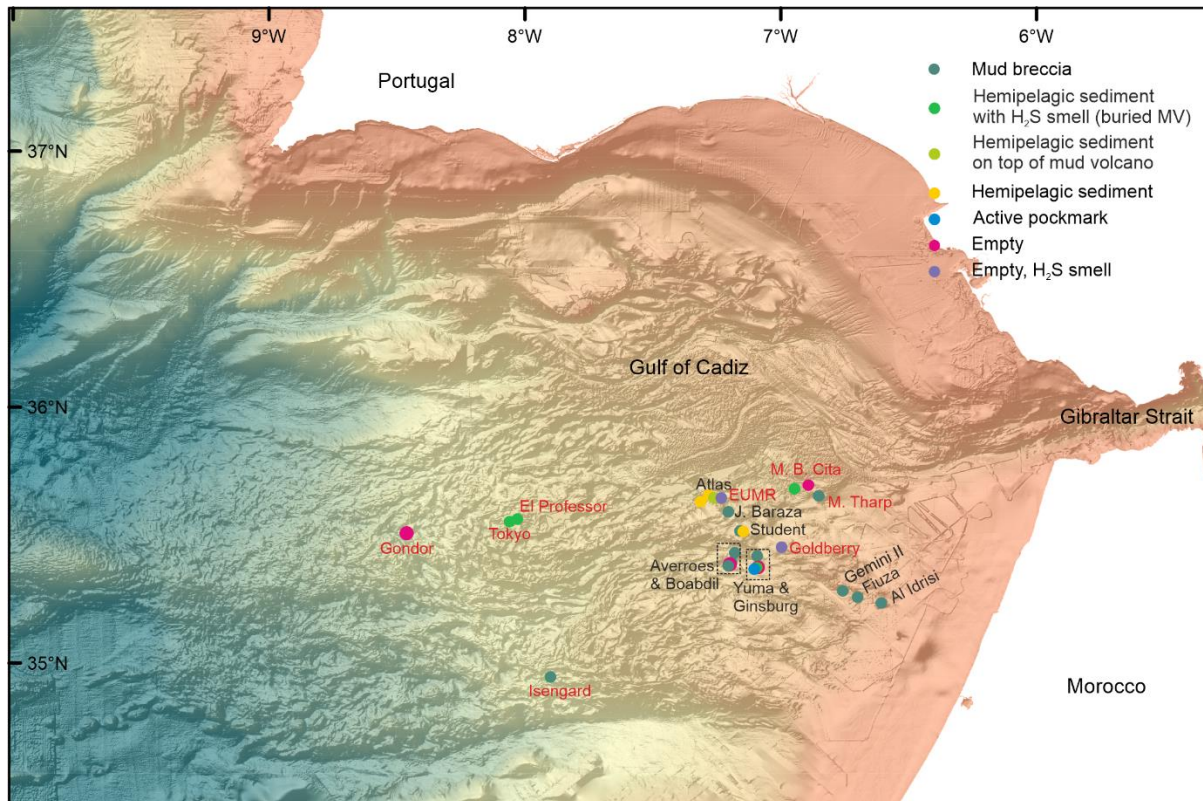


Figure 5.15: Distribution of the GCs collected in the M167 cruise, labelled by MV names (black, known MVs; red, discovered MVs). Color of the symbols utilized for the GC location are indicative of the main sedimentological facies (see legend).

5.3 Physical Properties

(J. Zhang, S. Xu)

5.3.1 Methodology

Physical properties are indicators of composition and environmental conditions, thus providing important constraints on characterization of sediments and rocks. Therefore, basic physical properties such as moisture and density (MAD) and thermal conductivity were measured during cruise M167.

MAD measurements were conducted on working halves of gravity cores and used to determine water content, wet and dry bulk density, grain density and porosity. Two specimens were sampled per meter. The measurements and calculations follow Blum (1997) and include a salt correction.

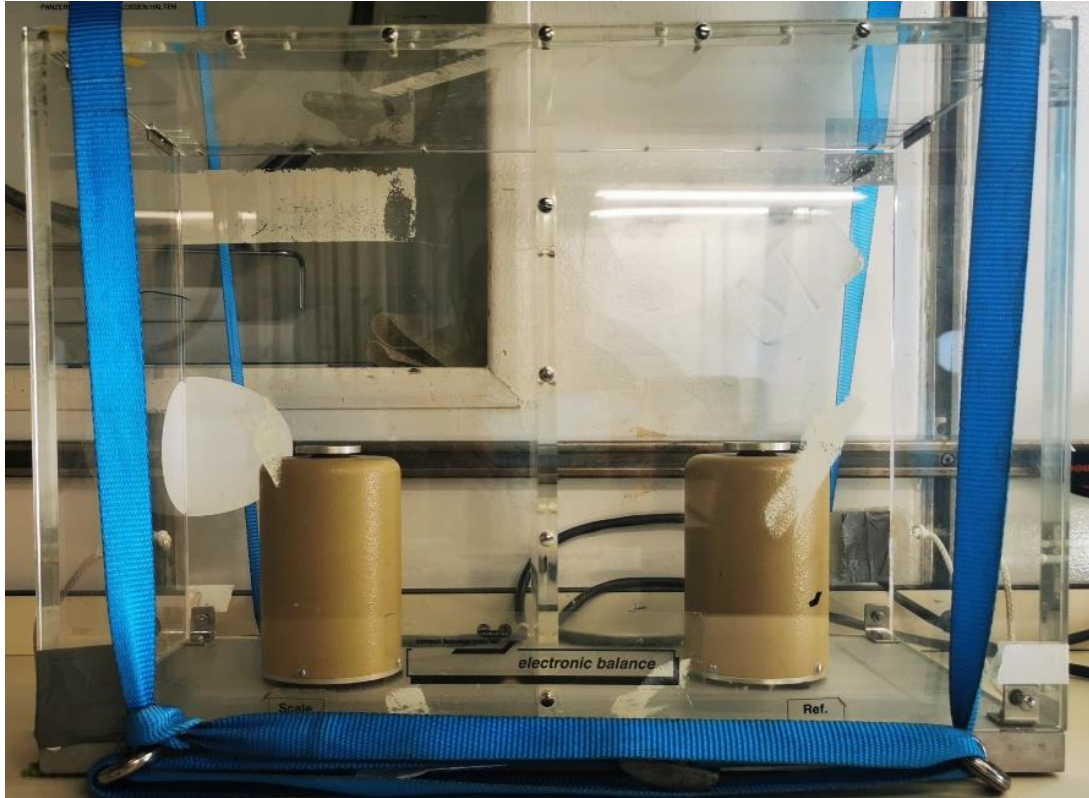


Figure 5.16: The motion-compensated paired balance system for onboard mass measurements.

A motion-compensated paired balance system was used onboard for mass measurements (Fig. 5.16). It was calibrated every 12 hours (more frequently under bad weather conditions) and yielded an error $< \sim 1\%$. The wet bulk specimen mass (M_b) was measured immediately after sampling. Subsequently, the wet specimens were placed in a convention oven to dry at 105°C . After 24 hours, the dry specimens were transferred to a desiccator to cool down to room temperature and their dry bulk mass (M_d) was measured 1 hour later. The mass of pore water (M_w) in the specimen is estimated by:

$$M_w = \frac{M_b - M_d}{1 - s}$$

where s is the standard seawater salinity ($s = 0.035$). The water content (w) is then calculated by:

$$w = \frac{M_w}{M_b - M_w}$$

After the measurements the dry bulk specimens were stored in sealed plastic bags. The specimens were re-dried and weighted once transported back to the University of Bremen. There the volume of dry specimens (V_d) was measured using a Quantachrome penta-pycnometer. For each instrument run, four specimens and one calibration sphere were placed in the chambers. The calibration sphere was to monitor errors and was rotated between all five chambers. The specimens and calibration sphere were measured five times respectively and the average values were taken. The dry specimen volume was corrected for the precipitated salt:

$$V_{d-cor} = V_d - \frac{M_w \cdot s}{\rho_{salt}}$$

where V_{d-cor} is the corrected dry specimen volume and ρ_{salt} is the salt density ($\rho_{salt} = 2.20 \text{ kg/cm}^3$). Assuming the seawater density $\rho_w = 1.024 \text{ kg/cm}^3$, the pore water volume (V_w) is given by:

$$V_w = \frac{M_w}{\rho_w}$$

Then the wet bulk density (ρ_b), dry bulk density (ρ_d), grain density (ρ_g) and porosity (ϕ) are calculated by:

$$\rho_b = \frac{M_b}{V_w + V_{d-cor}}$$

$$\rho_d = \frac{M_b - M_w}{V_w + V_{d-cor}}$$

$$\rho_g = \frac{M_b - M_w}{V_{d-cor}}$$

$$\phi = \frac{V_w}{V_w + V_{d-cor}}$$

The thermal conductivity was measured on working halves of gravity cores with a spacing of at least one measurement per section. The KD2 Pro thermal properties analyzer produced by Decagon Devices was used for this purpose. The thermal properties analyzer is equipped with three sensors, of which we employed a dual-needle 30 mm sensor (SH-1), capable of measuring thermal conductivity, specific heat capacity, thermal diffusivity and thermal resistivity. The sensor has accuracy within 7% for specific heat capacity and accuracy within 5% for thermal conductivity, thermal diffusivity and thermal resistivity, respectively. The performance of the sensor was verified every 12 hours. It was calibrated on a standard Delrin block of known thermal property values. Before taking every measurement, the sensor was inserted into the cores for one minute to allow equilibration to core temperature. A correlation coefficient (r^2) is displayed on the screen after measurements, which indicates the data quality. Good data sets ($r^2 > 0.9990$) were taken and data sets with $r^2 \leq 0.9990$ were discarded.

5.3.3 Preliminary Results

During cruise M167, 140 MAD and 109 thermal conductivity measurements were acquired on working halves of gravity cores from Gulf of Cadiz. The physical properties measurements provide constraints on characterization of the sediments.

For MAD data, no obvious difference is observed between MV and pockmark sediments (Fig. 5.17). The water content ranges from 40% to 80% and a general decreasing trend is visible at the first 100 cmbsf, followed by relatively constant water content values. The porosity is generally in a range of 50% to 70% and shows similar variation trend with water content. In contrast, the bulk density increases from 1.5 g/cm^3 at seafloor to as high as 1.8 g/cm^3 at 100 cmbsf and remains constant to 400 cmbsf.

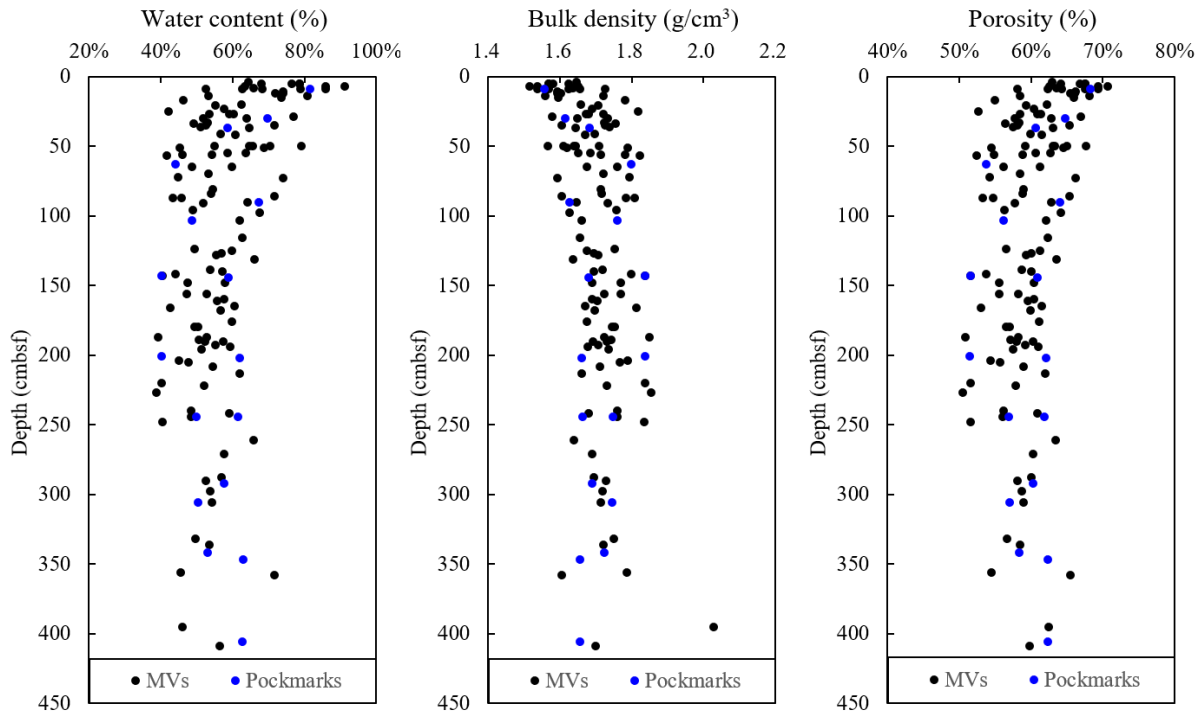


Figure 5.17: Water content, bulk density and porosity of gravity core samples from cruise M167.

In addition, the MAD data from Ginsburg and Yuma MVs were compared with that of cruise M149, which shows that the results in this cruise are consistent with that from cruise M149. For Ginsburg MV (Fig. 5.18), the water content decreases gradually from 80% at seafloor to 40% at 500 cmbfs although quite scattered data are observed at 300 - 420 cmbfs. Correspondingly, similar increasing and decreasing trends are visible in bulk density and porosity, respectively. In contrast, Yuma MV (Fig. 5.19) shows relatively stable values. The water content, bulk density and porosity of Yuma MV remain around 60%, 1.7-1.8 g/cm³ and 60%, respectively.

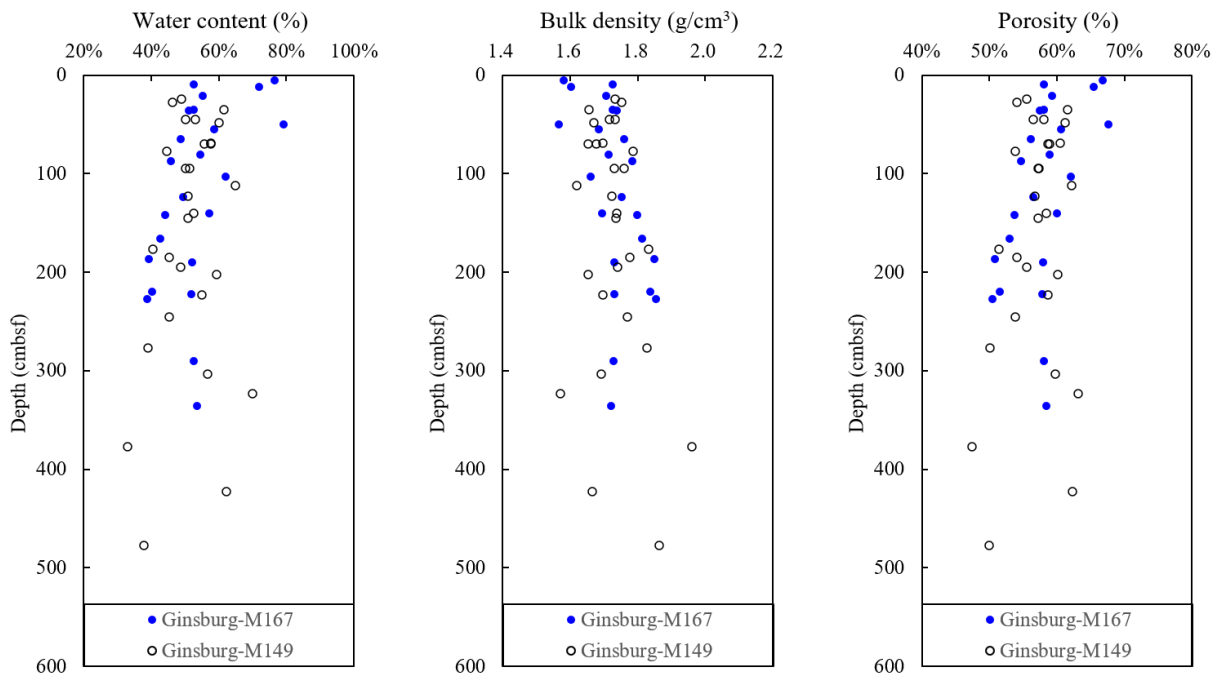


Figure 5.18: Water content, bulk density and porosity of Ginsburg gravity core samples from cruises M167 and M149.

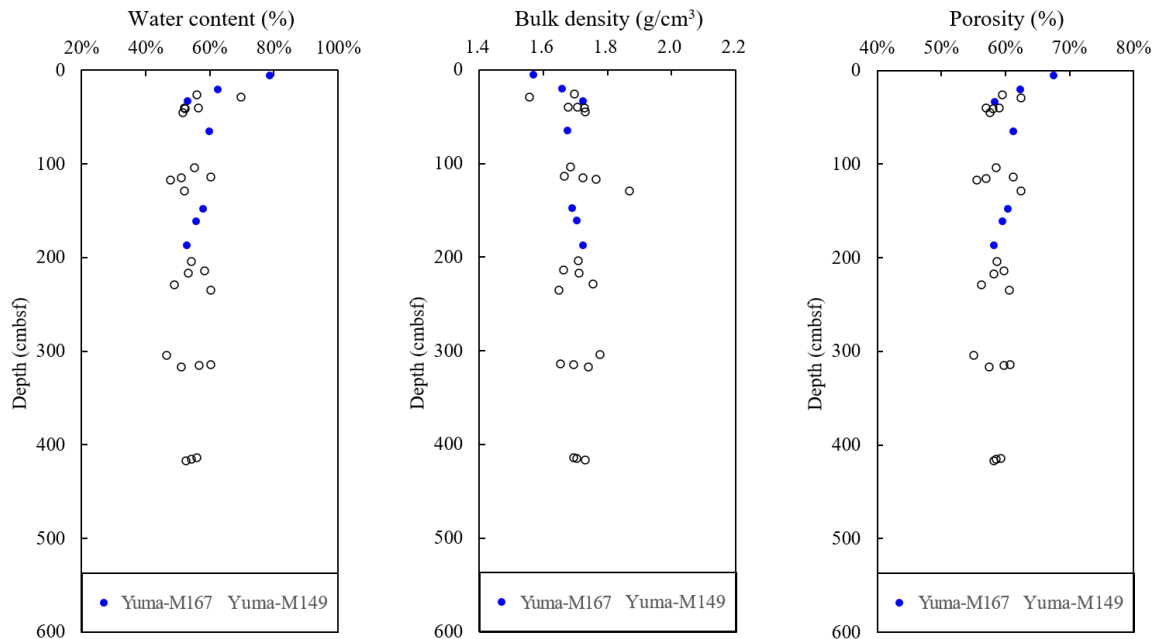


Figure 5.19: Water content, bulk density and porosity of Yuma gravity core samples from cruises M167 and M149.

For thermal conductivity data (Fig. 5.20), there is also no obvious difference between MV and pockmark sediments. The thermal conductivity generally increases from 0.8 W/m°C at seafloor to as high as 1.4 W/m°C at 100 cmbsf and remains relatively stable to 400 cmbsf, although it is quite scattered at 0-250 cmbsf and many low thermal conductivity values (0.8 W/m°C) are found. The scattered measurements are attributed to degassing, where fractures and widely distributed pores decrease the thermal conductivity of sediments. This is corroborated by the relationship between porosity and thermal conductivity. The thermal conductivity generally decreases with the increase of porosity. However, the anomalously low thermally conductivity data points caused by degassing obviously deviate from the general variation trend, since degassing cannot be reflected by porosity data.

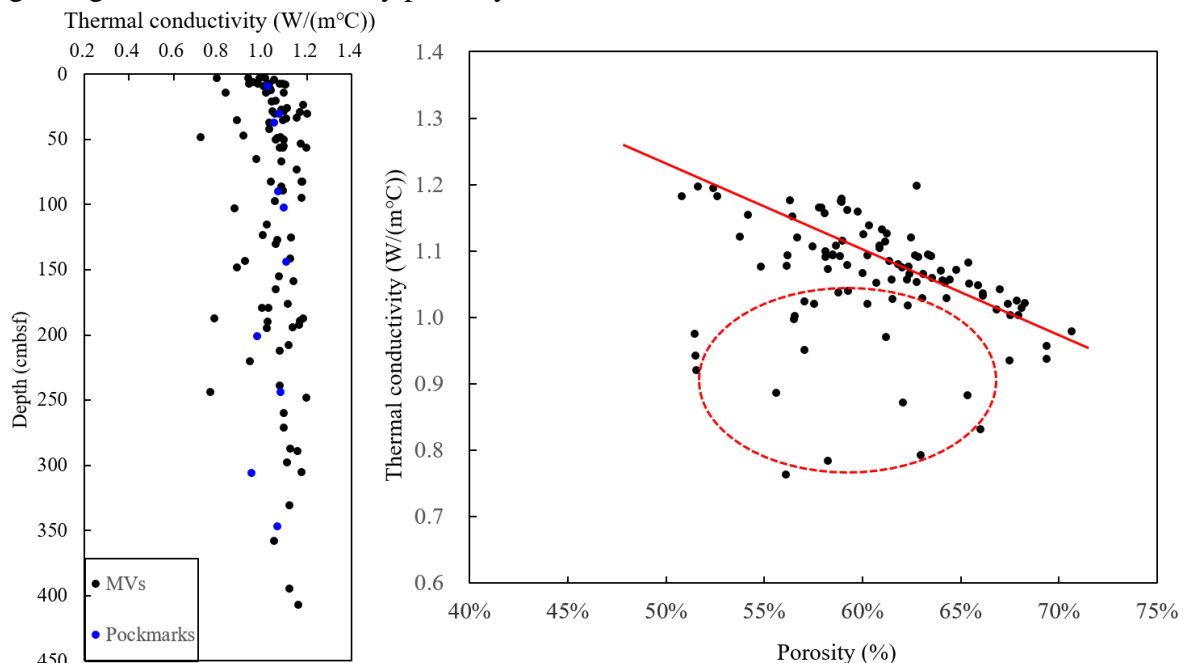


Figure 5.20: Thermal conductivity and the relationship between porosity and thermal conductivity for gravity core samples from cruises M167.

5.4 Pore water Sampling & Geochemistry

(C. Schmidt, H. Zehnle)

5.4.1 Methodology

Sediment samples were taken from gravity cores (GC) and ROV Squid push cores. The sampling was done in the geology laboratory of the ship. Upon core retrieval, we took 2-3 cm wide sediment slices from the working halves of the GC. The spacing of the sampling was chosen according to core recovery, but did normally not exceed 20 cm for GCs. Push cores were sampled every 2 cm. Sediments both at the splitted surface and in contact with the liner were not sampled to avoid potential contamination with seawater.

A GEOMAR argon-gas squeezer was used to extract porewater from the sediments (Fig. 5.21). With this instrument, 14 samples can be squeezed simultaneously. On average, it took 30 to 45 minutes to squeeze 5-10 ml of porewater. Squeezing was performed in the vessel's cold room at 4 °C. Gas pressure was monitored and seldom exceeded 5 bar during the squeezing. While squeezing, the porewater was filtered through 0.2 µm cellulose Whatman filters and collected in 20 ml plastic vials. In addition to the squeezing method, some gravity cores were treated with rhizons (purchased from Rhizosphere, Netherlands) in order to gain pore fluids from undisturbed whole cores (Fig. 5.21). Push cores were sampled only with rhizons. Therefore, small holes were drilled in the plastic liner and rhizons were placed in the sediments. The rhizons were connected with 10 ml syringes. Syringes were draw up and hold at the position with a wooden spacer in order to keep the vacuum. Extracted pore fluids were transferred afterwards into 20 ml plastic vials.



Figure 5.21: Rhizon sampling being performed in the Geolab of RV Meteor, and Geomar pore water press.

Total Alkalinity (TA) and Chloride titrations were done immediately after the extraction of porewater. Onboard analysis was performed in order to detect fluid venting during the cruise. We expected to observe increase in TA caused by the anaerobic oxidation of methane and negative as well as positive Cl anomalies. Negative Cl anomalies are caused by clay dehydration while positive anomalies show indication for salt dissolution in the subsurface. Further sub-

sampling for anion, cations, ammonium and isotope analyses was conducted after the onboard analyses were completed.

Table 5.4: Onboard chemical analyses and subsampling.

Onboard analysis	Treatment
Total alkalinity	Onboard titration
Chloride	Onboard titration
Porewater sub-sampling	
Anions (IC)	None
Cations (ICP)	Add 10 µl HNO ₃ per ml sample
Ammonium	None
δ¹⁸O/δD	None

Analyses for **total alkalinity (TA)** were carried out on board using a METROHM titration unit 876 Dosimat Plus. TA was determined by titration with 0.02 N HCl using a methyl red indicator. The solution was bubbled with argon to remove CO₂ and H₂S gas released during the titration. Onboard analyses for chloride (Cl) were carried out using a METROHM titration unit 876 Dosimat Plus. The **Cl concentration** was determined with AgNO₃ and a K-Chromat and K-Dichromat indicator. IAPSO seawater standard was used for both on board titration methods to check the reproducibility and accuracy of the chemical analyses. The error (± 1 SD) of the Cl and TA analyses amount to ± 2 mM (± 0.3 %) for Cl and ± 0.05 mEq. dm⁻³ (± 2 %) for TA, according to replicated analyses of the IAPSO standard. A full method description for both methods can be found on the GEOMAR website (www.geomar.de/mg-analytik).

5.4.2 Preliminary Results

Samples taken during M167 are listed in Table XYZ. Overall 203 samples could be retrieved during the cruise (194 GC samples and 9 PC samples). The ROV Squid Push Core samples are the only one taken in the Alboran Sea, all other samples were taken with the GC in the Gulf of Cadiz. For most of the samples sub samples were taken for further analysis for IC, ICP-OES, Ammonium and Isotopes on shore. On board analysis of Total Alkalinity and Cl could be performed for most of the samples taken.

Table 5.5: Station and sample list for porewater samples

Station	Location	No. Of samples	Gear	Method
GeoB24205-3	Carboneras Fault, Alboran Sea	9	PC	Rhizon
GeoB24206-1	Summit MV Ginsburg	10	GC	Squeezing
GeoB24207-1	MV Ginsburg- W Flank	14	GC	Rhizon
GeoB24208-1	Pockmarks SW Averroes MV	12	GC	Squeezing
GeoB24209-3	Averroes MV	5	GC	Rhizon
GeoB24211-1	Yuma MV	10	GC	Squeezing
GeoB24213-1	Background pockmark	17	GC	Squeezing
GeoB24214-1	Possible MV #1- N of Tangier MV	9	GC	Squeezing
GeoB24221-1	N Ginsburg MV area	17	GC	Rhizon
GeoB24222-1	Ginsburg MV	12	GC	Squeezing
GeoB24225-1	Gemini 2 MV	11	GC	Squeezing

GeoB24226-1	Fiuzza MV	6	GC	Squeezing
GeoB24228-1	Potential MV #1 Lineament South	4	GC	Squeezing
GeoB24229-1	Potential MV #3 Lineament Center	10	GC	Squeezing
GeoB24231-1	Potential MV#2 New MVs Field	8	GC	Squeezing
GeoB24233-1	Plain SW Atlas MV	7	GC	Rhizon
GeoB24234-1	Atlas MV	9	GC	Squeezing
GeoB24236-1	Potential MV E of Atlas MV	9	GC	Squeezing
GeoB24238-1	Depression W of Student MV	16	GC	Squeezing
GeoB24239-1	Student MV	8	GC	Squeezing

5.4.2.1 Mud Volcanoes

Overall, we got samples from 12 MVs, where 5 MV of where new discoveries. From the profiles of total alkalinity, we can estimate the depth of sulfate methane transition zone (SMTZ), where both sulfate and methane are exhausted due to AOM, at the horizon where total alkalinity is the highest (e.g. Chatterjee et al., 2011). Four of the MVs (GeoB24207-1/11-1/22-1/25-1) show a strong increase in TA to up to 30 meq/L in the upper 100 cm of the sediments (Fig 5.22). TA concentrations however, due not decrease with depth again, but rather stay at high levels. This increased level of alkalinity with depth can be explained by the incongruent dissolution of Na-feldspars (Hensen et al., 2007). Only GeoB24226-1 shows peak in TA of 7.52 meq/L at 92 cm depth indicating the depth of the STMZ. Sediments of GeoB24206-1 and GeoB24229-1 are marked by hemipelagic sediment cover of the mud breccia (see sedimentology). The same sedimentary stratigraphy can also be observed in the TA of both MVs. Up to a sediment depth of about 175 cm concentrations stay at seawater values. Below that, concentrations start to increase slowly to values of about 12.25 meq/L (GeoB24206-1) and 8.11 meq/L (GeoB24229-1). All other MVs do not show a significant increase in TA with depth, even though mud breccia was recovered from gravity cores. Therefore, these MVs can be considered as inactive or dormant.

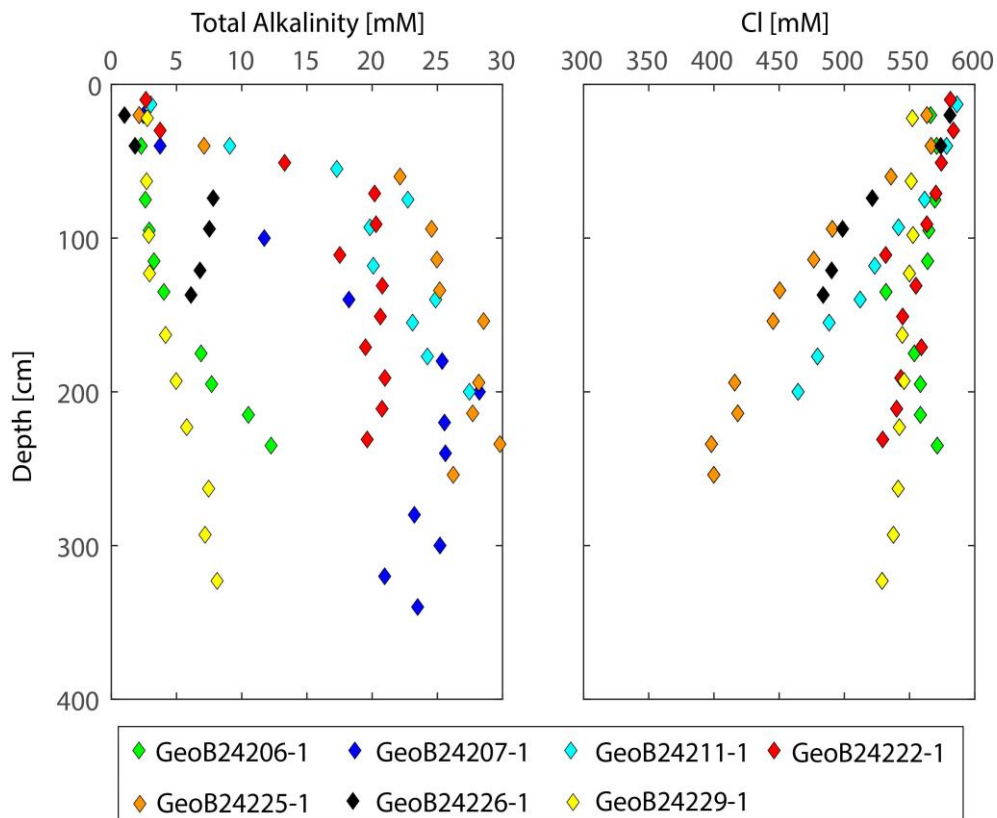


Figure 5.22: Porewater depth profiles for Total Alkalinity and Cl for selected GCs of several MVs in the Gulf of Cadiz.

Cl concentrations show slightly different picture for the MVs. Only GeoB24211-1/25-1/26-1 do show a strong decrease in Cl concentrations with depth compared to seawater (Fig XYZ). The lowest concentration is observed for Geob24225-1 with 399 mM at 254 cm depth. All other MVs show only a slight decrease in Cl to concentrations not below 530 mM. Cl decrease is a widespread phenomenon in the GoC. Fluids of the MVs are affected by fluid freshening caused most likely the transformation of smectite to illite (Hensen et al., 2007; Scholz et al., 2009). Potential source for these fluids are Mesozoic sediments of the accretionary wedge in the GoC (Hensen et al., 2015; Schmidt et al., 2018).

5.4.2.2 Pockmarks

During the cruise two possible pockmarks were sampled with the GC. One potential pockmark near Student MV (GeoB24238-1) does not show any signs for active fluid flow. TA and Cl values stay at seawater values with depth (Fig. 5.23). The depression can be rather described as collapse hole (León et al., 2010). The second sampled pockmark is located close to the Averroes MV (GeoB24208-1). Depth profiles for Cl and TA are shown in Fig. 5.23. In contrast to the neighboring MVs (Ginsburg Yuma), the Pockmark shows a strong increase to high Cl concentration compared to seawater of up to 1817 mM at 329 cm depth. High Cl concentrations are clear indication for a salt dome beneath the structure. Evaporite dissolution is widespread phenomena in the Gulf of Cadiz region and is described as Cl source for many MVs, e.g. Mercator MV (Haffert et al., 2013).

In addition to that, the TA also rises in the upper 50 cm to 14.49 meq/L and stays at this high level. The high TA can be explained here again by a combination of AOM and by the incongruent dissolution of Na-feldspars, similar to the MVs.

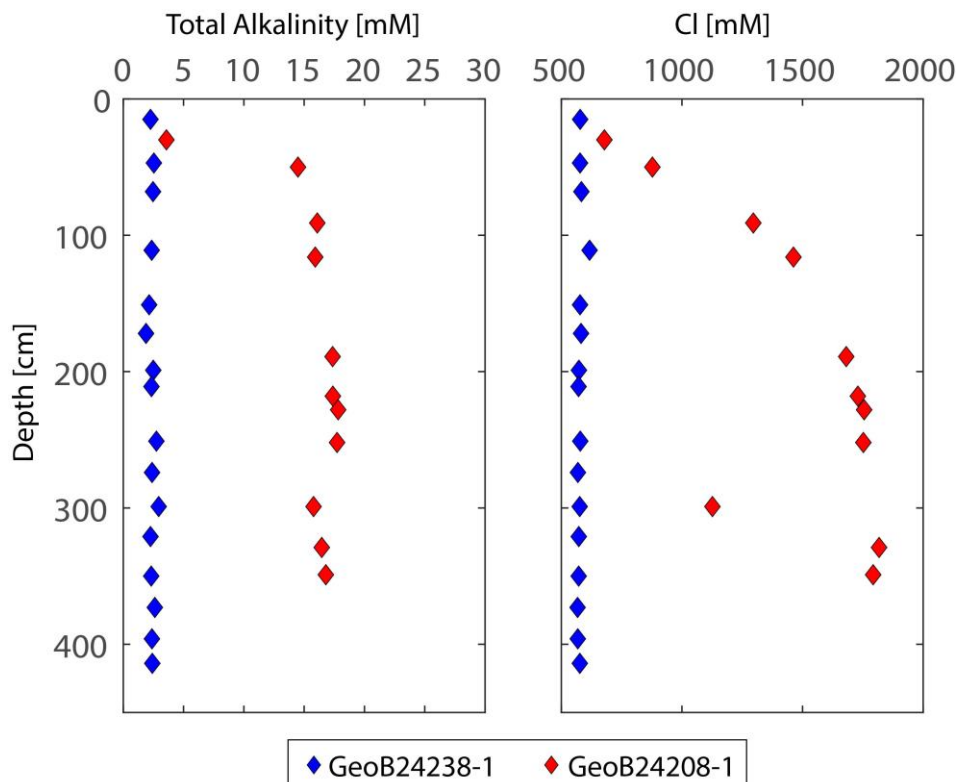


Figure 5.23: Porewater depth profiles for Total Alkalinity and Cl for selected GCs of two pockmarks in the Gulf of Cadiz.

5.5 Microbiology

(H. Zehnle)

5.5.1 Methodology

During M167, the seafloor was sampled with both push and gravity cores. 2 push cores of approximately 20 cm length were collected with ROV SQUID and 32 gravity cores of on average 174 cm length were recovered.

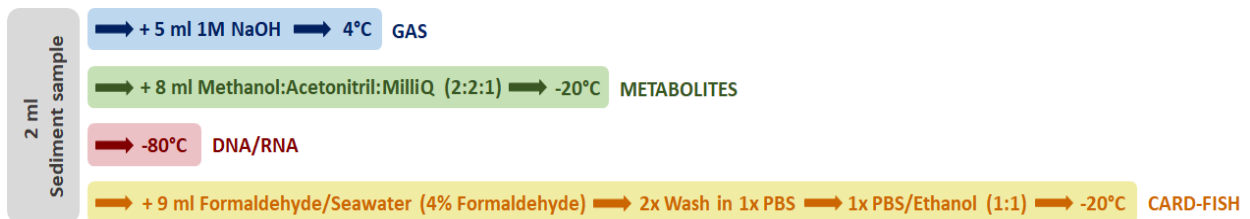


Figure 5.24: Processing scheme for sampling from push and gravity cores during M167 in order of priority. RNA and metabolite samples were only collected from push cores.

Push cores were moved to a 4 °C cold room immediately after recovery. Here, samples were taken every 2 cm (horizontal transects) (Fig. 5.24).

Samples for gas chromatography were taken first by transferring 2 ml of sediment to 20 ml crimp vials prepared with 5 ml 1M NaOH. The vials were sealed with butyl rubber stoppers and crimp caps. They were shaken to homogenize the sediment with the NaOH in order to stop microbial activity and to drive gasses into the headspace. The vials were then stored at 4 °C.

For DNA and RNA analysis, 2 ml of sediment were transferred to 15 ml Sarstedt tubes, respectively. DNA and RNA samples were frozen immediately at -80 °C.

For microbial metabolite analysis, 2 ml of sediment were added to 15 ml Sarstedt tubes containing 8 ml of a methanol:acetonitrile:MilliQ mixture (2:2:1 v/v/v). After sample homogenization, metabolite samples were stored at -20 °C.

For catalyzed reporter deposition fluorescence in situ hybridization (CARD-FISH), 2 ml of sediment were homogenized with 9 ml formaldehyde in seawater solution (4 % v/v final concentration) in 20 ml scintivials. Cells were fixed at 4 °C for 2-4 h. Afterwards, vials were shaken before transferring 2 ml of sample into 2 ml cryovials. After centrifugation at 3000 rpm for 3 min, the supernatant was discarded. Pellets were washed twice with 1.3 ml filter-sterilized (0.2 µm) phosphate-buffered saline (PBS), resuspending the pellet each time and centrifuging at 3000 rpm for 3 min. After the second PBS wash, pellets were resuspended in 1.5 ml filter-sterilized PBS/EtOH (1:1 v/v) and stored at -20 °C. The remainder of the samples in the scintivials was stored at 4 °C for cell counting.

For **gravity core** sampling, gas chromatography, DNA, and CARD-FISH samples were taken as described above from 24 of the 32 recovered cores (Fig. 5.24). However, the samples were taken directly on deck instead of in the cooling chamber. After recovery, gravity cores were split into 1 m sections. From the upper first section, samples for gas chromatography, DNA, and CARD-FISH were taken at 15 cm intervals. From the second section, gas chromatography and DNA samples were taken every 30 cm. From the third and fourth section, gas chromatography and DNA samples were taken every 50 cm.

The gas chromatography samples, including headspace samples, were taken before splitting the core pieces into working and archive halves to prevent gas venting. The other sample(s) were taken from the opened working halves on the same horizontal transect as the corresponding gas chromatography sample.

5.5.2 Preliminary Results

From the 2 recovered push cores, we collected 12 Gas, DNA, and FISH samples as well as 7 RNA and metabolite samples.

From the 24 sampled gravity cores, we collected 211 gas chromatography samples, 209 DNA samples, as well as 84 CARD-FISH samples. These samples were frozen or fixed until analyses can be done once back at MPI, in Bremen.

Gas samples will be subjected to gas chromatography in order to measure the presence and concentrations of methane and other small alkanes, such as ethane, propane, and butane. From DNA (and RNA, if applicable) samples, nucleic acids will be extracted and sequenced. The sequences will be analyzed bioinformatically to gain information on the microbial communities and their metabolic activity in the samples. In the case of push core, these results will be supported by the detection of metabolites via mass spectrometry. Additionally, CARD-FISH samples will be employed to detect specific microbial groups of interest using targeted oligonucleotide probes.

5.6 BlueROV

(S. Krupiński)

5.6.1 Introduction and Aim

The ocean research community benefits from a number of existing and constantly improved robotic tools such as ROVs, AUVs, camera skids and observatories. These have enabled carrying out tasks and measurement not otherwise possible and are on the way to mature into a dependable technology. Because of their complexity and the vulnerability of electronics and other components to the sea conditions, they must be typically attended by a trained and large crew. The logistics of transporting them and the deployment procedures tend to be complicated while the price of such instruments stays relatively high. Due these reasons, compounded by the restrictions on the scientific crew sizes due to the Covid-19 pandemic, it is interesting to explore the emerging lower-end vehicles as a lightweight alternative for research expeditions where the deep-diving and heavy instruments are not a requirement. With the miniaturization of some key scientific instruments, the increase in computational power available in small footprints as well as an increasing power density for batteries, small vehicles have become significantly more capable over the past few years. We have reached a point where the smaller vehicles have the potential for well-defined specific tasks to deliver part of the functionality of the bigger more capable tools, e.g. in instrument deployment or visual survey, but at a fraction operational complexity of the latter class. For these niche applications, the performance needs to be verified for the conditions encountered in the ocean research and the necessary adaptations need to be planned. It is therefore critical to gather the operational experience in this domain.

Expedition M167 was expected to enable advances in several aspects of adoption of small robot technology in the ocean research. The principal objectives are outlined below:

- 1 Test the small vehicle in open sea conditions and in the context of deck operations, setup and to better understand its potential role in science data collection. Determine the sea conditions limit and factors impeding/enabling operations.
- 2 Test modifications and improvements to the vehicle which will pave the way for new development of this type, including the motion controller of the autonomous underwater vehicle, the graphical user interface (GUI) and the electronics package.
- 3 Evaluate the maintenance and repair requirements based on the observed problems and circumstances.
- 4 Develop the safe and efficient procedures for deployment and retrieval, judge the minimal setup and roles of the support team for the vehicle.
- 5 Collect data for future experiments.

5.6.2 Methodology

A commercially available prosumer grade mini-ROV – MARUM BlueROV2 (Prof. R. Bachmayer Working Group) – was used as a testbed for component and operations tests. Its producer, BlueRobotics, also delivers a number of marine robotic components characterised by a reasonable performance and a low price tag which are an interesting basis for the researched technology. The existing electronics/computational system of the MARUM BlueROV was largely replaced by a set of components chosen for higher performance and improved connectivity in particular with respect to scientific data acquisition. At the same time, the original software was replaced by the open-source platform of robotic libraries (Robotic Operating System – ROS, version 2) and custom written control layer which is being evaluated as the future basis for the research applications.

MARUM BlueROV2 “heavy” is a small size prosumer grade ROV (albeit self-sufficient in energy) with dimensions of only 46x58x25 cm and a weight of about 12 kg in air (Fig. 5.25). The MARUM BlueROV2 is rated to a depth of 100 meters (with plastic housings) or 300m (with aluminium housings), although this can be significantly extended. Even in its basic, shallow diving version, it allows to cover large areas of interest for the Ocean Sciences, mainly continental shelf areas such as portions of the North Sea or the Baltic Sea, etc. It can be easily lifted by one person and the requirements for handling and deployment are minimal. At the front of the ROV is a mid-definition (720p, 30fps) wide-angle low-light camera optimized for use on the ROV. It’s mounted to a tilt mechanism so that the pilot can control the camera tilt to look up or down, even when the ROV is level. The ROV uses eight thrusters (T200 Thrusters in a vectored configuration), providing a high thrust-to-weight ratio and the ability to move in any direction and full six-degree-of-freedom control and feedback stability. Adjustable gain levels allow the pilot to have precision control at extremely low speeds as well as high power to overcome currents (~2-3 kn) and carry significant loads compared to its own weight. This configuration is needed to work at the expected current regimes in the central North Sea. The vehicle is equipped with an optional single-degree-of-freedom manipulator (a gripper). The unquestionable advantage of this hardware besides the low cost is its ease of operation, Of course, many capabilities of the professional ROVs are missing in this small vehicle such as a dexterous high-power manipulator, a professional-grade acoustic positioning solution or high-quality light and camera setup. Also due to the available propulsive forces produced on a work-class ROV it is also to lift or work with larger objects or samples.

One aspect where this technology can hope to contribute to improving scientific data collection is the search and evaluation of shallow water gas seeps. It is envisaged that the visual quantification of gas bubble emissions can be conducted with a funnel attached to a simple manipulator. Gas bubbles will be sampled for on-board analyses using an overflow compartment. The challenge of this initiative lies in the miniaturisation of the components and the impact that they will have on the behaviour of the vehicle. An experimental gas collection setup, currently suitable for the survey-class ROV was constructed which will be deployed in case an underwater gas seepage will be encountered during a dive.

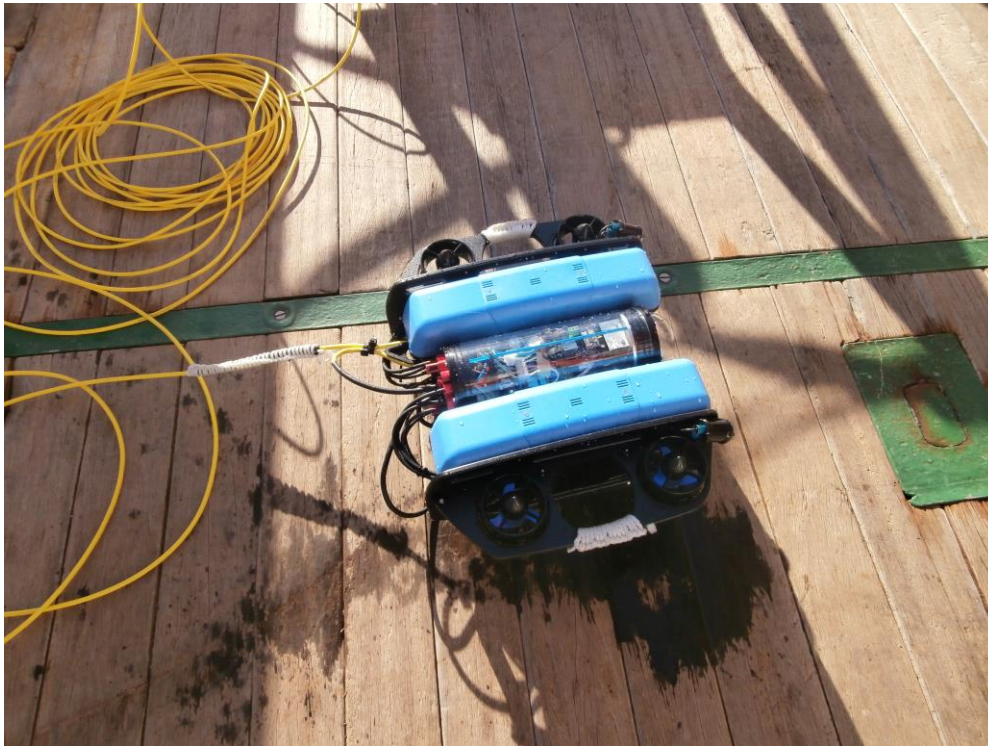


Figure 5.25: BlueROV robot in the "heavy" configuration on deck of RV Meteor after deployment.

5.6.3 Preliminary Results

ROV deployment

Table 5.5: Station list for BlueROV deployments

Deployment date	Principal aim	Duration	Max. diving depth	Station	Sea conditions
17.10.2020	System test, buoyancy check and basic control verification	25 min	5 m	Alboran Sea	Sea state 1 Wind 2 Bf
19.10.2020	Test deployment with depressor weight	1 h	25 m	Alboran Sea	Sea state 2 Wind 4 Bf
25.10.2020	Surface test 2, refinement of the depressor weight dive method	1.5 h	20 m	Gulf of Cadiz	Sea state 2 Wind 3 Bf
29.10.2020	Image collection and test of deployment from a different location of the ship (the bow)	40 min	7 m	Gulf of Cadiz	Sea state 2 Wind 5 Bf

As expected, the vehicle's deployment proved to be fast, manageable under different weather conditions and adapted for a small team. The deck operations necessary for deploying the ROV could be conducted by a team of two people, including the person necessary for crane/winch operations, if a crane was used for depressor weight management. However, in most situations, an additional person was helpful for managing the umbilical, coordinating the initial stages of the deployment and watching out for the vehicle on the surface.



Figure 5.26: An important consideration during the initial stages of deployment of the robot is avoiding direct proximity of the ship while on the surface. This photo shows the arrangement of the crane used as an attachment point for the snap tackle and the depressor weight

On several occasions, the ROV was deployed by the pilot simply lifting it over the railing and lowering it in the water by the umbilical. While quick and relied on few people, this way of operation was mostly used for test on surface and was found to be less advantageous in terms of controlling the robot underwater, as it did not provide any additional mechanism of controlling the umbilical. Care had to be taken to steer the vehicle away from the splash zone around the hull of the boat at all times in order to avoid collisions between the two (Fig. 5.26). This could be accomplished either by the pilot directly observing and controlling the vehicle from the deployment deck, or the additional team member giving directions to the pilot sitting at the control console by a walkie-talkie. In the first case, it was necessary to bring the surface control computer to the deck which was a small hindrance for later operation. A potential improvement would be to use long range (>20m) wireless controller coupled to the control computer in the control room. Using the embedded compass, the vehicle can also be initially driven away from the boat without the visual feedback by simply following the appropriate magnetic heading relative to the current heading of the deploying ship.

This simple procedure was also carried out from the bow of the ship without significant problems, as illustrated by **Error! Reference source not found.** Despite rougher seas, the vehicle's pendulum motion while being lowered did not cause collisions with the side of the

ship. Due to high freeboard, it was slightly more difficult to observe the vehicle's behavior on the surface.

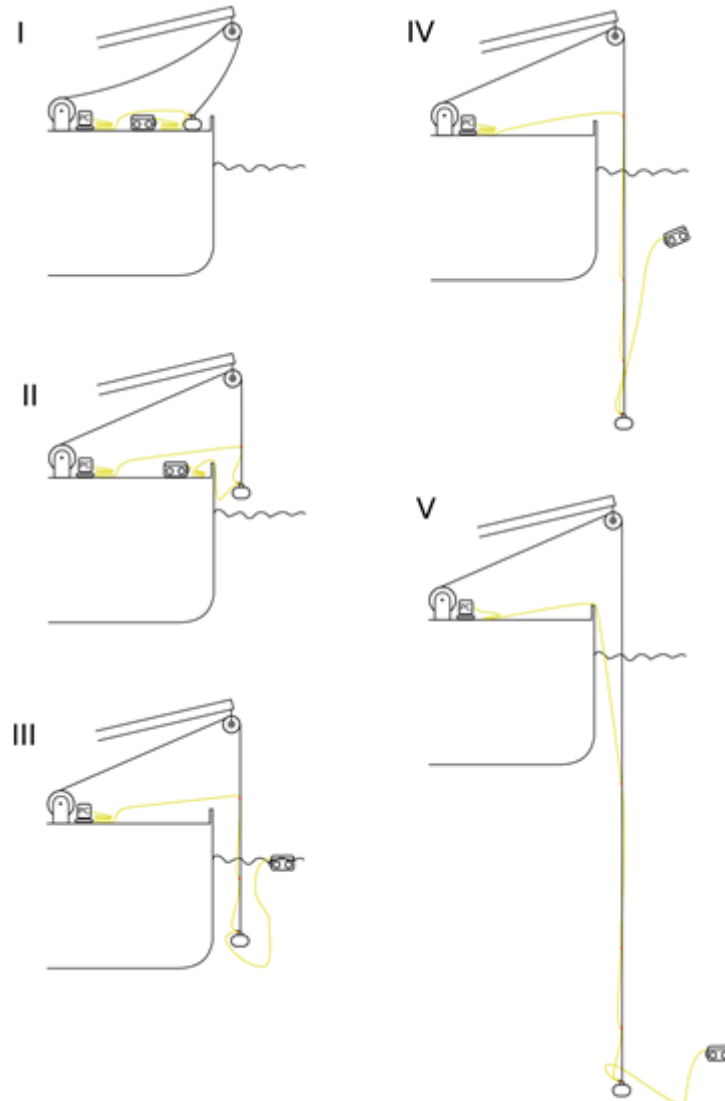


Figure 5.27: Deployment stages for the depressor weight-ROV system

The method of deploying the vehicle with the umbilical attached to the depressor weight was successfully used multiple times. The procedure is roughly sketched in **Error! Reference source not found.5.27**. While it slowed the deployment and the dive slightly (e.g. due to the need to attach the umbilical to the lifting rope every 5 m), it proved to be very advantageous. Firstly, it permitted to reduce the free length of the umbilical being affected by the current and drifting around, potentially getting close to risk areas such as the ship's propeller. Secondly, it stabilized the position of the vehicle – if the pilot stopped controlling the robot and let it drift freely, the depressor weight would keep its position directly underneath the deployment point and thus the vehicle would only have drifted away from it by the length of the free umbilical. Lastly, the depressor weight provided a visual reference for the robot in the open water column. The depressor object was chosen from commonly available items from the ship's mechanical store (**Error! Reference source not found.**), with the weight in the order of 10 kg determined to be sufficient for the operation. Aside from making it easy to manipulate, it also allowed to work

with any winch/crane of opportunity. Lowering such weight by hand could also be imagined if no mechanical means of lifting were available.

Two danger factors were identified during the trials that were related to deploying the vehicle from the research ship: the danger of contact with a moving propeller (either main propeller or the tunnel thruster) or the danger of entanglement on the structures protruding from the hull, such as sensors, rudder, or bilge keels. The first danger was deemed to be a minor risk, since the currents caused by these devices were usually not strong enough in the deployment zone to pull the robot in before the deck observer would notice. The other danger was only present if the ROV would navigate around the boat (e.g. for hull inspection). In most scientific missions, the vehicle would be deployed directly to the target depth. However, on at least one occasion, the lack of visual reference points or temporary control problems, the vehicle was accidentally allowed to drift along the hull or even underneath it, which increased the entanglement risk.

Since the ROV used in these trials was powered by the internally carried battery, which had positive impact on the small umbilical diameter and the simplicity of electronics, an additional question had to be answered, to what extent the battery charge would be enough to perform the activities related to the scientific missions. It was observed during the expedition that even longer deployments did not lead to the battery being completely discharged, thus confirming that this setup can be applicable to more complicated fieldwork.



Figure 5.28: Typical elements of ship's rigging and hoisting devices can be used as a depressor weight of opportunity for deploying small robots, here ranging from 7 to 15kg, Finally, the middle block was chosen for the role.

Setup and demobilisation time: ultimately, the preparation of the robot, including moving it to the side of the ship, running the appropriate checklists and powering it up, would require 15 minutes, which meant that the robot could be deployed on short notice and that the time spent of

this stage was short compared to the useful dive time. It was also a positive factor for managing the research station schedule, as it offered more flexibility. The post-dive demobilisation, which in turns included coiling the umbilical, rinsing, drying and removing the vehicle from deck, would typically not exceed 20 minutes.

Means and hardware involved: one or two-people team, preferably equipped with means of communication, a winch with a fixed point to hang a tackle from at the level of the freeboard or a small crane/winch system (Fig. 5.29). Fully manual deployment, even in the depressor weight setup, is also theoretically possible.



Figure 5.29: Deployment using a depressor weight slightly increases the complexity of the operation with the deck personnel required to control the winch or crane

Weather limitations: in all deployments, the weather was deemed to be well within the operational envelope for the robot (sea state 1-2, wind up to 5 Bf). It was observed that in higher wind conditions more attention is needed to prevent the robot from drifting out of the safe zone of deployment due to the surface current). While operating in higher waves, the only issue was to move rapidly from first entering the splash zone to full control of the robot during the lowering of the robot into water and upon picking it up (Fig. 5.30).



Figure 5.30: Deployment of the robot off the ship's bow included working with a significantly higher freeboard

ROV control

Since the vehicle's control system was developed in-house, it had to undergo a number of tests to ensure stability and correct output. Most of the initial work had been done in the testing pool but the practical deployment of the vehicle in the sea conditions had put the vehicle in conditions which were not possible to replicate at small scale.

The biggest challenge to the stability of the control of the vehicle was the near constant presence of sea current during the trials. In effect, the research ship, even if it is positioned on station, tends to be exposed to surface current. This applies a constant force on the vehicle and carries it away from the deployment point, if the pilot does not correct the situation.

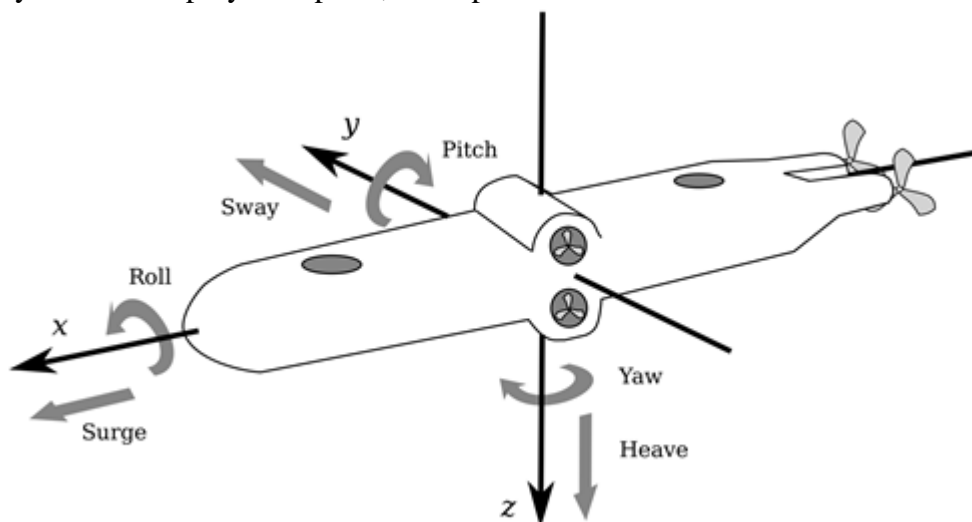


Figure 5.31: Each of the degrees of freedom of the vehicle was part of the control scheme. The vehicle's design made it naturally stable in pitch and roll but rapid motions in other directions are known to cause disturbance in this equilibrium

The control objectives for the vehicle were threefold:

1. to assure that the vehicle stays level at all times, implying controlling pitch and roll (**Error! Reference source not found.**5.31) to zero
2. to keep heading and depth at a constant level during certain parts of the mission
3. to assure that the motion of the vehicle in surge, sway, heave and yaw is smooth and efficient

These objectives were gradually satisfied during the sea trials but some harsher conditions were still proving difficult to work in, revealing challenges resulting, for example, from the chosen deployment method.

Regarding the first control objective, the natural stability of the vehicle was largely sufficient to guarantee that the vehicle keeps the correct attitude. However, due to initial problems with the third control objective, the actions of the pilot in yaw or sway could lead to a temporary loss of this stability and, if not stopped quickly, lead to a large roll (typically), including a possibility that the vehicle “tumbles over”. While this did not lead to any danger for the vehicle, it was a nuisance for the pilot and a source of inefficiency during the mission. This problem was partially resolved by allowing a finer tuning of the power of lateral thrusters and increasing the coefficients for the roll and pitch control. It was nevertheless quite clear that the controller of the vehicle must consider the interaction of multiple degrees of freedom (Fig. 5.32).

The depth controller was functional and helpful for the navigation of the vehicle but the attempts to control the heading revealed some problems with the heading sensor, which seemed to be burdened by a high noise level, thus rendering the control rather chaotic.

Another problem with the heading control stemmed from the current interacting with the vehicle: if the vehicle was allowed to drift, the umbilical would be quickly stretched and the force pulling the rear of the vehicle to one side would introduce significant disturbance to the heading control. At the time, the heading controller was not configured aggressively enough to counter this effect in stronger currents.



Figure 5.32: Images from the vehicle mounted camera show the position of the depressor weight and the free umbilical during deployment. Here, the depressor weight is lowered pass the bilge keels. In such videos it was also observed how the umbilical, rather taut due to the current, interacts with the vehicle

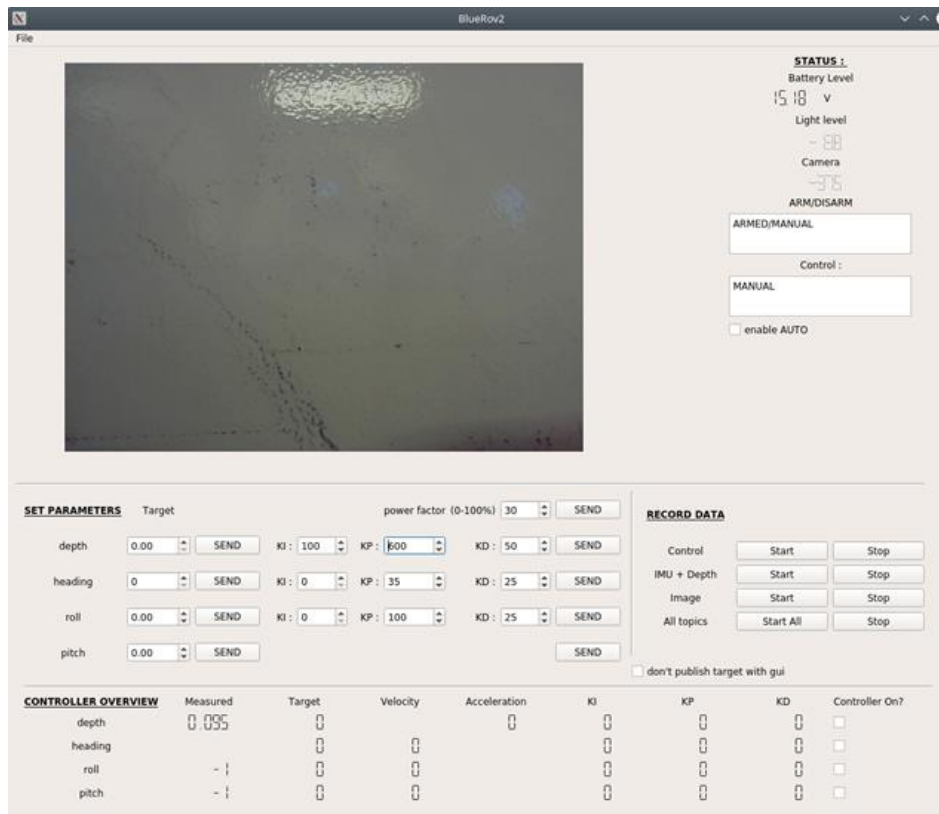


Figure 5.33: Graphical user interface for the robot developed at MARUM

The partial conclusions obtained during the deployment of the vehicle indicated that the inertial measurement unit (IMU) sensor providing orientation data has to be either reprogrammed or upgraded to a higher specifications sensor, while the control system must be perfected as to allow high-gain command while maintaining roll and pitch stability.

A simple user interface (GUI) developed in-house, shown in **Error! Reference source not found.5.33**, was used to provide the pilot feedback about the output of the sensors and thus increase the situational awareness about the state of the vehicle. The initial GUI's functionalities were centered on the tuning of the controllers and capturing data necessary for the further development of the vehicle (as *.bag files, specific to the Robotic Operating System (ROS) libraries). Future interfaces will contain similar information presented in more synthetic and graphical manner while the system tuning functionality can be moved to a sub-window, as it is not necessary for carrying out the mission.

ROV maintenance and repair

The practicality of a small robotic tool for ocean science in terms of logistics simplification was perceivable already at the stage of expedition preparations – the system together with the accessories, tools, an exhaustive set of spares and a range of optional accessories could be transported in two one-man portable standard shipping boxes. Due to the small size of the robot, both tools and the spare components were also of small dimensions.

The maintenance procedures preceding and following the deployments were limited to quick functionality checks and vehicle rinsing. They were successfully carried out by one person. As a benefit of the small size of the vehicle, most of the maintenance actions could be carried out in the enclosed laboratory space, thus shielding the operator from the weather conditions. Another

part of the routine maintenance operations was charging of the batteries, which was rendered more practical by rotating through a set of 3 batteries.

Table 5.6: Station list for BlueROV deployments

Problem / issue	Maintenance / repair actions
Camera pan-and-tilt (P&T) unit orientation to optimize	Remove the control container and open it, remove the electronics shelf mechanical support, remove the bulkhead and drill and additional hole in it for a M3 screw, remount the P&T unit in the new orientation, assemble all elements in the reverse order, close, mount and vacuum-test the container.
Exchange of umbilical for one suitable for deeper dives	Remove the control container and open it, dismantle the old umbilical together with its through-hull and mount the new one. Close, mount and vacuum-test the control container.
One of the thrusters not responding to commands	Remove and open the control container, inspect the electronics for superficial damages (none found), connect a spare thruster in place of the non-responding one (result: still no response), replace the ESC, reassemble the electronics, close, mount and vacuum-test the control container

During the expedition lasting approximately one month, there were very few instances of need for repair. The only actual failure which occurred was a malfunction of one of the electronic speed controllers (ESCs), detected due to a visible change of behavior of one of the thrusters. The initial diagnostic conducted to identify the source of the problem required about 1 hour of work and the replacement of the components took about 1.5 hour. The complication arose mostly due to cramped cable arrangement in the relatively cramped electronic canister of the vehicle.

Given the small robot size and the relatively basic hardware specifications (limited sources of sensor feedback of the components, little spare computational power, etc.), the current setup does not contain embedded mechanisms for pointing out the sources of failures. However, due to high availability and very high affordability of the spare parts, the user can easily bring a replacement part for virtually every element of the robot to the expedition. It enables a fault-finding strategy where, in case of an apparent failure of a component, the source of the problem can be found by swapping every element of the chain (e.g. control computer – power supply – ESC – motor) until the functionality is reestablished when the faulty element is swapped for a working one (Table 5.6). It was concluded that the selected set of spares and tools was adequate. In one or two cases, the missing tools were found in the ship's workshops.

5.7 ROV SQUID

(T. Leymann, V. Vittori, H. A. Mai, T. Fleischmann, W. Menapace)

5.7.1 Introduction and Aim

MARUM-Squid is a light work-class ROV manufactured by SAAB Seaeeye (UK) for operations down to 2000 m. The powerful, yet compact ROV system is realized on a comparably small footprint at a considerably low weight (< 10 t) and can be shipped within a single 20" ISO container. The system was adapted for marine research at MARUM and put into service in July

2015. During the cruise Meteor 167, the ROV-Squid was used as a platform to test new underwater technologies and to recover three observatories in the western Mediterranean Sea and Gulf of Cadiz (Fig 5.34).



Figure 5.34: ROV MARUM-Squid deployment during M167.

Mobilization

The system consists of three major components: the ROV, the winch with 2250 m supply cable (tether) and the topside equipment for power supply and control. During mobilization, the winch and the ROV were placed on the working deck of RV Meteor. Unlike most ROV systems, MARUM-Squid has no dedicated control van in order to keep the system as small and compact as possible. Part of the concept is to use a ship laboratory and convert it into an operational control room for the ROV. The entire topside equipment including the 3kV transformer with corresponding filter box and the portable flight cases containing devices for vehicle control, navigation, video display and data/video recording, were installed in the “Groß Nass-Labor” of the vessel (Fig. 5.35). The ship’s USBL system Posidonia (IXBlue) was used for positioning and navigation during operation.

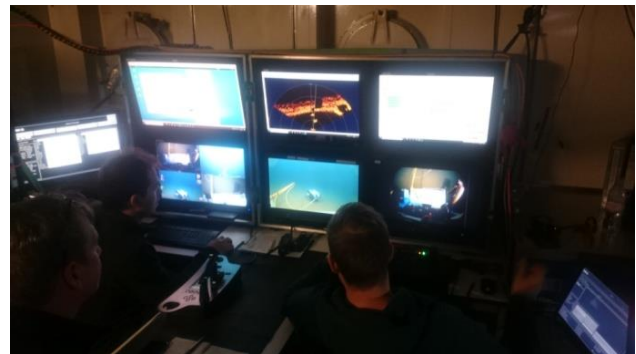


Figure 5.35: ROV and winch on the working deck (left); Nass-Labor serving as ROV control room (right)

Deployment and recovery

Prior to the deployment, an Imenco locklatch for releasing and recovering the ROV is slipped over the supply cable and the ROV's gimball which is the main attachment point of the system. Afterwards the locklatch is hooked into the ship's main crane. A sheave for guiding the supply cable from the winch overboard was mounted to the side A-Frame during mobilization. 50 m of supply cable with attached floats between the ROV and the depressor weight was laid loose on deck. The depressor weight, directly attached to the cable, is used as a weight to pull the supply cable straight down during operation. The 50 m between the depressor and the ROV is the actual operation radius of the system. Once the ROV is deployed and floating at the surface, the locking mechanism of the locklatch is released by pulling on a rope and pulled back on deck. Afterwards the ROV flies away off the starboard side of the vessel. In the meantime, the supply cable is laid inside the sheave behind the depressor weight and lifted overboard with the ROV winch. When the depressor is lowered to the surface, the ROV starts to dive and the winch pays out supply cable simultaneously until it reaches the seafloor. Recovery of the system is done in reverse order.

5.7.2 Methods

Dimensions and power

Vehicle dimensions are 2.1 x 1.2 x 1.9 m (L x B x H) and total weight of the ROV is 1.5 t. The transformer on the ROV converts 3kV to 500 V for the thrusters and hydraulics and 24 V for the low power devices such as cameras, Pan and Tilt unit or LEDs. Overall power of the ROV is 45 KW. The vehicle is equipped with a total of 11 thrusters; 8 horizontal thrusters providing a forward bollard pull of ~500 kgf each and 3 vertical thrusters.

Navigation

The MARUM-Squid is equipped with a standard ROV navigation sensor package such as a Valeport MiniPOS depth sensor and a Tritech PA500 altimeter which measures the height of the ROV above the seafloor. These sensors are used for auto altitude and auto depth hold maneuvers with an accuracy of 10 cm. Furthermore, the MARUM-Squid is equipped with two independent navigation devices, the 16CP and the MiniPOS, that can be used in alternation, providing a redundancy in case one of the device fails. The 16CP navigation pod consists of an integrated 3D magnetometer (3D compass) with an embedded processor capable of calculating roll, pitch and yaw in real-time. Using the 16CP navigation pod, Auto Heading as well as Pitch/Roll hold are possible with the ROV. The CDL MiniPOS/NAV3 navigation system provides the same functions as the 16CP, but also allows advanced autofunctions like station-keeping or -displacement. Furthermore, the MiniPOS calculates an additional, absolute position of the ROV by using all vehicle sensors and an input from any USBL positioning system. The MiniPOS is a fully self-contained Attitude Heading and Reference System (AHRS). It comprises a gyro compass based around a Monolithic Ring Laser Gyrocompass (MRLG). Together with the MRLG, three axis accelerometers make the MiniPOS a full inertial system. The MiniPOS is coupled to a RDI Workhorse Doppler Velocity Log (DVL) which increases the quality of the positioning when the ROV is operating close to the seafloor.

Additionally, the vehicle is equipped with a Tritech Seaking - dual frequency forward looking sonar operating at 325/650 kHz. The device is installed on the upper porch for 360° obstacle detection/avoidance.

Cameras & Optics

The ROV is equipped with 5 cameras. Two PAL DSPL MultiseaCams serve as forward looking and rear looking camera. The latter monitors the orientation of the tether during operation. Another camera mounted vertically on the front porch, the DSPL Wide-I, is giving a full overview of the area in front of the vehicle. An Imenco Tigersharks stills acquires images at a resolution of 14 megapixel and is mounted on the Pan and Tilt unit of the vehicle. The external flashgun of the stills is installed at a 45° angle on the upper porch. The main working camera is an Insite Pacific MiniZEUS MKII, likewise mounted on the ROVs Pan and Tilt unit. The MiniZEUS is a full HD camera with a resolution of 2.38 megapixel. The MiniZEUS has an hemispherical dome port and a fully corrected optical lens with a 10 x optical zoom. The optical lens corrects for chromatic, geometric and radial distortion that occur when using optical systems underwater. Two Imenco Dusky Shark line lasers are installed on the Pan and Tilt unit. They project two parallel laser beams at a distance of 29 cm for size measurements of objects on the seafloor (Fig. 5.36).

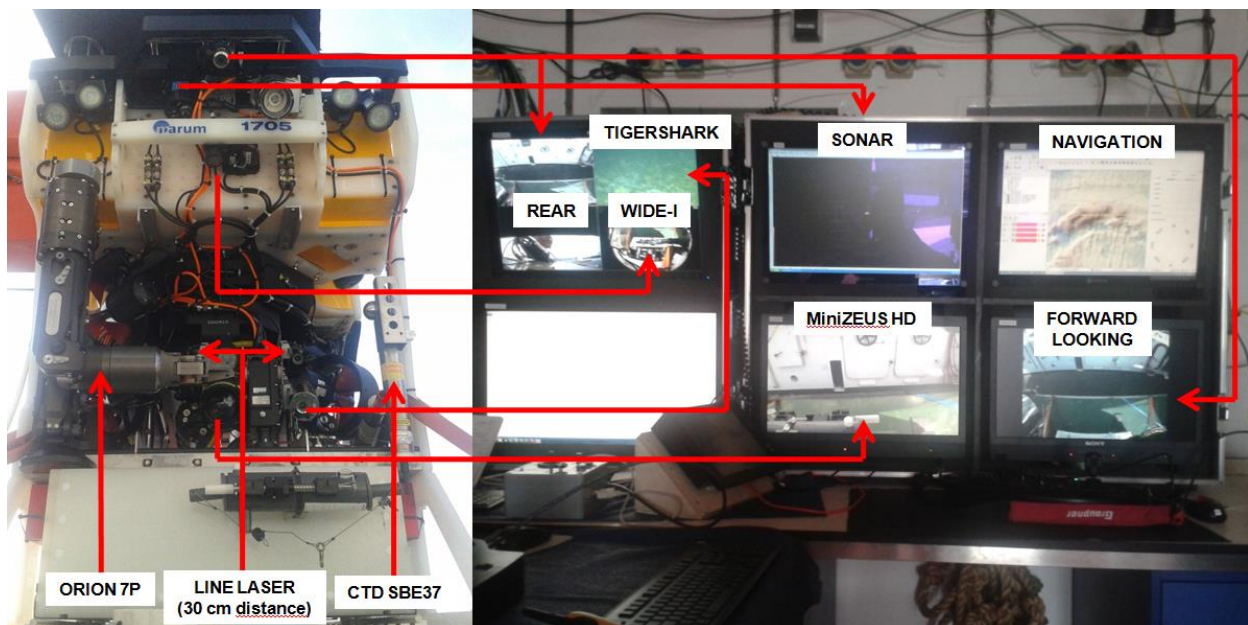


Figure 5.36: front of MARUM-Squid and video/navigation monitors

Lights

The ROV comes with 6 x 24V dimmable LEDs at 3520 lumens. One pair is installed on the starboard side and the second pair on the port side of the ROV. The other two LEDs are placed on the Pan and Tilt unit and on the upper porch facing backwards towards the ROV umbilical.

Hydraulics

A 4.5kW integrated hydraulic power unit (iHPU) onboard the vehicle, provides a maximum operating pressure of 210 bar and a maximum flow rate of 11.6 l/min. The pump supplies the vehicle's Orion 7P manipulator and the 7-stations valve pack with hydraulic power.

The Orion 7P manipulator, manufactured by Schilling Robotics, is installed on the starboard side of the vehicle. It is a fully proportional, hydraulic manipulator with 7 degrees of freedom. The reach of the arm is 1.5 m and has a lifting capacity of 68 kg. The Orion is remotely controlled via a Master Controller, which is a miniature of the Slave-Arm installed on the vehicle. The movement of the Master Controller directly translates into proportional movements of the Slave Arm, allowing precise operations in the centimeter range.

The Hydro-Lek HLK 73000 is a 7-station valve pack with solenoid valves to which a large variety of different hydraulic tools can be connected and operated (see tools chapter). It is primarily used to open and close the sample box on the tools kit, mounted underneath the ROV.

Vehicle telemetry

The ROV uses a single mode fiber optic telemetry in combination with a Coarse Wave Division Multiplexer (CWDM). The CWDM increases the telemetry capabilities as it splits the light in several wavelength ranges that serve as individual channels for a variety of telemetry boards for video and data. The entire vehicle telemetry runs on one single mode fiber. Solely the MiniZEUS requires a dedicated fiber, due to the large bandwidth of the HD video signal.

In addition, the ROV-Squid has a Small Survey Pod mounted inside the vehicle's frame for the integration of additional scientific sensors. Six ports for serial communication, a 1 Gigabit Ethernet link for sensors that require a high bandwidth and 2 additional PAL video channels are available.

Positioning

During RV Meteor cruise 167, the ship's USBL system POSIDONIA (IXBLUE, FR) was used for positioning the ROV. The data telegram was fed into the ROV's navigation computer and control system. In addition to the position provided by the USBL system, the MiniPOS navigation unit calculates its own position by using all vehicle sensors and the USBL input. Once the MiniPOS is aligned, the Aided Navigation mode becomes active. When available, the MiniPOS sends precise position updates at a much higher frequency compared to USBL systems. Furthermore, the Aided Navigation allows the vehicle to go into the stationkeep mode, that holds the ROV on position without being displaced in X or Y direction by the currents. While stationkeeping, the vehicle can be shifted in any X and/or Y direction at given distances with an accuracy of 10 cm.

The Squid's navigation software is a Plug-In called Posiview, coded for the open source ArcGis software QGis. A georeferenced TIFF navigation map is used as the background, displaying the ship's and ROV's heading as well as their position.

Video and Data

All navigation data from the ROV and the vessel are stored in a separate navigation file. The videos and still images contain a timestamp so they can be geo-referenced using the navigation file. The videos of the MiniZEUS and the 2x2 tiling of the four PAL camera were recorded on hard disk in the MP4 video format.

Winch and supply cable

The winch was designed and constructed by Mac-Gregor Hatlapa and weighs 4.7 t including the cable. Overall dimensions are 2.1 x 1.9 x 1.9 m (L x B x H). Maximum Line-Pull is 2.5 t on the lower layer and maximum spooling velocity are 30 m/min. The 19 mm soft umbilical was manufactured by Norddeutsche Seekabelwerke (NSW) and has a total length of ~2300 m. The inner consists of three Aramid layers, resulting in a breaking strain of 120 kN and a safe working load of 20 kN. Three 4² copper conductors supply the ROV with electrical power and 7 drain wires serve as protective earth. A total of 6 loose fitted single mode fibers are available in pairs stored inside three individual metal tubes.

Topside equipment

The 3kV topside transformer weighs 400 kg and its dimensions are 800 x 550 x 1500 mm (LxBxH). The transformer receives 400 V from the ship and converts them to 3000 VAC at 800 Hz to be supplied to the onboard transformer of the ROV. The corresponding filter box, for compensating unwanted power peaks, weighs 100 kg and has a size of 400 x 600 x 1800 mm (LxBxH).

The devices required to operate the ROV, such as the main computer with the control system, are installed into a double sized 19" flight case. Two more flight cases with Intel NUC navigation computers and monitors displaying the ROVs cameras, the sonar and navigation map, are part of the topside equipment.

5.7.3 ROV Dives

During the Meteor cruise M167 a total of 7 dives (#54-#60, Fig. 5.37) were carried out down to a maximum diving depth of 1021 mbsl (Table 5.7). The MARUM-Squid spent around 18 hours at the seafloor for the recovery of three observatories as well as three mosaic-type flights and some additional push core sampling. The same amount of time is available as MiniZEUS HD and as Tiling of four analog cameras, which were recording for the duration of the scientific work program at the seafloor. In addition, several thousands of high resolution still pictures were taken.

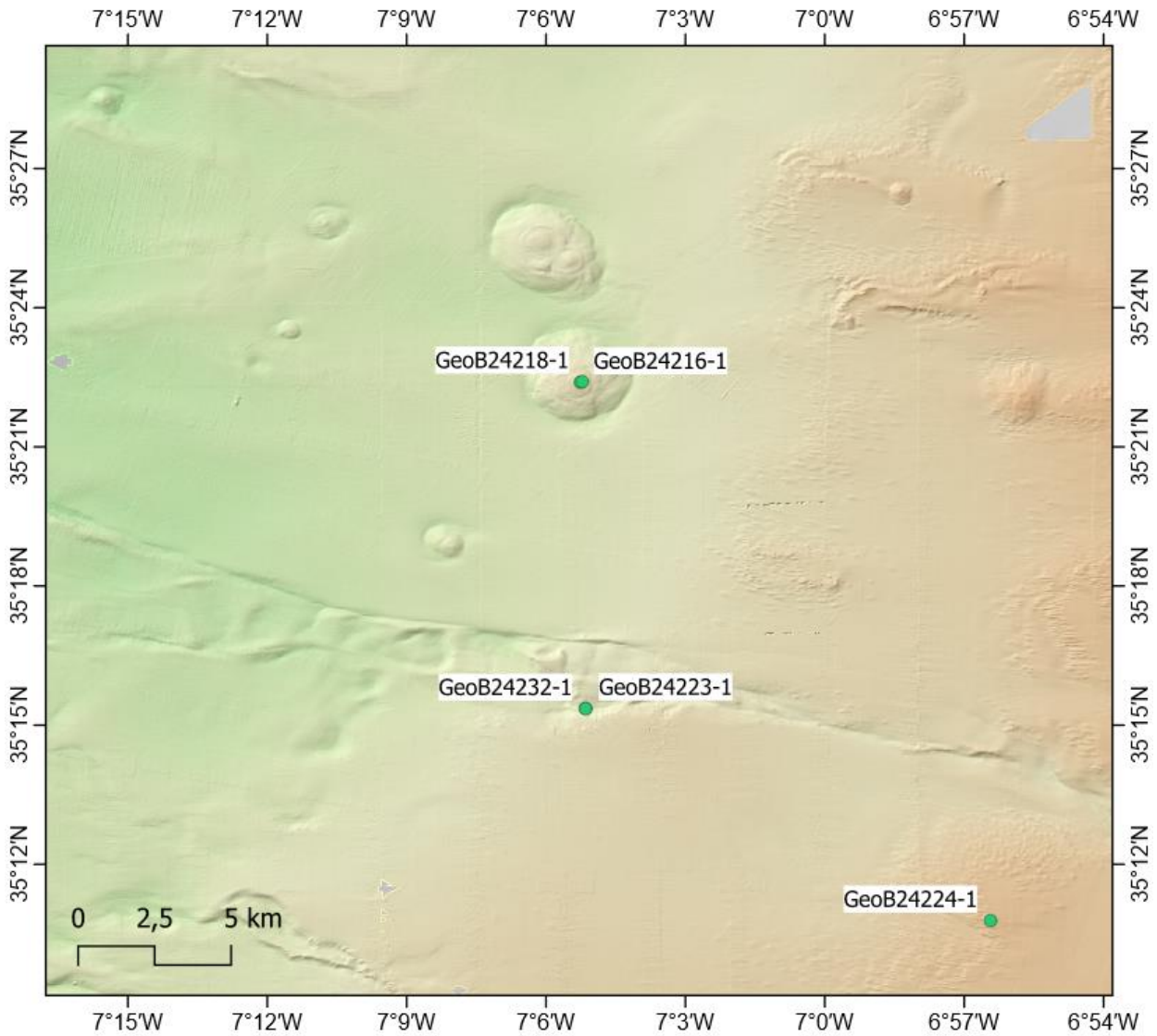


Figure 5.37: Map of ROV SQUID dives in the Gulf of Cadiz

Table 5.7: List of ROV SQUID dives during the M167

Dive#	Date	Launch Time (UTC)	Launch Position	Recovery Position	Recovery Time (UTC)	Bottom Time (hh:mm)	Max. Depth (m)
54	18.10.2020	13:13	36°23.3517'N / 02°52.2174'W	36°23.3047'N / 02°52.1749'W	17:50	02:42	964
55	19.10.2020	07:15	36°23.3440'N / 02°52.2414'W	36°23.3167'N / 02°52.2510'W	12:05	02:58	960
56	22.10.2020	13:25	35°22.3674'N / 07°5.3049'W	35°22.3747'N / 07°5.3104'W	17:48	02:32	903
57	23.10.2020	07:31	35°22.4090'N / 07°5.2415'W	35°22.3902'N / 07°5.2621'W	12:32	03:11	906

58	24.10.2020	10:05	35°15.3683'N / 07°5.1564'W	35°15.3310'N / 07°5.1558'W	13:43	01:46	1021
59	25.10.2020	08:13	35°10.7411'N / 06°56.4628'W	35°10.7247'N / 06°56.4668'W	13:25	03:25	725
60	28.10.2020	06:36	35°15.3580'N / 07°5.1866'W	35°15.3570'N / 07°5.1866'W	09:56	01:29	1020

Observatory recovery and in-situ mosaicking work

The ROV MARUM-Squid was used as a platform to recover three logging devices located inside borehole casings by the MARUM MeBo drilling system during the expedition M149 in 2018. During Dive #54 and #55, the MeBo CORK in the Alboran Sea (Carboneras fault) was first located, then brought back on deck with the help of the Orion arm (Fig 5.38).

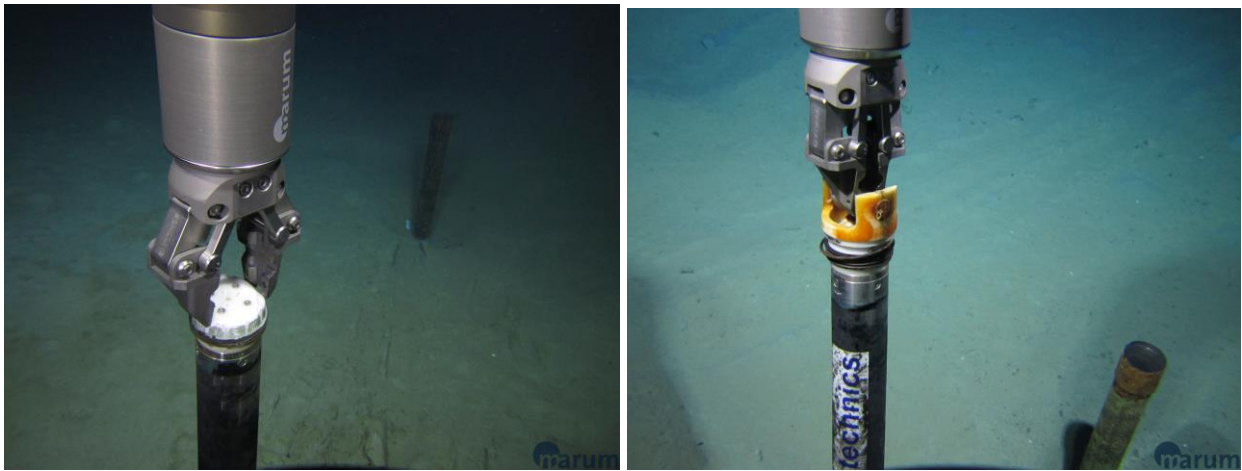
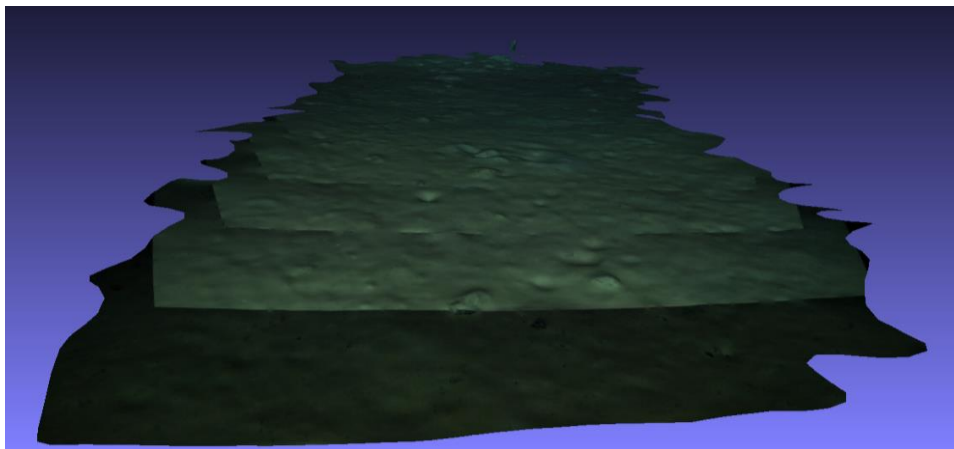


Figure 5.38: CORK recovery operations during dive #55 (left) and dive #56 (right).

On Dive #56 the second CORK was located on the summit of Ginsburg MV, in the Golf of Cadiz, and subsequently recovered (Fig 5.38). Dive #57 gave us the chance to perform the first mosaic tracks of an area of roughly 20 m² on Ginsburg MV (Fig 5.39). Unfortunately Dive #58, due to the failure of the hydraulic system, could only be used to confirm the position of the third CORK as well as to do some mosaicking work around the same CORK position (Fig 5.39).



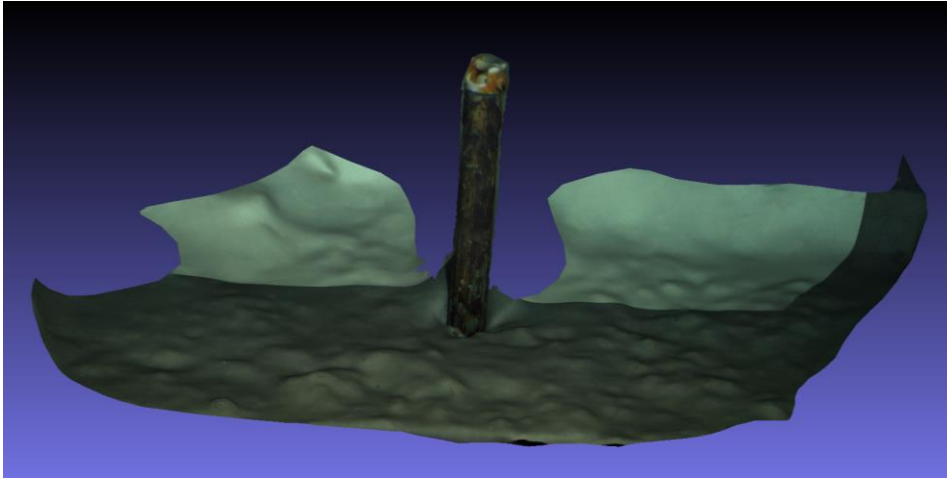


Figure 5.39: Preliminary photomosaicking results of dive #57 (upper picture) and dive #58 (lower picture).

Dive #59 was used to test again the photomosaicking technique on a coral mound. Finally, dive #60 gave us the opportunity to test a new CORK recovery procedure that does not involve any hydraulic system. As shown in the following pictures, two new tools have been custom-made on board for this specific purpose (Fig. 5.40).

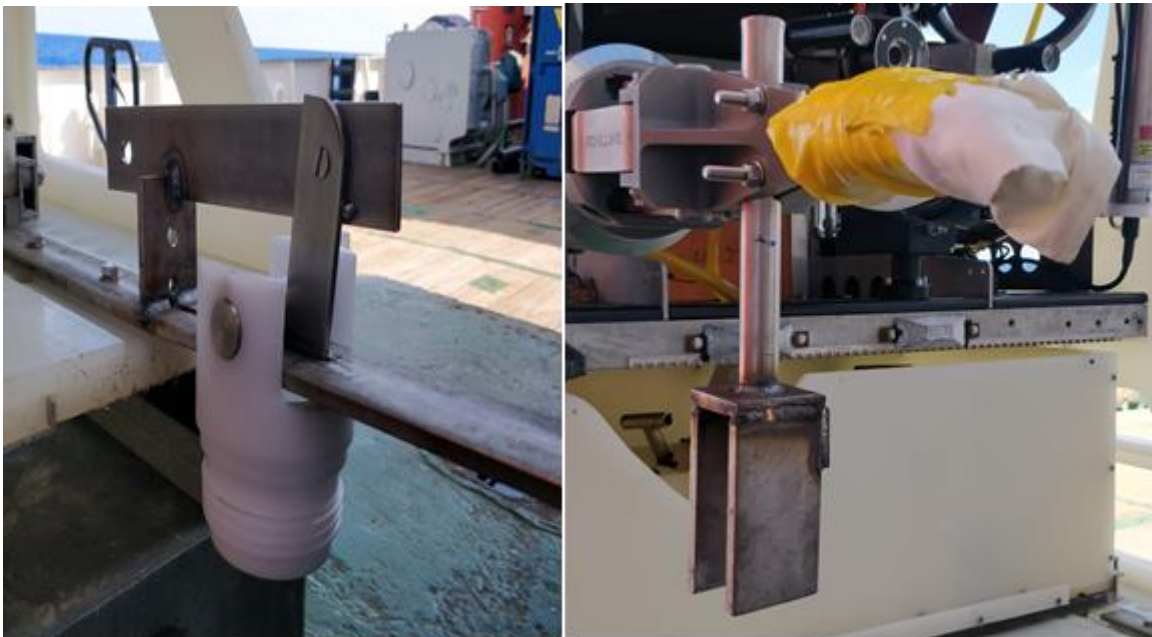


Figure 5.40: The CORK Catcher mounted on the porch (left) and the CORK Screw fixed to the inactive Orion arm(right) and used during dive #60.

5.7.4 MeBo CORKs (T. Fleischmann)

Introduction

A MeBo observatory consists of a tubular stainless-steel pressure housing that is 667 mm long, has a diameter of 76 mm and is able to withstand a pressure equivalent to 2000 m water depth (Fig. 5.41). From the lower end of the pressure housing a temperature and, if wanted, a conductivity sensor is protruding into the borehole. The temperature sensor is a high precision, long-term stable model from the IST company (Modell TSIC 501F with a -10 to 60°C

measurement range and an accuracy of $\pm 0.1^\circ\text{C}$). The conductivity sensor was purchased from Sea & Sun Technology and measures in a range from 0-60 mS/cm with an accuracy of 0.002 mS/cm.

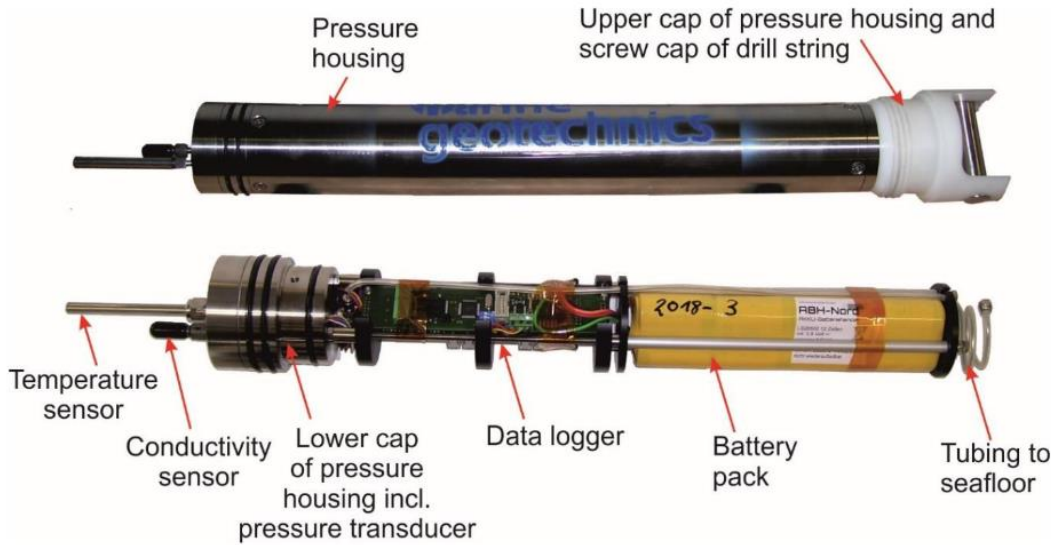


Figure 5.41: In the upper picture is illustrated the pressure housing of an observatory with the screw cap on the right side. The lower picture shows the interior of an observatory. See text for details.

An additional port connects the borehole to a differential pressure transducer (High Precision Pressure Transmitter 33X purchased from manufacturer Keller; 100 kPa differential pressure range with an accuracy of 0.05% FS). The other side of the pressure transducer is connected to the seafloor.

Preliminary Results

For the installation of each observatory, a borehole was drilled into the seafloor with MeBo during the 2018 RV Meteor M149 expedition and the casing was left in place. After reaching the target depth, the Final drill rod was replaced with one which had the observatory already screwed on. The observatory on top of the last drill rod seals the borehole from the overlying ocean water. The whole assembly was pushed down the seafloor so that approximately 50-100 cm drill pipe protruded into the water column.

Table 5.8: List of recovered observatories

Obs. Name	GeoB#	SQUID Dive#	Date / Time of recovery	Lat. / Long.	Water depth (mbsl)	Location
Christian	24205	55	19.10.2020 10:46	36°23.308'N 2°52.275'W	960	Carboneras fault
Helen	24216	56	22.10.2020 16:22	35°22.3728'N 7°5.3115'W	902	Ginsburg MV

Mechthild	24232	60	28.10.2020	35°15.3459'N	1019	Lineament Center
			08:52	7°5.1579'W		

On the cruise M167, all three observatories were successfully recovered from the sea floor by the ROV Squid team (Table 5.8). During dive 55 on October 19, 2020, the observatory called “Christian” was successfully removed from the borehole in the Alboran Sea. Unfortunately, the housing was flooded for reasons that have yet to be clarified. It is therefore unlikely that the data contained can be extracted (see Fig. 5.42). The next dive three days later took place at Ginsburg MV, in the gulf of Cadiz. There, the ROV team recovered “Helen” (Fig. 5.43). Upon opening the housing, we found a still-operating system and performed some basic system tests. After this, we disconnected the observatory from the power source and secured it for the way back to Bremen, since the data download had to be done in a properly equipped laboratory. The last observatory was recovered from the sea floor on October 28, 2020. Unfortunately, this instrument was also leaky and exploded in the water column during the ascent process. The electronics were shot back into the abyss.



Figure 5.42: Observatory “*Christian*” recovered from the Carboneras fault in the Alboran sea. The housing has leaked over the years, seriously damaging the electronics.

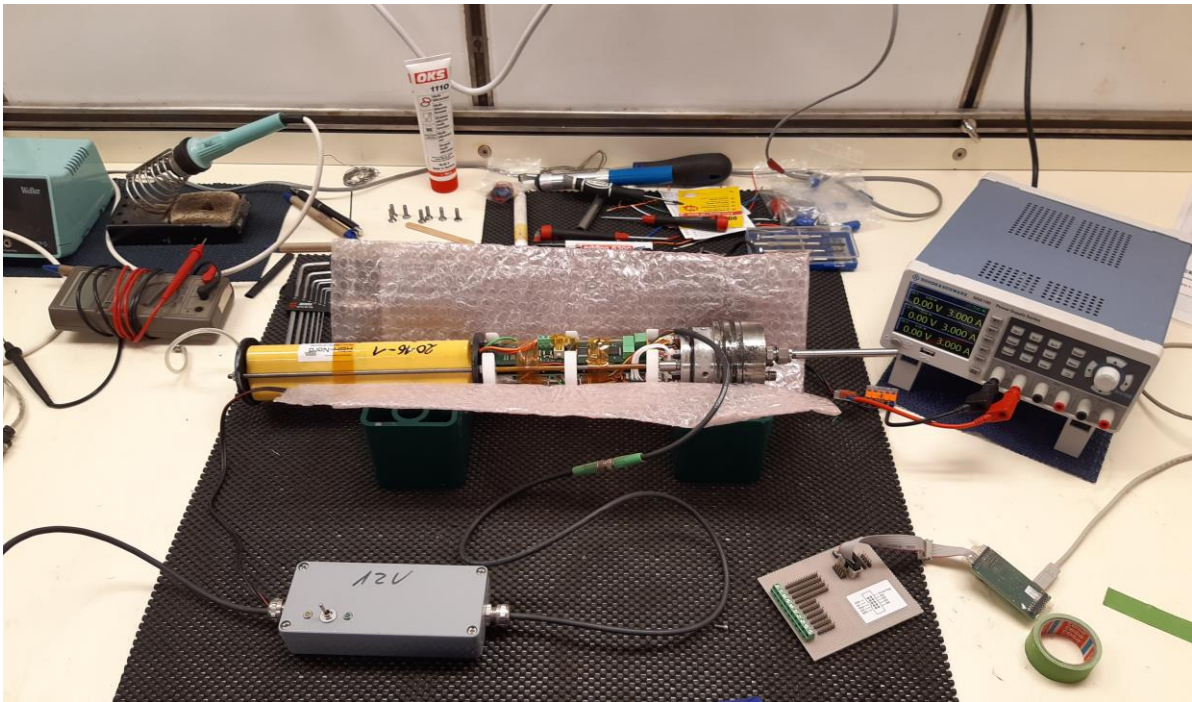


Figure 5.43: Observatory “Helen” recovered from Ginsburg MV. After opening the housing, we could successfully conduct a system test.

6 Ship’s Meteorological Station

(C. Heitmann-Bacza)

The research expedition M167 started in Emden on Sunday afternoon of Oct 11th 2020. Transfer to the research area began after passing through the sluice of Emden, with a moderate to fresh, north-west wind accompanied by occasional gale force gusts. Mainly good visibility allowed a view of the two bordering countries when arriving at the English Channel. During the track through the English Channel, a low-dominated weather with showers and gusts was predominant. Between a ridge over the Bay of Biscay and an eastward moving low north-westerly wind, wind speed increased to average 6-7 Bft with gusts of 8 Bft on Oct 13th. Significant sea reached 2 to 3 m. Afterwards, north to northeasterly wind weakened again to 4-5 Bft while sailing towards southwest along the Bay of Biscay. A high ridge over the western Mediterranean Sea caused light breeze from mainly eastern directions, with a significant sea between 0.5 and 1 m, until arriving into the Alboran Sea. During the passage of the Strait of Gibraltar, easterly to northeasterly wind temporarily reached up to 5 Bft.

After the RV Sonne crossed the RV Meteor research area in the evening of Oct 17th, the station work in the Alboran Sea began. A northeasterly wind blew around 3 Bft, a light breeze at times, significant sea was mostly around 0.5 m in the research area. Weather conditions were very good with air temperatures between 17° to 20°C, water temperatures between 18° to 22°C and fair cloud cover.

The RV Meteor left the Alboran Sea on the 20th and sailed through the Strait of Gibraltar to the Gulf of Cadiz research area in the night of the 21st. A low trough with showers, southwesterly winds of 6 Bft (later 8 Bft) and gale force gusts passed through during that night. Significant sea rose from 2 to 3 m, the swell was coming from west to southwest. Following, the

wind blew continuously from southwest with 5-6 Bft. Another trough followed with occasional showers during the night of 22nd, then northerly winds of 6 to 7 Bft and 2 to 3 m significant sea followed.

In the subsequent days, a high moved to the Azores and an associated ridge influenced the research area with westerly to northwesterly winds around 3 Bft; 5 Bft were briefly measured. Gales crossed the North Atlantic, from where a 2 m swell moved to the research area from northwest. A cold front approached from northwest, wind veered southwest to west with 5-6 Bft, and gusts of up to 8 Bft were measured in the night of Oct 26th. After that, a north-westerly wind blew with 5 Bft and the significant sea rose to 3- 3.5 m at times.

Subsequently, another Azores high ridge expanded again towards the Gulf of Cadiz, wind veered north to northeast at 4 Bft. A swell of 2 m from the northwest continued in the research area. Air temperature apart during rain showers was between 20°C to 21°C and water temperature was 22°C during research work.

The RV Meteor left the research area and began the transit to Emden on Tuesday at noon, Oct 27th. A new high-pressure area developed at the Azores and a high ridge passed over the Iberian Peninsula on 28th. At the same time, a low trough extended from Ireland to the Bay of Biscay and wind speed rose up to 5-6 Bft at times. The significant sea reached 3 m, with swell coming from the northwest.

Sailing to the north, a cold front moved across the Bay of Biscay from Oct 30th to Nov 01st. Southwesterly winds reached force 8, in gusts of 9 to 10 Bft. Rain and showers occurred sporadically. The significant wave rose to 4-5 m. During transit through the English Channel on Nov 02nd, the wind shifted to westerly directions and weakened temporarily to 6-7 Bft; the significant wave height reached 3 to 3.5 m. A small-scale low trough followed on 3rd November and the wind increased to 8 Bft again at noon. Shower gusts up to 10 Bft were measured. Once passed this trough the wind slowly decreased. Finally, the RV Meteor reached the sluice of Emden with westerly wind of 4 to 5 Bft on Wednesday, November 04th 2020 around 3 o'clock pm.

7 Station List M167

7.1 Overall Station List

GeoB Number: Curation number of the MARUM core repository

Abbreviations: EM122/ParaS = Ship-mounted Multibeam and Parasound systems; XBT = expendable bathythermograph; ROV = Remotely Operated Vehicle SQUID; B_ROV = Remotely Operated Vehicle BlueROV; GC = Gravity Corer.

NOTE: Date/Time/LAT/LONG/Water Depth are relative to either start of the operation (for EM122/ParaS, ROV, XBT, B_ROV) or seafloor conditions (GC, ROV_CORK, ROV_PHOTOMOSAIC)

GeoB Station No.	METEOR Station No.	Name/Area	Gear Type	Date	Time (UTC)	LAT (°N)	LONG (°W)	Water Depth (m)	Recovery (cm)
GeoB24201-1	M167_1-1	Carboneras Fault, Alboran Sea	EM122	17.10.2020	23:00	36°22.624'N	2°42.340' W	1205	
GeoB24201-2	M167_1-1	Carboneras Fault, Alboran Sea	XBT	17.10.2020	08:32	36°10.450'N	3°59.047'W	1230	
GeoB24202-1	M167_2-1	Carboneras Fault, Alboran Sea	ROV	18.10.2020	07:17	36° 23.336' N	2° 52.231' W	953	
GeoB24202-2	M167_3-1	Carboneras Fault, Alboran Sea	EM122	18.10.2020	09:14	36°23.149'N	2°52.306'W	963	
GeoB24203-1	M167_4-1	Carboneras Fault, Alboran Sea	ROV	18.10.2020	14:11	36°23.3149'N	2°52.22545'W	961	
GeoB24204-1	M167_5-1	Carboneras Fault, Alboran Sea	ParaS	18.10.2020	19:21	36°15.182'N	3°01.367'W	914	
GeoB24204-2	M167_7-1	Carboneras Fault, Alboran Sea	XBT	19.10.2020	07:58	36°23.342'N	2°52.166'W	957	
GeoB24205-1	M167_6-1	Carboneras Fault, Alboran Sea	ROV	19.10.2020	08:13	36°23.3257'N	2°52.2100'W	960	
GeoB24205-2	M167_6-1	Carboneras Fault, Alboran Sea	ROV	19.10.2020	10:46	36°23.3196'N	2°52.2828'W	938	
GeoB24205-5	M167_6-1	Carboneras Fault, Alboran Sea	B_ROV	19.10.2020	13:08	36°23.312'N	2°52.245'W	958,5	
GeoB24206-1	M167_9-1	Summit MV Ginsburg	GC	20.10.2020	11:45	35°22.300'N	7°05.618'W	936	255
GeoB24206-2	M167_8-1	W Morocco, Atlantic Ocean	XBT	20.10.2020	09:52	35°26.718'N	6°58.904'W	1991	
GeoB24207-1	M167_10-1	MV Ginsburg- W Flank	GC	20.10.2020	13:24	35°22.0237'N	7°06.1676'W	1012	360
GeoB24208-1	M167_11-1	Pockmarks SW Averroes MV	GC	20.10.2020	15:33	35°22.8020'N	7°12.2334'W	1190	369
GeoB24209-1	M167_12-1	Averroes MV	GC	20.10.2020	17:16	35°23.5773'N	7°11.4617'W	1100	100
GeoB24209-2	M167_13-1	N Ginsburg MV area	EM122+ParaS	20.10.2020	18:33	35°25.482'N	7°10.179'W	1678	
GeoB24209-3	M167_14-1	Averroes MV	GC	21.10.2020	08:15	35°23.5677'N	7°11.4806'W	1100	61
GeoB24210-1	M167_15-1	Boabdil MV	GC	21.10.2020	10:00	35°25.8418'N	7°10.7104'W	1100	46
GeoB24210-2	M167_15-2	Boabdil MV	GC	21.10.2020	11:34	35°25.8408'N	7°10.7099'W	1094	69

GeoB24211-1	M167_16-1	Yuma MV	GC	21.10.2020	13:23	35°25.0561'N	7°05.4521'W	950	225
GeoB24212-1	M167_17-1	Averroes MV	GC	21.10.2020	15:15	35°23.5124'N	7°11.5472'W	1116	0
GeoB24213-1	M167_18-1	Background pockmark	GC	21.10.2020	16:37	35°23.1351'N	7°11.9814'W	1146	416
GeoB24213-2	M167_19-1	NE Ginsburg MV	EM122+ParaS	21.10.2020	17:53	35°25.709'N	7°12.294'W	1158	
GeoB24214-1	M167_20-1	Possible MV #1- N of Tangier MV	GC	22.10.2020	08:00	35°40.7983'N	6°56.7317'W	975	215
GeoB24215-1	M167_21-1	Possible MV #2- N of Tangier MV	GC	22.10.2020	09:40	35°41.710'N	6°53.4879'W	890	0
GeoB24215-2	M167_21-2	Possible MV #2- N of Tangier MV	GC	22.10.2020	10:35	35°41.686'N	6°53.496'W	868	0
GeoB24216-1	M167_22-1	Ginsburg MV	ROV	22.10.2020	14:23	35°22.3910'N	7°05.2618'W	902	
GeoB24216-2	M167_22-1	Ginsburg MV	ROV	22.10.2020	16:22	35°22.3812'N	7°05.3114'W	910,5	
GeoB24217-1	M167_23-1	N Ginsburg MV area	EM122+ParaS	22.10.2020	18:31	35°23.570'N	7°06.757'W	1158	
GeoB24218-1	M167_24-1	Ginsburg MV	ROV	23.10.2020	08:30	35°22.4061'N	7°05.2280'W	905	
GeoB24218-2	M167_24-1	Ginsburg MV	ROV	23.10.2020	09:42	35°22.4043'N	7°05.2317'W	903,8	
GeoB24219-1	M167_25-1	Ginsburg MV	GC	23.10.2020	14:12	35°22.389'N	7°05.2620'W	899	129
GeoB24220-1	M167_26-1	Possible MV W of Al Gacel	GC	23.10.2020	15:59	35°27.0857'N	6°59.7623'W	833	0
GeoB24221-1	M167_27-1	Possible MV #3	GC	23.10.2020	18:05	35°39.0864'N	6°51.0523'W	858	430
GeoB24221-2	M167_28-1	N Ginsburg MV area	EM122+ParaS						
GeoB24222-1	M167_29-1	Ginsburg MV	GC	24.10.2020	07:30	35°22.4042'N	7°05.4620'W	915	241
GeoB24223-1	M167_30-1	Lineament center	ROV	24.10.2020	11:07	35°15.3582'N	7°05.1501'W	1021	
GeoB24223-2	M167_30-1	Lineament center	ROV	24.10.2020	11:50	35°15.3516'N	7°05.1554'W	1020,3	
GeoB24223-3	M167_31-1	E lineaments area	EM122+ParaS	24.10.2020	14:59	35°14.035'N	6°52.446'W	759	
GeoB24224-1	M167_32-1	Coral Mound	ROV	25.10.2020	09:04	35°10.7838'N	6°56.4353'W	735	
GeoB24224-2	M167_32-1	Coral Mound	ROV	25.10.2020	10:34	35°10.7679'N	6°56.4482'W	730,5	
GeoB24224-3	M167_32-2	Coral Mound	XBT	25.10.2020	08:12	35°10.741'N	6°56.464'W	741	
GeoB24224-4	M167_32-3	Coral Mound	B_ROV	25.10.2020	13:43	35°10.720'N	6°56.459'W	740	
GeoB24225-1	M167_33-1	Gemini 2 MV	GC	25.10.2020	16:54	35°16.863'N	6°45.433'W	421	274
GeoB24226-1	M167_34-1	Fiuzza MV	GC	25.10.2020	18:00	35°15.363'N	6°41.946'W	387	161
GeoB24227-1	M167_35-1	Al Idrisi MV	GC	25.10.2020	19:01	35°14.085'N	6°36.371'W	211	67
GeoB24227-2	M167_36-1	Southern accretionary prism	EM122+ParaS	25.10.2020	19:43	35°13.722'N	6°36.546'W	225	
GeoB24228-1	M167_37-1	Potential MV #1 Lineament South	GC	26.10.2020	07:51	34°56.7181'N	7°53.9750'W	2030	65
GeoB24228-2	M167_37-2	Potential MV #1 Lineament South	GC	26.10.2020	09:50	34°56.7051'N	7°53.9616'W	2017	0

GeoB24229-1	M167_38-1	Potential MV #3 Lineament Center	GC	26.10.2020	15:26	35°30.4016'N	8°27.6926'W	2276	343
GeoB24229-2	M167_39-1	Newly discovered MV field	EM122+ParaS	26.10.2020	16:54	35°30.425'N	8°28.492'W	2373	
GeoB24230-1	M167_40-1	Potential MV#1 New MVs Field	GC	27.10.2020	06:36	35°33.6676'N	8°01.7118'W	1670	31
GeoB24231-1	M167_41-1	Potential MV#2 New MVs Field	GC	27.10.2020	08:26	35°33.1070'N	8°03.5386'W	1717	266
GeoB24231-2	M167_42-1	Lineament North	EM122+ParaS	27.10.2020	11:05	35°31.483'N	7°56.250'W	1594	
GeoB24231-3	M167_42-2	Lineament North	XBT	27.10.2020	13:30	35°20.320'N	7°53.940'W	1727	
GeoB24232-1	M167_43-1	Lineament Center	ROV	28.10.2020	07:32	35°15.3530'N	7°05.1529'W	1019	
GeoB24232-2	M167_43-1	Lineament Center	ROV	28.10.2020	08:52	35°15.3387'N	7°05.1619'W	1018,9	
GeoB24233-1	M167_44-1	Plain SW Atlas MV	GC	28.10.2020	12:57	35°37.7627'N	7°18.7322'W	1413	145
GeoB24234-1	M167_45-1	Atlas MV	GC	28.10.2020	14:31	35°39.3028'N	7°16.8160'W	1302	272
GeoB24235-1	M167_46-1	Pockmark E of Atlas MV	GC	28.10.2020	16:15	35°38.6690'N	7°15.6359'W	1380	0
GeoB24236-1	M167_47-1	Potential MV E of Atlas MV	GC	28.10.2020	17:42	35°38.6229'N	7°13.892'W	1194	241
GeoB24236-2	M167_48-1	Lineament North	EM122+ParaS	28.10.2020	20:13	35°42.358'N	7°35.039'W	1441	
GeoB24237-1	M167_49-1	Jesus Baraza MV	GC	29.10.2020	06:29	35°35.4288'N	7°12.0791'W	1090	132
GeoB24238-1	M167_50-1	Depression W of Student MV	GC	29.10.2020	08:32	35°30.959'N	7°09.410'W	1131	433
GeoB24239-1	M167_51-1	Student MV	GC	29.10.2020	09:49	35°30.807'N	7°08.755'W	950	209
GeoB24239-2	M167_51-1	Student MV	B_ROV	29.10.2020	10:25	35°30.807'N	7°08.750'W	948	

7.2 Profiles Station List

Survey No.	GeoB	Start (UTC)		End (UTC)		Location	Instruments	PS70 Profiles		EM122 Lines		EM710 Lines		Remarks
		Date	Time	Date	Time			from	to	from	to	from	to	
0	-	15.10.2020	09:13	16.10.2020	18:31	Transit to the Alboran Sea	EM122 (PS70)			001	061			Underway transit, data will not be further processed
1	GeoB24201-1	17.10.2020	23:00	18.10.2020	05:50	Caboneras Fault, Alboran Sea	EM122, EM710			001	018	001	016	
2	GeoB24202-2	18.10.2020	09:15	18.10.2020	12:46	Caboneras Fault, Alboran Sea	EM122			019	028			
3	GeoB24204-1	18.10.2020	19:20	19.10.2020	06:35	Caboneras Fault, Alboran Sea	PS70	1	15					
4	-	19.10.2020	12:11	20.10.2020	11:20	Transit from the Alboran Sea to the Gulf of Cadiz	EM122			029	071			Transit to the Gulf of Cadiz, only lines 060 to 070 were processed
5	GeoB24209-2	20.10.2020	18:31	21.10.2020	06:53	N Ginsburg MV area	EM122			072	103			
6	GeoB24213-2	21.10.2020	17:47	22.10.2020	07:22	N Ginsburg MV area	EM122, PS70	16	27	104	140			different settings for the Parasound (SLF = 3.5 khz)
7	-	22.10.2020	11:45	22.10.2020	12:39	Transit to MV Ginsburg	EM122			141	142			
8	GeoB24217-1	22.10.2020	18:28	23.10.2020	06:53	N Ginsburg MV area	EM122, PS70	28	39	143	179			
9	-	23.10.2020	16:47	23.10.2020	18:07	Transit to possible Mudvolcano in the northern Gulf of Cadiz	EM122			180	183			
10	GeoB24221-2	23.10.2020	19:17	24.10.2020	06:51	N Ginsburg MV area	EM122, PS70	40	53	184	224			
11	GeoB24223-2	24.10.2020	14:49	25.10.2020	07:31	E Lineament area	EM122, EM710, PS70	54	69	225	275	017	056	
12	-	25.10.2020	16:12	25.10.2020	20:42	Transit to GC stations	EM122			276	287			
13	GeoB24227-2	25.10.2020	20:42	26.10.2020	16:44	Western Gulf of Cadiz, transit between GC	EM122, PS70	70	77	288	332			No PS data for about 2h due to technical problems, no PS data during the transits

						stations							
14	GeoB24229-2	26.10.2020	16:46	27.10.2020	10:50	Potential mudvolcano field	EM122, PS70	78	86	333	375		
15	GeoB24231-2	27.10.2020	11:06	28.10.2020	06:11	Potential mudvolcano field - western Gulf of Cadiz	EM122, PS70	87	95	376	427		
16	GeoB24236-2	28.10.2020	18:40	29.10.2020	06:06	North Lineament	EM122, PS70	96	101	429	451		
17	-	29.10.2020	11:47	31.10.2020	04:02	Transit in Portuguese Waters	EM122			452	536	Underway transit, data will not be further processed	

8 Data and Sample Storage and Availability

Metadata of the cruise and the Station List were submitted to the Pangaea data bank (www.pangaea.de). Sediment cores recovered during the M167 cruise are stored at the University of Bremen, in the MARUM Core Repository: (www.marum.de/Infrastruktur/MARUM-GeoB-Kernlager.html). Samples from these cores are available upon request to the Chief Scientist Walter Menapace (menapace@uni-bremen.de). Shipboard collected pore water and headspace samples remain with the Geotechnics group at MARUM (contact person: A. Kopf, akopf@marum.de). Interested scientists can request samples after the three years moratorium period. In addition, further data will be submitted to Pangaea along with upcoming scientific publications.

Table 8.1 Overview of data availability

Type	Database	Available	Free Access	Contact
Station List	PANGAEA	Online	✓	menapace@uni-bremen.de
Termosalinograph data	PANGAEA	Online	✓	menapace@uni-bremen.de
Hydroacoustic Data (Multibeam, Parasound)	PANGAEA	October 2021	October 2024	menapace@uni-bremen.de
Lithologs	Attached to this report	October 2021	✓	menapace@uni-bremen.de
Onboard Porewater geochemistry	PANGAEA	October 2021	October 2024	menapace@uni-bremen.de
Sediments physical properties	PANGAEA	October 2021	October 2024	menapace@uni-bremen.de

9 Acknowledgements

All participants of Expedition M167 thank the countries of Morocco, Portugal and Spain for the permission of research in their Exclusive Economic Zone. The captain and crew of R/V Meteor are thanked for their support, which immensely contributed to the success of the expedition. Particular gratitude goes also to the German Research Foundation, the German Research Fleet Coordination Centre and the shipping company Briese Research, for the tremendous support they have provided. This cruise was funded by the EU Marine Robots project and it was planned, coordinated and carried out with the help of MARUM “Center for Marine Environmental Sciences” at the University of Bremen.

10 References

- Blum, P. (1997). Physical properties handbook: a guide to the shipboard measurement of physical properties of deep-sea cores.
- Caress, D.W. and Chayes, D.N. (1996). Improved processing of Hydrosweep DS multibeam data on the R/V Maurice Ewing. *Marine Geophysical Researches* 18, 631–650.
- Chatterjee, S., Dickens, G. R., Bhatnagar, G., Chapman, W. G., Dugan, B., Snyder, G. T., and Hirasaki, G. J., (2011). Pore water sulfate, alkalinity, and carbon isotope profiles in shallow sediment above marine gas hydrate systems: A numerical modeling perspective: *Journal of Geophysical Research*, v. 116, no. B9, p. B09103.

- Crutchley, G. J., Berndt, C., Klaeschen, D., & Masson, D. G. (2011). Insights into active deformation in the Gulf of Cadiz from new 3-D seismic and high-resolution bathymetry data. *Geochemistry, Geophysics, Geosystems*, 12(7).
- Cunha, T. A., Matias, L. M., Terrinha, P., Negredo, A. M., Rosas, F., Fernandes, R. M. S., & Pinheiro, L. M. (2012). Neotectonics of the SW Iberia margin, Gulf of Cadiz and Alboran Sea: a reassessment including recent structural, seismic and geodetic data. *Geophysical Journal International*, 188(3), 850-872.
- Duarte, J. C., Rosas, F. M., Terrinha, P., Schellart, W. P., Boutelier, D., Gutscher, M. A., & Ribeiro, A. (2013). Are subduction zones invading the Atlantic? Evidence from the southwest Iberia margin. *Geology*, 41(8), 839-842.
- Gomez de la Pena, L., Ranero, C. R., & Gràcia, E. (2018). The crustal domains of the Alboran Basin (western Mediterranean). *Tectonics*, 37(10), 3352-3377.
- Gutscher, M. A., Dominguez, S., Westbrook, G. K., Gente, P., Babonneau, N., Mulder, T., ... & Terrinha, P. (2009). Tectonic shortening and gravitational spreading in the Gulf of Cadiz accretionary wedge: Observations from multi-beam bathymetry and seismic profiling. *Marine and Petroleum Geology*, 26(5), 647-659.
- Gutscher, M. A., Dominguez, S., Westbrook, G. K., Le Roy, P., Rosas, F., Duarte, J. C., ... & Sallarès, V. (2012). The Gibraltar subduction: A decade of new geophysical data. *Tectonophysics*, 574, 72-91.
- Haffert, L., Haeckel, M., Liebetrau, V., Berndt, C., Hensen, C., Nuzzo, M., Reitz, A., Scholz, F., Schönfeld, J., Perez-Garcia, C., and Weise, S. M., (2013). Fluid evolution and authigenic mineral paragenesis related to salt diapirism - The Mercator mud volcano in the Gulf of Cadiz: *Geochimica et Cosmochimica Acta*, v. 106, p. 261-286.
- Haffert, L., & Haeckel, M. (2019). Quantification of non-ideal effects on diagenetic processes along extreme salinity gradients at the Mercator mud volcano in the Gulf of Cadiz. *Geochimica et Cosmochimica Acta*, 244, 366-382.
- Hebbeln, D., Bender, M., Gaide, S., Titschack, J., Vandorpe, T., Van Rooij, D., Wintersteller, P. and Wienber, C. (2019). Thousands of cold-water coral mounds along the Moroccan Atlantic continental margin: Distribution and morphometry. *Marine Geology* 411, 51-61.
- Hensen, C., Nuzzo, M., Hornibrook, E., Pinheiro, L. M., Bock, B., Magalhães, V.H. and Brückmann, W. (2007). Sources of mud volcano fluids in the Gulf of Cadiz—indications for hydrothermal imprint. *Geochimica et Cosmochimica Acta* 71, Issue 5, 1232-1248.
- Hensen, C., Scholz, F., Nuzzo, M., Valadares, V., Gràcia, E., Terrinha, P., Liebetrau, V., Kaul, N., Silva, S., Martínez-Lorient, S., Bartolome, R., Piñero, E., Magalhães, V. H., Schmidt, M., Weise, S. M., Cunha, M., Hilario, A., Perea, H., Rovelli, L., and Lackschewitz, K., (2015). Strike-slip faults mediate the rise of crustal-derived fluids and mud volcanism in the deep sea: *Geology*, v. 43, no. 4, p. 339-342.
- Hüpers, A., Menapace, W., Magalhaes, V., Freudenthal, T., and Cruise Participants (2020). Report and preliminary results of R/V METEOR cruise M149: Shipboard and Post-Cruise Analyses, Recurrence of tsunamigenic hazards from MeBo drilling records and hazard mitigation using MeBo observatories, Las Palmas (Canary Islands) – Cadiz (Spain), 24.07.2018 – 24.08.2018. doi.org/10.26092/elib/100
- Ivanov, M. K., Kenyon, N., Nielsen, T., Wheeler, A., Monteiro, H., Gardner, J., ... & Akhmetzhanov, G. (2000). Goals and principal results of the TTR-9 cruise. *IOC. UNESCO Worksh Rep*, 168, 3-4.
- Judd, A. and Hovland, M. (2007). *Seabed Fluid Flow: The Impact on Geology, Biology and the Marine Environment*. Cambridge University Press, 475 pp.
- León, R., Somoza, L., Medialdea, T., Hernández-Molina, F. J., Vázquez, J. T., Díaz-del-Río, V., and González, F. J., (2010). Pockmarks, collapses and blind valleys in the Gulf of Cádiz: *Geo-Marine Letters*, v. 30, no. 3-4, p. 231-247.
- Levitus, S. (1982). *Climatological Atlas of the World Ocean*, NOAA/ERL GFDL Professional Paper 13, Princeton, N.J., 173 pp. (NTIS PB83-184093)
- Manga, M., Brumm, M., & Rudolph, M. L. (2009). Earthquake triggering of mud volcanoes. *Marine and Petroleum Geology*, 26(9), 1785-1798.
- Medialdea, T., Vegas, R., Somoza, L., Vázquez, J. T., Maldonado, A., Díaz-del-Río, V., ... & Fernández-Puga, M. C. (2004). Structure and evolution of the “Olistostrome” complex of the Gibraltar Arc in the Gulf of Cádiz (eastern Central Atlantic): evidence from two long seismic cross-sections. *Marine Geology*, 209(1-4), 173-198.

- Medialdea, T., Somoza, L., Pinheiro, L. M., Fernández-Puga, M. C., Vázquez, J. T., León, R., ... & Vegas, R. (2009). Tectonics and mud volcano development in the Gulf of Cádiz. *Marine Geology*, 261(1-4), 48-63.
- Menapace, W., Völker, D., Sahling, H., Zoellner, C., dos Santos Ferreira, C., Bohrmann, G., & Kopf, A. (2017). Long-term in situ observations at the Athina mud volcano, Eastern Mediterranean: Taking the pulse of mud volcanism. *Tectonophysics*, 721, 12-27.
- Munsell Color Co. (1975). *Munsell Soil Color Charts*. Munsell Color, Macbeth Division of Kollmorgen Corporation, Maryland.
- Pinheiro, L.M., Ivanov, M.K., Sautkin, A.P., Akhmanov, G.G., Magalhães, V.H., Volkonskaya, A., Monteiro, H., Somoza, L., Gardner, J., Hamouni, N. and Cunha, M.R. (2003). Mud volcanism in the Gulf of Cadiz: results from the TTR-10 cruise. *Mar. Geol.* 195, 131–151
- Platt, J. P., Behr, W. M., Johannesen, K., & Williams, J. R. (2013). The Betic-Rif arc and its orogenic hinterland: a review. *Annual Review of Earth and Planetary Sciences*, 41, 313-357.
- Rutter, E.H., Faulkner, D.R. and Burgess, R. (2012). Structure and geological history of the Carboneras Fault Zone, SE Spain: Part of a stretching transform fault system. *Journal of Structural Geology* 45, 68-86.
- Schmidt, C., Burwicz, E., Hensen, C., Wallmann, K., Martinez-Lorient, S., and Gracia, E., (2018). Genesis of mud volcano fluids in the Gulf of Cadiz using a novel basin-scale model approach: *Geochimica et Cosmochimica Acta*, v. 243, p. 186-204.
- Scholz, F., Hensen, C., Reitz, A., Romer, R. L., Liebetrau, V., Meixner, A., Weise, S. M., and Haeckel, M., (2009). Isotopic evidence ($^{87}\text{Sr}/^{86}\text{Sr}$, $\delta^7\text{Li}$) for alteration of the oceanic crust at deep-rooted mud volcanoes in the Gulf of Cadiz, NE Atlantic Ocean: *Geochimica et Cosmochimica Acta*, v. 73, no. 19, p. 5444-5459.
- Silva, S., Terrinha, P., Matias, L., Duarte, J. C., Roque, C., Ranero, C. R., ... & Zitellini, N. (2017). Micro-seismicity in the Gulf of Cadiz: Is there a link between micro-seismicity, high magnitude earthquakes and active faults? *Tectonophysics*, 717, 226-241.
- Somoza, L., Díaz-del-Río, V., León, R., Ivanov, M., Fernández-Puga, M. C., Gardner, J. M., ... & Maestro, A. (2003). Seabed morphology and hydrocarbon seepage in the Gulf of Cadiz mud volcano area: Acoustic imagery, multibeam and ultra-high resolution seismic data. *Marine geology*, 195(1-4), 153-176.
- Spakman, W., Chertova, M. V., van den Berg, A., & van Hinsbergen, D. J. (2018). Puzzling features of western Mediterranean tectonics explained by slab dragging. *Nature Geoscience*, 11(3), 211.
- Toyos, M. H., Medialdea, T., León, R., Somoza, L., González, F. J., & Meléndez, N. (2016). Evidence of episodic long-lived eruptions in the Yuma, Ginsburg, Jesús Baraza and Tasyo mud volcanoes, Gulf of Cádiz. *Geo-Marine Letters*, 36(3), 197-214.
- Vanneste, H., James, R. H., Kelly-Gerreyn, B. A., & Mills, R. A. (2013). Authigenic barite records of methane seepage at the Carlos Ribeiro mud volcano (Gulf of Cadiz). *Chemical Geology*, 354, 42-54.
- Wessel P. and Smith, W.H.F. (1998). New, improved version of generic mapping tools released. *Eos, Trans. Am. Geophys. Union* 79, 579. [dx.doi.org/10.1029/98EO00426](https://doi.org/10.1029/98EO00426)
- Zitellini, N., Gràcia, E., Matias, L., Terrinha, P., Abreu, M.A., DeAlteriis, G., Henriot, J.P., Dañobeitia, J.J., Masson, D.G., Mulder, T., Ramella, R., Somoza, L. and Diez, S. (2009). The quest for the Africa–Eurasia plate boundary west of the Strait of Gibraltar. *Earth and Planetary Science Letters*, 280, 13-50.

11 Appendices

11.1 Lithologs

R/V METEOR M167	Station: M167_ GeoB 24206-1
Location: Summit Ginsburg MV	Date: 20.10.20, 11:14:00 (UTC)
Latitude: 35°22.300'N	
Longitude: 7° 05.651'W	
Water depth: 936 m	Recovery: 255.00 cm

Depth (cmbsf)	LITHOLOGY				Description	
	Photos	Log	Color	Struct.		
0			10YR 5/2	⊗	0 - 2.5 cm: filling foam	
2.5 - 16 cm			H ₂ S	☼	2.5 - 16 cm: oxidized mud breccia covered by a water-saturated hemipelagic sediment layer (2.5 - 4 cm), bearing sand (likely foraminifera). Gradual contact with the underlying sediments	
16 cm					⊗	16 cm: sub-cm bioclast (bivalve shell)
16 - 255 cm						16 - 255 cm: mud breccia with sparse mm-size polygenetic clasts (mud, lithic and bioclasts). Anoxic, H ₂ S smell. Constant colour through the core until ca. 130 cm, where light gray mud clasts and patches appear on the splitted surface.
21 cm					○	21 cm: cm-size echinoderm spine fragment
25 - 27 cm					○	25 - 27 cm: sub-cm dark gray mud clast (10YR 3/1)
89 - 92 cm					H ₂ S	89 - 92 cm: cm greenish gray mud clast (GLEY 2 10G 5/1)
121 - 123 cm					○	121 - 123 cm: 3-cm light gray mud clast (GLEY 1 10Y 7/1). Potential high carbonate content
146 cm					○	146 cm: sub-cm greenish gray clast (GLEY 1 10GY 5/1)
146.5 - 147.5 cm						146.5 - 147.5 cm: greenish gray patch (GLEY 1 5G 5/1)
167.5 - 171 cm						167.5 - 171 cm: greenish gray patch (GLEY 1 5G 5/1)
191 - 194.5 cm					○	191 - 194.5 cm: 3-cm dark gray mud clast (10YR 3/1)
210 - 215 cm					H ₂ S	210 - 215 cm: greenish gray patch (GLEY 1 5G 6/1)
231 - 232 cm					○	231 - 232 cm: cm-size mud clast
235 - 246 cm					☼	235 - 246 cm: coral fragments (<i>L. pertusa</i>)
241 - 245 cm					☼	241 - 245 cm: 4-cm coral fragment (<i>L. pertusa</i>) covered by bryzoans(?)
252 - 255 cm						252 - 255 cm: empty portion, core-catcher material
300						
350						
400						
450						
500						
550						

R/V METEOR M167

Station: M167_GeoB 24207-1

Location: Ginsburg MV, western flank

Date: 20.10.20, 13:24:00 (UTC)

Latitude: 35°22.0237'N

Longitude: 7° 06.1676'W

Water depth: 1012 m

Recovery: 360.00 cm

LITHOLOGY				
Depth (cmbsf)	Photos	Log	Color	Description
0			2.5Y 5/4	0 - 6,5 cm: filling foam
0-50				6.5 -13 cm: oxidized mud breccia. Water saturated (6.5 - 8 cm). High content of mm-size clasts (likely foraminifera).
0-360				13 - 360 cm: mud breccia with sparse mm-size poligenetic clasts (mud, lithic and bioclasts). Anoxic, H ₂ S smell, decreasing to the bottom. Constant color through the core until ca. 180 cm, where dark gray patches appear on the splitted surface.
85.5-86.5				85.5 - 86.5 cm: cm-size mud clast
163				163 cm: sub-cm mud clast
181-183				181 - 183 cm: sub-cm sandy mud clast
196-201				196 - 201 cm: dark grey patch
225-226				225 - 226 cm: sub-cm greenish grey mud clast (GLEY 5G 5/1)
227.5-232				227.5 - 232 cm: dark gray layered patches (GLEY 1 5/N)
274-276				274 - 276 cm: light gray patch (GLEY 1 10Y 7/1)
313-314				313 - 314 cm: sub-cm mud clast (10YR 5/1)
325-328				325 - 328 cm: elongated cm. mud clast (10YR 5/1)
333-339				333 - 339 cm: elongated dark gray patch (GLEY 1 5/N)
342-344				342 - 344 cm: dark gray sub-cm mud clast (GLEY 1 5/N)
357-358				357 - 358 cm: greenish gray sub-cm mud clast (GLEY 1 5G 5/1)

R/V METEOR M167

Station: M167_ GeoB 24208-1

Location: Pockmark SW Averroes MV

Date: 20.10.20, 15:33:00 (UTC)

Latitude: 35°22.8020'N

Longitude: 7°12.2334'W

Water depth: 1190 m

Recovery: 369.00 cm

LITHOLOGY					
Depth (cmbsf)	Photos	Log	Color	Struct.	Description
0			10YR 6/3	☉	0 - 6 cm: filling foam
50				H ₂ S	6 - 7 cm: oxidized surface sediments. Silty mud bearing fine sand (likely foraminifera)
100			GLE Y 1 5G 5/1	☉	7 - 369 cm: silty mud bearing fine sand (likely microfossil). Anoxic, H ₂ S smell. Occurrence of moussy texture in several locations. Gas hydrates inferred from empty portions at different depths, unexpected larger water release during the removal of the core from the gravity corer pipe, anoxic conditions, site location (pockmark)
150				☉	7 - 47 cm: relative high amount of water compared to the rest of the core
200				H ₂ S	74 - 75 cm: moussy texture in an elongated lens
250				☉	77 - 78 cm: cm-size bioclast
300				☉	84 - 85 cm: moussy texture in a circular lens
350				H ₂ S	88 - 89 cm: moussy texture in an oval lens
400				☉	89.5 - 94 cm: moussy texture in a sub-circular lens
450				☉	100 - 101 cm: moussy texture in an oval lens
500				☉	107 - 119 cm: elongated moussy structure. Likely gas-rich fluid escaping structure, with a core centered at 115 - 119 cm
550				☉	127 - 139 cm: empty interval (filled by foam, after line-scansion)
				☉	139 - 152.5 cm: relative higher concentration of microfossils and/or mm-size bioclasts
				☉	144 - 150 cm: moussy texture, interrupted by the underlying cavity
				☉	152.5 - 164.5 cm: empty interval (filled by foam, after line-scansion)
				☉	169 - 176 cm: layer with diffuse moussy texture
				☉	176 - 178 cm: sub-horizontal shear deformation
				☉	182 - 187 cm: scaphopod
				☉	189 - 194 cm: layer with diffuse moussy texture
				☉	196.5 - 199 cm: moussy structure in a sub-circular lens, associated to cm-size bioclast (bivalve shell fragment).
				☉	213 - 220 cm: layer with diffuse moussy texture
				☉	222 - 232 cm: layer with diffuse moussy texture
				☉	236 - 242.5 cm: moussy texture in a sub-circular lens
				☉	244 - 252 cm: moussy texture in an elongated lens, located along the plastic liner
				☉	255 - 259 cm: moussy texture in a sub-circular lens, associated with cm-size bioclast
				☉	264 - 269 cm: deformation cracks
				☉	269 - 272 cm: partially empty portion
				☉	276 - 369 cm: stiff highly-coesive sediment
				H ₂ S	276 - 292 cm: sub-horizontal shear fractures
				☉	307 - 309 cm: sub-horizontal shear fracture
				☉	333.5 - 336.5 cm: sub-horizontal shear fracture
				☉	346 - 348 cm: cm-size bioclast (bivalve shell fragment), with associated minor fragments
				☉	354.5 - 369 cm: empty portion (core catcher), filled by foam after line-scansion

R/V METEOR M167

Station: M167_GeoB 24209-1

Location: Averroes MV

Date: 20.10.20, 17:16:00 (UTC)

Latitude: 35°23.5773'N

Longitude: 7°11.4617'W

Water depth: 1100 m

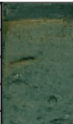


Recovery: 100.00 cm

LITHOLOGY					
Depth (cmbsf)	Photos	Log	Color	Struct.	Description
0			10YR 5/4		0 - 15 cm: filling foam on the left side
0 - 6 cm					oxidized mud breccia covered by a water-saturated hemipelagic sediment layer (0 - 2 cm), bearing fine sand (likely foraminifera). Gradual contact with the underlying sediments
2 - 3 cm					2-cm-size bioclast (bivalve shell)
6 - 100 cm					mud breccia with sparse mm-size polygenetic clasts (mud, lithic and bioclasts). Anoxic, H ₂ S smell.
6 - 35 cm					yellowish brown patches (10YR 5/4), likely derived from the upper oxidized layer.
26 - 29 cm					elongated dark gray patch (GLEY 1 5/N)
36 cm					dark gray patch (GLEY 1 5/N)
44 - 46 cm					dark gray patch (GLEY 1 5/N)
46 - 52 cm					imprint of a large mud clast (working half)
48.5 - 54 cm					large mud clast, poorly lithified
52.5 - 56.5 cm					imprint of a large mud clast (working half)
54 - 58 cm					large mud clast, poorly lithified
62 - 63.5 cm					cm-size mud clast
77.5 - 85 cm					imprint of a large mud clast, conglomerate with polygenetic clasts likely lithified by carbonate-rich cement (working half)
87 - 90 cm					large mud clast, poorly lithified
50			GLEY 1 6/N	H ₂ S 	
100					
150					
200					
250					
300					
350					
400					
450					
500					
550					








R/V METEOR M167	Station: M167_ GeoB 24209-3
Location: Averroes MV	Date: 21.10.20, 08:15:00 (UTC)
Latitude: 35°23.5677'N	
Longitude: 7°11.4806'W	
Water depth: 1100 m	Recovery: 61.00 cm

Depth (cmbsf)	LITHOLOGY				Description
	Photos	Log	Color	Struct.	
0			10YR 5/4	⊗	0 - 2 cm: filling foam 2 - 6.5 cm: oxidized mud breccia covered by a water-saturated hemipelagic sediments (2 - 4 cm), bearing fine sand (likely foraminifera). Gradual contact with the underlying sediments 6.5 - 61 cm: mud breccia with sparse mm-size poligenetic clasts (mud, lithic and bioclasts). Anoxic, H ₂ S smell. Gradually colour change from upper oxidized layer until 18.5 cm 22 - 26.5 cm: large size mud clast (likely carbonate-cemented) 28 - 30.5 cm: coral fragment(?), likely covered by bryzoans 42 - 46 cm: carbonate-cemented large sandy mud clast
50			10YR 6/2 GLEY 1 6/N	⊗ ⊗	
100					
150					
200					
250					
300					
350					
400					
450					
500					
550					

R/V METEOR M167	Station: M167_GeoB24210-1
Location: Boabdil MV	Date: 21.10.20, 10:00:00 (UTC)
Latitude: 35°25.8418'N	
Longitude: 7°10.7104'W	
Water depth: 1100 m	Recovery: 46.00 cm

Depth (cmbstf)	LITHOLOGY				Description
	Photos	Log	Color	Struct.	
0			10YR 5/4 GLEY 1 6/N		<p>0 - 6.5 cm: filling foam</p> <p>6.5 - 8 cm: oxidized mud breccia covered by a water-saturated hemipelagic sediments bearing fine sand (likely foraminifera). Gradual contact with the underlying sediments</p> <p>8 - 46 cm: mud breccia with sparse mm-size poligenetic clasts (mud, lithic and bioclasts). Anoxic, H₂S smell. Gradually colour change from upper oxidized layer until 28 cm</p> <p>20.5 - 25 cm: bioturbation hole with oxydized sediments</p> <p>26.5 - 29 cm: large bioclast (bivalve shell fragment)</p> <p>32 - 34 cm: dark gray patch (GLEY 1 5G 4/1)</p> <p>34 - 37 cm: cm-size mud clast (carbonate-cemented)</p> <p>41 - 42 cm: sub-cm bioclast (bivalve shell fragment)</p> <p>43 - 46 cm: large mud clast with an altered surface (GLEY 1 5G 5/2)</p>
50					
100					
150					
200					
250					
300					
350					
400					
450					
500					
550					

R/V METEOR M167	Station: M167_GeoB24210-2
Location: Boabdil MV	Date: 21.10.20, 11:34:00 (UTC)
Latitude: 35°25.8408'N	Recovery: 69.00 cm
Longitude: 7°10.7099'W	
Water depth: 1094 m	

Depth (cmbsf)	LITHOLOGY				Description
	Photos	Log	Color	Struct.	
0			2.5Y 6/4		0 - 8.5 cm: filling foam
50			GLEY 1 6/N	 	8.5 - 10 cm: oxidized mud breccia covered by a water-saturated hemipelagic sediment, bearing fine sand (likely foraminifera). Gradual contact with the underlying sediments 10 - 61 cm: mud breccia with sparse mm-size polygenetic clasts (mud, lithic and bioclasts). Anoxic, H ₂ S smell 28 - 32 cm: large bioclast (bivalve shell fragment) 42 - 44 cm: cm-size greenish gray mud clast (GLEY1 5G 5/1) 61 - 69 cm: filling foam
100					
150					
200					
250					
300					
350					
400					
450					
500					
550					

R/V METEOR M167

Station: M167_GeoB24211-1

Location: Yuma MV



Date: 21.10.20, 13:23:00 (UTC)

Latitude: 35°25.0561'N

Longitude: 7°05.4521'W

Water depth: 950 m

Recovery: 225.00 cm

LITHOLOGY				
Depth (cmbsf)	Photos	Log	Color	Description
0			10YR 4/4	<p>0 - 2 cm: filling foam</p> <p>2 - 4 cm: oxidized mud breccia covered by a water-saturated hemipelagic sediment, bearing fine sand (likely foraminifera). Gradual contact with the underlying sediments.</p> <p>4 - 225 cm: mud breccia with sparse mm-size poligenetic clasts (mud, lithic and bioclasts). Anoxic, H₂S smell. Gradual increase of cohesion through the core. Several sub-cm holes (fluid releasing structure likely formed after core splitting)</p> <p>14.5 - 15.5 cm: sub-cm dark gray mud clast (GLEY 1 5/N)</p> <p>23 - 24 cm: sub-cm light gray mud clast (5Y 7/1)</p>
50			GLEY 1 5G 5/1	<p>103/105.5 - 107/109.5 cm: filling foam (inclined)</p> <p>130 - 133 cm: sub-horizontal expansion crack</p> <p>153 - 157 cm: small sub-horizontal expansion cracks</p> <p>165 - 167 cm: sub-horizontal expansion crack</p> <p>169 - 174 cm: sub-horizontal expansion crack</p> <p>182 - 183 cm: sub-cm mud clast</p>
100				
150				
200				212 - 225 cm: core catcher material
250				
300				
350				
400				
450				
500				
550				

R/V METEOR M167	Station: M167_ GeoB24213-1
Location: Background Pockmark	Date: 21.10.20, 16:37:00 (UTC)
Latitude: 35°23.1351'N	Recovery: 416.00 cm
Longitude: 7°11.9814'W	
Water depth: 1146 m	

LITHOLOGY					
Depth (cmbsf)	Photos	Log	Color	Struct.	Description
0					0 - 6.5 cm: filling foam
50			10YR 5/4 10YR 5/3 10YR 6/2	☉	6.5 - 416 cm: silty mud bearing fine sand (likely foraminifera), water saturated (6.5 - 16) and high water content through the whole core. Variable coloration through the core. Oxidized layer (6.5 - 18 cm). The whole sequence is interpreted as hemipelagic sediments (likely foraminifera-bearing nannofossil ooze).
100			10YR 6/1	☉	80 - 88 cm: light olive brown (2.5Y 5/4) 92 - 94 cm: cm-size lens with high concentration of microfossil 94 - 97 cm: light olive brown (2.5Y 5/4)
150					136 - 137 cm: gray patch (2.5 Y 5/1) 137 - 140 cm: light olive brown patches (2.5 Y 5/6)
200					166 - 167 cm: gray layer (2.5 Y 5/1)
250			2.5Y 5/6		196 - 197 cm: light olive brown patches (2.5 Y 5/6)
300			10YR 6/1	☉	211.5 - 213.5 cm: gray patch (2.5 Y 5/1)
350			10YR 5/2	?	233 - 237 cm: layered light olive brown patch (2.5Y 5/6)
400			10YR 6/4 2.5Y 7/2 10YR 6/2	?	250 - 254 cm: light olive brown patch (2.5Y 5/6) 258 - 259 cm: lens with high concentration of microfossils and bioclasts
450			10YR 5/3		320 - 327 cm: dark grey patches (GLEY 1 5G 4/1) 338 - 346 cm: layered light olive brown patch (2.5Y 5/6)
500					386 - 390 cm: light olive brown patch (2.5Y 5/6)
550					400 - 416 cm: imprints from the core catcher

R/V METEOR M167

Station: M167_ GeoB24214-1

Location: Possible MV #1- N of Tangier MV
(Marie Tharp MV)

Date: 22.10.20, 08:00:00 (UTC)

Latitude: 35°40.7983'N







Longitude: 6°56.7317'W

Water depth: 975 m

Recovery: 215.00 cm

LITHOLOGY					
Depth (cmbsf)	Photos	Log	Color	Struct.	Description
0			10YR 5/6	☉	0 - 2 cm: filling foam
2			10YR 5/2	☉	2 - 9.5 cm: oxidized mud breccia covered by a water-saturated hemipelagic sediment bearing fine sand (likely foraminifera). Large content of cm-size coral rubble. Gradual contact with the underlying sediments.
9.5				☉	9.5 - 39 cm: intermediate layer oxidized-anoxic mud breccia. Large content of cm-size coral rubble (<i>L. pertusa?</i>)
39				☉	39 - 215 cm: mud breccia with sparse mm-size poligenetic clasts (mud, lithic and bioclasts). Anoxic, H ₂ S smell. Several coral-rich intervals
60				H ₂ S	60 - 66 cm: large coral fragment (<i>L. pertusa</i>) and small coral rubble
86				☉	86 - 115 cm: sparse greenish gray mud clasts (d.<0.5 cm, G. 1 5G 5/1)
94				☉	94 - 96.5 cm: greenish gray lens (GLEY 1 5G 5/1)
115			GLEY 1 6/N	☉	115 - 116 cm: sub-cm greenish gray mud clast (GLEY 1 5G 5/1)
141				☉	141 - 142 cm: sub-cm greenish gray mud clast (GLEY 1 5G 5/1)
142				☉	142 - 215 cm: sparse cm-size light olive gray patches (2.5 5/4)
151.5				☉	151.5 - 154.5 cm: dark graysh brown gray mud clasts remains (2.5 Y 3/2)
164				☉	164 - 166 cm: sub-horizontal layered dark gray patch (GLEY1 4/N)
171				☉	171 - 172 cm: sub-cm graysh green mud clast (GLEY 1 5G 5/2)
181				☉	181 - 182 cm: sub-cm dark greenish gray mud clast (GLEY 1 5G 4/1)
201				H ₂ S	201 - 215 cm: core catcher material
204				☉	204 - 205 cm: sub-cm light gray mud clast (5Y 7/1)
250					
300					
350					
400					
450					
500					
550					

R/V METEOR M167	Station: M167_ GeoB24219-1
Location: Ginsburg MV	Date: 23.10.20, 14:12:00 (UTC)
Latitude: 35°22.389'N	Recovery: 129.00 cm
Longitude: 7°05.262'W	
Water depth: 899 m	

Depth (cmbsf)	LITHOLOGY				Description			
	Photos	Log	Color	Struct.				
0			GLEY 1 6/N	H ₂ S    	0 - 10.5 cm: filling foam 10.5 - 129 cm: mud breccia with sparse mm-size poligenetic clasts (mud, lithic and bioclasts). Anoxic, H ₂ S smell. Costant colour through the core. 14 - 21 cm: yellowish brown patches on the right side (upper oxidized sediments, 10YR 5/4) 27 cm: sub-cm greenish gray clast (GLEY 1 5G 5/1) 55 - 129 cm: mud breccia less cohesive, characterized by sparse mussy texture and higher water content compare to the upper layer (10.5 - 55 cm) 55 - 63 cm: large mud clast with sub-cm clasts associated			
50								
100								
150								
200								
250								
300								
350								
400								
450								
500								
550								

117 - 129 cm: half empty (core catcher)

R/V METEOR M167

Station: M167_GeoB24221-1

Location: Possible MV #3 (Maria Bianca Cita MV)

Date: 23.10.20, 18:05:00 (UTC)

Latitude: 35°39.0864'N

Longitude: 6°51.0523'W

Water depth: 858 m

Recovery: 430.00 cm

LITHOLOGY					
Depth (cmbsf)	Photos	Log	Color	Struct.	Description
0			10YR 5/6		0 - 2 cm: filling foam
			10YR 5/4		2 - 230 cm: silty mud with fine sand (foraminifera, other microfossil), water saturated (2-10 cm) and high water content through the whole core. Gradual oxydation and color change through the core. Several layers with coral rubble (fragments of <i>L. pertusa</i> frameworks)
			10YR 6/6		7 - 18 cm: cm-size coral rubble
50			10YR 5/1		20 - 30 cm: sparse sub-cm bioclasts (bivalve shells and coral rubble)
					31 - 32 cm: cm-size bioclast (bivalve shell fragment)
					32.5 - 40.5 cm: sparse sub-cm coral rubble
100					93 - 115 cm: dense layer of coral rubble (large to sub-cm size)
			2.5Y 5/2		136 - 141 cm: dark gray patches (2.5Y 4/2)
150					166 - 173 cm: cluster of sub-cm bioclasts (coral rubble and bivalve shell fragments)
					176 - 181 cm: yellowish brown patches (10YR 6/4)
200					196 - 199 cm: cluster of sub-cm bioclasts (coral rubble and bivalve shell fragments)
					202 - 207 cm: cluster of sub-cm bioclasts (coral rubble and bivalve shell fragments). Brown patches (10YR 5/3)
					214.5 - 217 cm: sub-cm coral rubble
250			GLE Y 1 10Y 6/1		230 - 430 cm: silty mud with fine sand (foraminifera, other microfossil). Anoxic conditions, H ₂ S smell at core opening
				H ₂ S	258 - 293 cm: layer with dense concentration of coral frameworks and coral rubble (<i>L. pertusa</i>)
300					302 - 314 cm: layer with dense concentration of coral rubble
					327 - 329 cm: large coral fragment
			GLE Y 1 10Y 5/1		335 - 336.5 cm: small greenish gray lens with muddy silt (GLE Y 1 5G 5/1)
350				H ₂ S	376 - 393 cm: sparse coral rubble
400					396 - 428 cm: layer with dense concentration of coral frameworks and coral rubble (<i>L. pertusa</i>)
					428 - 430 cm: filling foam
450					
500					
550					

R/V METEOR M167	Station: M167_ GeoB24222-1
Location: Ginsburg MV	Date: 24.10.20, 07:30:00 (UTC)
Latitude: 35°22.4042'N	Recovery: 241.00 cm
Longitude: 7°05.4620'W	
Water depth: 915 m	

Depth (cmbstf)	LITHOLOGY			
	Photos	Log	Color	Struct.
0				
0 - 2.5 cm				filling foam
2.5 - 10 cm				oxidized mud breccia covered by a water-saturated hemipelagic sediment layer (2.5 - 4.5 cm), bearing sand (likely foraminifera). Gradual contact with the underlying sediments
8.5 cm				sub-cm olive brown mud clast (2.5Y 5/6)
10 - 241 cm				mud breccia with sparse mm-size polygenetic clasts (mud, lithic and bioclasts). Anoxic, H ₂ S smell. Increase in cohesion with depth
29 - 34 cm				large lithic clast (or well-consolidated mud clast)
36 - 39 cm				mud clast
41 - 100 cm				empty space on the side (coring permutation)
57.5 - 58 cm				sub-cm ligh gray mud clasts (2.5Y 7/1)
65 - 74 cm				sparse mm-size ligh gray mud clasts (2.5Y 7/1)
86 - 87 cm				sub-cm ligh gray mud clast (2.5Y 7/1)
91 cm				sub-cm ligh brownish gray mud clast (2.5Y 6/2)
102 - 138 cm				sparse sub-cm mud clasts
141 - 230 cm				coring pertubation on the side of the core
150.5 - 151.5 cm				sub-cm greenish gray mud clast (GLEY 1 5G 5/1)
152 - 154 cm				cm-size dark grayish brown mud clast (10YR 4/2)
163 cm				sub-cm light gray mud clast (2.5 Y 7/1)
186 - 187 cm				sub-cm greenish gray mud clast (GLEY 1 5G/5/1)
192 - 193 cm				sub-cm greenish gray mud clast (GLEY 1 5G/5/1)
226 - 231 cm				sparse sub-cm mud clasts
230 - 241 cm				empty portion (core catcher)

R/V METEOR M167

Station: M167_GeoB24225-1

Location: Gemini II MV

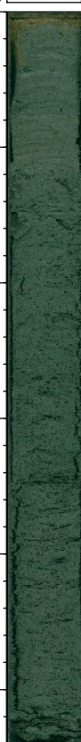

Date: 25.10.20, 16:54:00 (UTC)

Latitude: 35°16.863'N

Longitude: 6°45.433'W

Water depth: 421 m

Recovery: 274.00 cm

LITHOLOGY						
Depth (cmbsf)	Photos	Log	Color	Struct.	Description	
0			10YR 5/4	☉	0 - 2 cm: filling foam	
2			☉	2 - 4.5 cm: oxidized mud breccia covered by a water-saturated hemipelagic sediment layer (2 - 3 cm), bearing sand (likely foraminifera). Gradual contact with the underlying sediments. Oxidized material on the side of the underlying sediments as coring permutation. Gradual increase of cohesion with depth		
5			☉		4.5 - 270 cm: mud breccia with sparse mm-size poligenetic clasts (mud, lithic and bioclasts). Anoxic, H ₂ S smell	
21.5			☉		21.5 - 22 cm: sub-cm mud clast	
22			☉		22 - 36 cm: sparse mm-size light gray mud clasts (GLEY 1 7/N)	
39.5			☉		39.5 - 41.5 cm: sub-cm light gray mud clasts (2.5Y 7/1)	
60			☉		60 - 74 cm: sparse moussy texture	
87			☉		87 - 87.5 cm: sub-cm mud clast	
94			☉		94 - 274 cm: decompression cracks along the sides of the core	
104.5			☉		104.5 - 106.5 cm: large light gray mud clast (2.5Y 7/1)	
112			☉		112 - 113 cm: sub-cm mud clast	
113.5			☉		113.5 - 140 cm: sub-cm greenish gray mud clast (GLEY 1 5G 5/1)	
136			☉		136 - 139.5 cm: sub-cm mud clasts	
174.5			☉		174.5 cm: sub-cm mud clast	
195.5			☉		195.5 cm: sub-horizontal decompression crack	
201			☉		201 - 202 cm: sub-cm mud clast	
229			☉		229 cm: sub-horizontal decompression crack	
250			☉		250 - 251 cm: sub-cm dark gray mud clast (GLEY 1 5/N)	
256.5			☉		256.5 cm: sub-cm greenish gray mud clast (GLEY 1 5G 5/1)	
270			☉		270 - 274 cm: filling foam	
300						
350						
400						
450						
500						
550						

R/V METEOR M167	Station: M167_ GeoB24226-1
Location: Fiuza MV	Date: 25.10.20, 18:00:00 (UTC)
Latitude: 35°15.363'N	Recovery: 161.00 cm
Longitude: 6°41.946'W	
Water depth: 387 m	

Depth (cmbsf)	LITHOLOGY				Description
	Photos	Log	Color	Struct.	
0			10YR 5/6	⊗	0 - 2 cm: filling foam
2			GLE Y 1 5/N	○	2 - 7 cm: oxidized mud breccia covered by a water-saturated hemipelagic sediment layer (2 - 3 cm), bearing fine sand (likely foraminifera). Gradual contact with the underlying sediments. Oxidized material on the side of the underlying sediments as coring permutation. Gradual increase of cohesion with depth
5			G.1 5G 5/1	○	7 - 152 cm: mud breccia with sparse mm-size poligenetic clasts (mud, lithic and bioclasts). Anoxic, H ₂ S smell. High content of mud clasts (d. <0.5 cm). Sparse moussy texture. Intervals of greenish gray mud breccia are more cohesive than gray mud breccia
10			G.1 5/N	○	23 - 24 cm: sub-cm mud clast
15			5G 5/1 5Y 7/2	○	38.5 - 40.5 cm: large graysh mud clast (2.5 Y 4/2)
20			GLE Y 1 5/N	○	45 - 50 cm: carbonate-rich silty mud lens (nannofossil ooze?). Layer marking the contact between two mud flows
25					46 cm: cm-size mud clast at the contact between greensih mud breccia and underlying carbonate-rich hemipelagic sediments
30					94 cm: sub-cm greenish gray mud clast (GLE Y 1 5G 5/1)
35					117.5 cm: sub-cm greenish gray mud clast (GLE Y 1 5G 5/1)
40					122 - 128 cm: large lithified clast (arenite)
45					152 - 161 cm: filling foam
50					
55					

R/V METEOR M167	Station: M167_ GeoB 24228-1
Location: Potential MV #1 Lineament South (Isengard MV)	Date: 26.10.20, 07:51:00 (UTC)
Latitude: 34°56.7181'N	
Longitude: 7°53.9750'W	
Water depth: 2030 m	Recovery: 65.00 cm

Depth (cmbstf)	LITHOLOGY				Description
	Photos	Log	Color	Struct.	
0					0 - 5 cm: filling foam
5			10YR 5/4 10YR 6/3	⊗	5 - 14 cm: oxidized mud breccia covered by a water-saturated hemipelagic sediment layer (2 - 3 cm), bearing fine sand (likely foraminifera). Gradual contact with the underlying sediments. Oxidized material on the side of the underlying sediments as coring permutation.
14			GLEY 1 5/N	H ₂ S	14 - 65 cm: mud breccia with sparse mm-size poligenetic clasts (mud, lithic and bioclasts). Anoxic, H ₂ S smell. High content of carbonate in the mud matrix. High content of sandy particles. High cohesion compared to average mud breccia from other MVs
50			GLEY 2 5BG 5/1		50 - 54 cm: large dark gray mud clast (GLEY 1 4/N)
51			GLEY 1 5G 4/1		51 cm: sub-cm light gray mud clast (2.5Y 7/1)
60					60 - 65 cm: muddy gravel (mud clasts likely cemented by authigenic carbonate)
100					
150					
200					
250					
300					
350					
400					
450					
500					
550					

R/V METEOR M167

Station: M167_GeoB24229-1

Location: Potential MV #3 Lineament Center
(Gondor MV)

Date: 26.10.20, 15:26:00 (UTC)

Latitude: 35°30.4016'N

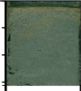

Longitude: 8°27.6926'W

Water depth: 2276 m

Recovery: 343.00 cm

LITHOLOGY					
Depth (cmbsf)	Photos	Log	Color	Struct.	Description
0			10YR 5/4 10YR 5/2 10YR 6/4	☉	0 - 2 cm: filling foam
50			2.5Y 6/1	☾	2 - 88 cm: muddy silt bearing fine sand (hemipelagic sediments). Oxidized layer. Likely nannofossil ooze bearing foraminifera. Gradual change of colour with depth. Light signs of bioturbation
100			GLE Y 1 7/1	(=)	73 - 80 cm: slightly bedded interval, with sign of bioturbation
150				☾	88 - 343 cm: muddy silt bearing fine sand (hemipelagic sediments). Anoxic, H ₂ S smell (buried mud volcano). High content of carbonate. Likely nannofossil ooze bearing foraminifera. Variable colours. Light to intermediate signs of bioturbation
200			GLE Y 1 5G 5/1	☾	
			GLE Y 1 7/N	☾☾	
			GLE Y 1 6/N	☾	
250			GLE Y 1 7/N	H ₂ S	
300			GLE Y 1 8/N	☾☾	275 - 283 cm: lens with light gray colour (high carbonate content)
350			GLE Y 1 7/N	☾☾	335 - 343 cm: partially empty portions (core catcher)
400					
450					
500					
550					

R/V METEOR M167	Station: M167_ GeoB24230-1
Location: Potential MV#1 New MVs Field (El Profesor MV)	Date: 27.10.20, 06:36:00 (UTC)
Latitude: 35°33.6676'N	
Longitude: 8°01.7118'W	
Water depth: 1670 m	Recovery: 31.00 cm

Depth (cmbsf)	LITHOLOGY				Description
	Photos	Log	Color	Struct.	
0			2.5Y 6/6 2.5Y 6/2 2.5Y 6/1	⊗	<p>0 - 2 cm: filling foam</p> <p>2 - 5 cm: oxidized mud breccia covered by a water-saturated hemipelagic sediments (2 - 3 cm), bearing fine sand (likely foraminifera). Gradual contact with the underlying sediments. Oxidized material on the side of the underlying sediments as coring permutation</p> <p>5 - 31 cm: mud breccia with sparse mm-size poligenetic clasts (mud, lithic and bioclasts). Anoxic, H₂S smell</p> <p>9 -14 cm: patches from the overlying oxidized sediments</p>
50			GLEY 1 6/N	H ₂ S	
100					
150					
200					
250					
300					
350					
400					
450					
500					
550					

R/V METEOR M167

Station: M167_GeoB24231-1

Location: Potential MV#2 New MVs Field
(Tokyo MV, unconfirmed)
Latitude: 35°33.1070'N
Longitude: 8°03.5386'W
Water depth: 1717 m

Date: 27.10.20, 08:26:00 (UTC)
Recovery: 266.00 cm

LITHOLOGY					
Depth (cmbsf)	Photos	Log	Color	Struct.	Description
0			10YR 6/4	⊗	0 - 4 cm: filling foam
50			2.5Y 6/1	⊗ ?	4 - 166 cm: silty mud bearing fine sand (likely foraminifera), water saturated (4 - 5 cm) . Gradual oxydation and color change through the core. Oxidized material (4 - 105 cm). 8.5 - 15.5 cm: yellowish brown patches (oxidized material, 10YR 6/4)
100				?	50 - 51 cm: muddy silt lens (GLEY 1 10GY 4/1) 57 - 58 cm: muddy silt lens (GLEY 1 10GY 4/1)
150			GLEY 1 6/N	?	66 - 68 cm: grayish brown lens (2.5Y 5/2)
200			GLEY1 10GY 4/1 10GY 5/1 10GY 4/1 5GY 4/1 10GY 5/1 10GY 4/1 5GY 6/1 10GY 4/1 mix	⊗ H ₂ S ? ?	166 - 266 cm: muddy silt bearing sand (likely foraminifera). High colour variability. Greenish gray layer are likely mud breccia-derived materia. Anoxic, H ₂ S smell 190 cm: light gray patch (GLEY 1 10GY 7/1) 213 - 262.5 cm: patches with several colour (GLEY 5GY 6/1, 10GY 5/1-4/1-6/1) 216 - 219 cm: light gray patch (GLEY 1 10GY 7/1)
250			10GY 4/1 5GY 6/1 10GY 5/1	?	
300			10GY 6/1	?	252 - 262.5 cm: empty portions (core catcher) 262.5 - 266 cm: filling foam
350					
400					
450					
500					
550					

R/V METEOR M167	Station: M167_ GeoB 24233-1
Location: Plain SW Atlas MV	Date: 28.10.20, 12:57:00 (UTC)
Latitude: 35°37.769'N	Recovery: 145.00 cm
Longitude: 7° 18.743'W	
Water depth: 1413 m	

Depth (cmbsf)	LITHOLOGY				
	Photos	Log	Color	Struct.	
0					
0 - 4				⊗	0 - 4 cm: filling foam
4 - 145					4 - 145 cm: silty mud bearing fine sand (microfossil), water saturated (4-5 cm) and high water content through the whole core. Gradual oxydation and color change through the core. Empty portions along the sides on the plastic liner.
19 - 20					19 - 20 cm: brownish yellow patches (10YR 6/8)
66 - 68					66 - 68 cm: grayish brown lens (2.5Y 5/2)
106 - 107					106 - 107 cm: light gray layer (2.5Y 7/2)
122 - 123					122 - 123 cm: light gray patches (2.5Y 7/2)
123					123 cm: horizontal empty portion (0.5 cm large-deep, 6 cm-long)
134					134 cm: dark gray patch (2.5Y 4/1)
150					
200					
250					
300					
350					
400					
450					
500					
550					

R/V METEOR M167	Station: M167_GeoB 24234-1
Location: Atlas MV	Date: 28.10.20, 14:31:00 (UTC)
Latitude: 35°39.3028'N	Recovery: 272.00 cm
Longitude: 7°16.8160'W	
Water depth: 1302 m	

Depth (cmbsf)	LITHOLOGY				Description
	Photos	Log	Color	Struct.	
0			10YR 5/4 10YR 5/2*	☉	0 - 6.5 cm: filling foam
50			10YR 5/2 2.5Y 5/2	☉ ☉	6.5 - 42 cm: silty mud bearing fine sand (likely foraminifera), water saturated (6.5-9 cm) and high water content through the whole core. Oxidized layer (6.5 -19 cm). Gradual oxidation with depth. Empty portions along the sides on the plastic liner 42 - 137 cm: muddy silt bearing fine sand (likely foraminifera)
100				☉ ☉ ☉	
150			2.5Y 5/1	☉	130 - 136 cm: tusk shell (scaphopod) 137 - 272 cm: mud breccia with sparse mm-size polygenetic clasts (mud, lithic and bioclasts). Anoxic, H ₂ S smell. High content of sandy particles. Sparse mud clasts (<0.5 cm) 150 - 151 cm: dark gray patches (GLEY 1 5/N)
200			GLEY 1 5GY 5/1	H ₂ S ☉	200 - 202 cm: cm-size mud clast 212 - 218 cm: light gray patches (GLEY 1 5/N) 237 - 241 cm: light gray patches (GLEY 1 10Y 7/1)
250					258 - 272 cm: core catcher material
300					
350					
400					
450					
500					
550					

R/V METEOR M167

Station: M167_ GeoB24236-1

Location: Potential MV E of Atlas MV (EUMR MV)

Date: 28.10.20, 17:42:00 (UTC)

Latitude: 35°38.6229'N

Longitude: 7°13.892'W

Water depth: 1194 m

Recovery: 241.00 cm

LITHOLOGY								
Depth (cmbsf)	Photos	Log	Color	Struct.	Description			
0				♂	0 - 4 cm: filling foam			
4				4 - 5.5 cm: mixed dark grey-yellowish gray sandy (likely foraminifera) water-saturated silt layer. Dark grey material is likely organic-rich sediments				
5.5				H ₂ S	5.5 - 241 cm: mud breccia with sparse mm-size polygenetic clasts (mud, lithic and bioclasts). Anoxic, H ₂ S smell. Sparse large bioclasts. Cohesion of the mud breccia above the average. Increase of the cohesion and decrease of water content with depth			
55					33 - 38 cm: large coral fragment (<i>Eguchipsamnia?</i>)			
					37 - 40 cm: large coral fragment (<i>L. pertusa</i>)			
					45.5 - 47 cm: cluster of mud clasts (<0.5 cm)			
100					51 cm: sub-cm bioclast (bivalve shell fragment)			
					57 cm: sub-cm mud clast			
					60 cm: sub-cm bioclast (bivalve shell fragment)			
					64.5 - 65.5 cm: cm-size mud clast			
					67.5 - 68 cm: cm-size bioclast (bivalve shell fragment)			
					84 - 85 cm: cm-size mud clast			
					85 - 89 cm: layer with high concentration of sub-cm clasts			
150					128 - 129 cm: three sub-cm mud clasts			
					179 - 180 cm: dark gray patches (GLEY 14/N)			
					191 - 192 cm: dark gray patches (GLEY 14/N)			
					216 - 217 cm: light gray patches (GLEY 110Y 6/1)			
					222 cm: carbonate encrustation, likely authigenic carbonates			
					222 - 227 cm: below the carbonate encrustation, light gray mud breccia (10Y 6/1), likely high concentration of calcium carbonate			
					227 - 241 cm: core catcher material			
250								
300								
350								
400								
450								
500								
550								

R/V METEOR M167	Station: M167_GeoB 24237-1
Location: Jesus Baraza MV	Date: 29.10.20, 06:29:00 (UTC)
Latitude: 35°35.4288'N	
Longitude: 7°12.0791'W	
Water depth: 1090 m	Recovery: 132.00 cm

Depth (cmbsf)	LITHOLOGY				Description
	Photos	Log	Color	Struct.	
0			2.5Y 5/3		0 - 2 cm: filling foam
50			GLE Y 1		2 - 4.5 cm: oxidized mud breccia covered by a water-saturated hemipelagic sediment layer (2 - 3 cm), bearing fine sand (likely foraminifera). Gradual contact with the underlying sediments. Oxidized material on the side of the underlying sediments as coring permutation.
100			10Y 5/2		4.5 - 132 cm: mud breccia with sparse mm-size poligenetic clasts (mud, lithic and bioclasts). Anoxic, H ₂ S smell. High content of sub-cm mud clasts (<0.5 cm).
150			GLE Y 1		10 - 10.5 cm: sub-cm mud clast
200			10Y 6/1		14.5 - 15 cm: sub-cm mud clast
250			GLE Y 1		18 - 20 cm: dark grey patches (GLE Y 1 10Y 4/1)
300					19 - 27 cm: cluster of mud clasts of variable sizes (likely a unique clast fractured during core opening)
350					32 - 41 cm: filling foam
400					41 - 64 cm: cavities along the sides
450					68 cm: decompression crack
500					70 - 71 cm: cm-size light gray mud clast (GLE Y 1 10Y 7/1)
550					73 - 132 cm: high concentration of poligenetic mud clasts (<0.5 cm)
					77 - 132 cm: sparse moussy texture
					117 - 122 cm: moussy texture

R/V METEOR M167

Station: M167_GeoB24238-1

Location: Depression W of Student MV

Date: 29.10.20, 08:32:00 (UTC)

Latitude: 35°30.959'N

Longitude: 7°09.410'W

Water depth: 1131 m

Recovery: 433.00 cm

LITHOLOGY					
Depth (cmbsf)	Photos	Log	Color	Struct.	Description
0			10YR 5/4	☉	0 - 2 cm: filling foam
			10YR 5/2	☉	2 - 14 cm: muddy silt bearing fine sand (foraminifera), oxidized layer high water content
			2.5Y 5/2	☉	14 - 27 cm: silty mud
				☉	16 - 17 cm: cluster of mm-size bioclasts
				☉	18 - 19 cm: sub-cm size bioclast (bivalve shell)
				☉	19 - 22 cm: cluster of sub-cm bioclasts (bivalve shells)
				☉	21 - 27 cm: olive yellow patches (2.5Y 6/6)
				☉	26.5 - 28 cm: cm-size coral fragment
				☉	27 - 104 cm: silty mud bearing fine sand (likely foraminifera)
				☉	30 cm: sub-cm bioclast (bivalve shell)
				☉	31 - 33 cm: cm-size coral fragment
			2.5Y 4/2	☉	38 - 76 cm: large content of coral fragments (<i>L. pertusa</i>)
				☉	82 - 85 cm: dark gray patches (2.5Y 3/2)
				☉	92 - 103 cm: yellowish brown patches (10YR 5/6)
				☉	104 - 132 cm: silty mud with sand nodules
				☉	106 - 108 cm: sand nodule
				☉	117 - 118 cm: sand nodule
				☉	120.5 - 122 cm: sand nodule
			2.5Y 5/2	☉	123 - 125 cm: solitary coral skeleton (<i>D. diantus</i>)
				☉	128 - 132 cm: yellowish brown patches (2.5Y 4/1)
				☉	128 - 132 cm: sand nodule
			10YR 5/2	☉	132 - 173 cm: muddy silt with sand (mostly occurring as nodules)
				☉	135 - 135 cm: sand nodule
			10YR 5/3	☉	146 - 155 cm: sand nodule (on left side of the core)
			10YR 6/3	☉	159 - 165 cm: cm-size sand nodules
				☉	173 - 232 cm: sandy silt with mud
			10YR 5/2	☉	201 - 210 cm: layer with high sand concentration
				☉	213 cm: dark gray patch (10YR 5/2)
				☉	232 - 432 cm: muddy silt with sand (mostly in nodules, likely derived from bioturbation)
			10YR 6/2	☉	232 - 236 cm: sand nodules
				☉	238 - 242 cm: sand nodule
				☉	246 - 255 cm: sand-rich layer
			G.1 10Y 5/1	☉	254 - 259 cm: yellowish brown patches (10YR 5/6)
				☉	261 - 264 cm: dark gray patches (GLEY 1 4/N)
			2.5Y 5/2	☉	284 - 286 cm: sand nodule
			10YR 5/2	☉	286 - 307 cm: brown patches
			2.5Y 5/4	☉	292 - 298.5 cm: sand-rich layer
			10YR 5/2	☉	300 - 311 cm: sand-rich layer
				☉	324 - 332 cm: sand-rich layer
			10YR 4/2	☉	332 - 334 cm: sand nodule
			2.5Y 5/3	☉	
			10YR 5/2	☉	374 - 381 cm: sand-rich layer
			2.5Y 4/3	☉	381 - 395 cm: sand nodules
			10YR 6/3	☉	388 - 403 cm: yellowish brown patches (10YR 6/4 and 5/3)
			10YR 6/2	☉	395 - 398 cm: sand-rich layer
			10YR 5/2	☉	398 - 411 cm: sand nodules
			2.5Y 5/2	☉	411 - 415 cm: sand-rich layer
			10YR 5/2	☉	415 - 419 cm: sand nodule
450					
500					
550					

R/V METEOR M167

Station: M167_GeoB 24239-1

Location: Student MV

Date: 29.10.20, 09:49:00 (UTC)

Latitude: 35°30.807'N

Longitude: 7°08.755'W

Water depth: 950 m

Recovery: 209.00 cm

LITHOLOGY					
Depth (cmbsf)	Photos	Log	Color	Struct.	Description
0			10YR 5/6	☉	0 - 2 cm: filling foam
				☉	2 - 9 cm: large mud clast covered by water-saturated oxidized sediments.
				☉	9 - 209 cm: mud breccia with sparse mm-size poligenetic clasts (mud, lithic and bioclasts). Anoxic, H ₂ S smell. Sparse mm-size microfossils (foraminifera)
50			GLE Y 1 10GY 5/1	☉	20 - 21 cm: cm-size mud clast (on the liner, left side)
				☉	23 - 25 cm: cm-size whitish grey mud clast (GLE Y 1 7/N)
				☉	33.5 - 35.5 cm: cm-size mud clast
				☉	44 - 48 cm: cm-size mud clast
			GLE Y 1 10GY 4/1	☉	52 - 53.5 cm: light grey patches (GLE Y 1 10Y 7/1)
				☉	59 - 60 cm: two patches, GLE Y 1 4/N (right) and GLE Y 1 5G 5/1 (left)
100				☉	75 - 79 cm: light grey patch (GLE Y 1 7/N)
				☉	76 - 77 cm: greenish gray patch (GLE Y 1 5G 5/1)
			GLE Y 1 10GY 5/1	☉	85 - 88 cm: light gray patch (GLE Y 1 7/N)
				☉	105 cm: light gray patch (GLE Y 1 7/N)
				☉	117.5 cm: light gray patch (GLE Y 1 7/N)
				☉	124 cm: light gray patch (GLE Y 1 7/N)
150			G.1 5GY 7/1 GLE Y 1 10GY 5/1 G.1 5GY 5/1	☉	163 - 166 cm: light greenish gray patch (G.1 5GY 7/1)
				☉	187 - 188 cm: greenish gray patch (G.1 5GY 7/1)
200			GLE Y 1 10GY 5/1		201 - 209 cm: empty space (core catcher)
250					
300					
350					
400					
450					
500					
550					